ABSTRACT

Title of Dissertation: INTEGRATED VARIABLE SPEED LIMIT AND RAMP METERING CONTROL FOR MANAGING RECURRENT FREEWAY CONGESTION

Yang (Carl) Lu, Doctor of Philosophy, 2017

Dissertation directed by: Gang-Len Chang, Professor, Department of Civil & Environmental Engineering

Recurrent congestion due to highway bottlenecks is one major factor contributing to daily commuting delays in most traffic corridors. The resulting traffic queues often start from the bottleneck, and then spill back to further upstream segments to block their on-ramps and off-ramps. Consequently, the entire corridor -- freeways and their connected local arterials -- often suffers from severe gridlocks. To address such a critical issue, this research aims to develop an integrated control system, using both ramp metering and variable speed limits to improve the operational efficiency and to keep the traffic flows moving steadily near roadway capacity. The control system developed in this study includes a traffic state prediction model, a local bottleneck control module, and integrated corridor control strategies.

The primary objective of the traffic state prediction model is to reliably predict the evolution of traffic conditions under the implemented control strategies, such as variable speed limit (VSL) and ramp metering. Based on the estimated compliance rate of drivers, the developed system with VSL is capable of capturing traffic flow dynamics – made up of VSL-

complying and non-complying vehicles – and adjusting model parameters in real time, based on the on-line detected traffic data. The system's predicted traffic dynamics will in turn serve as the basis for exercising a local and/or corridor integrated control.

Grounded on the embedded mixed traffic flow model, the second component of this developed system is a local bottleneck control module, using both ramp metering and variable speed limits to tackle the recurrent congestion. This module is capable of selecting the activation time for each available control strategy – based on predicted traffic information – and determining the number of VSLs to be activated so as to ensure that the flow rate at the bottleneck segment will not exceed its capacity. The local control module can also activate the ramp metering in a timely manner to support the VSL operations within the target segment. The system under the local control state can also have the flexibility to select different control objectives based on the monitored traffic patterns.

When traffic demand exhibits a sustained increase, the local bottleneck control alone may not be enough to prevent the freeway from breaking down. Hence, this study has further developed an integrated corridor control module, which can dynamically incorporate the upstream highway segments into control boundaries and exercise ramp metering controls to distribute excess volumes among different on-ramps. This will concurrently address both operational efficiency and equity concerns between freeway and ramp vehicles.

INTEGRATED VARIABLE SPEED LIMIT AND RAMP METERING CONTROL FOR MANAGING RECURRENT FREEWAY CONGESTION

by

Yang (Carl) Lu

Dissertation submitted to the Faculty of the Graduate School of the
University of Maryland, College Park, in partial fulfillment
of the requirements for the degree of
Doctor of Philosophy
2017

Advisory Committee:
Dr. Gang-Len Chang, Chair
Dr. Cinzia Cirillo
Dr. Ali Haghani
Dr. Chung C. Fu (serves as replacing committee member)
Dr. Martin Dresner, Dean's Representative

Dedication

To my wife, Gengwen Zhao, my father, Jianping Lu, and my mother, Xing Liu

for their love and support.

Acknowledgement

First and foremost, my deepest sense of gratitude goes to my dissertation advisor, Dr. Gang-Len Chang, for his invaluable guidance and inspiration throughout my Ph.D. study at the University of Maryland, College Park. His long-term commitment to research and unconditional pursuit for perfection will significantly influence my future career.

I am grateful to the members of my doctoral examination committee, Dr. Cinzia Cirillo, Dr. Ali Haghani, Dr. David Yang, Dr. Chung C. Fu, and Dr. Martin Dresner, for their constructive comments and suggestions on my research work. Special thanks go to Dr. Chung C. Fu for agreeing to serve as the replacing committee member when Dr. David Yang cannot attend the final defense due to emergency issues.

Also, very special thanks go to my colleagues in Traffic Safety and Operations Lab: Dr. Xianfeng Yang, Yao Cheng, Liu Xu, Hyeonmi Kim, Dr. Sung Yoon Park, Dr. Mark Franz, Dr. Chien-Lun Lan, Anna Petrone, Gregory Kramida, Dr. Woon Kim, and Dr. Xin Zhang, for the enlightening discussion during my Ph.D. study.

Furthermore, I sincerely thank many friends at University of Maryland, especially: Dr. Lei Feng, Dr. Chenfeng Xiong, Dr. Yang Lu, Dr. Wenxin Qiao, Dr. Yongjie Lin, Dr. Shanjiang Zhu, Dr. Xiang He, Liang Tang, Han Dong, Yan Liu, Dr. Yanshuo Sun, Xuechi Zhang, Di Yang, and Zheng Zhu, for the enjoyable moments we shared.

And finally, I would like to express my deepest appreciation to my wife, Dr. Gengwen Zhao, my father, Jianping Lu, and my mother, Xing Liu, for their long-time constant love, support, and encouragement, without which this dissertation could not be completed.

Table of Contents

List of Tables

List of Figures

Chapter 1: Introduction

1.1 Research Background

The transportation community and general public have long considered contending with traffic congestion to be a priority due to the potential significant impacts on traffic delay, safety, vehicle emissions, and fuel consumption. As shown in the most recent Urban Mobility Report (TTI & INRIX, 2015), traffic congestion has resulted in 6.9 billion additional hours and 3.1 billion gallons of additional fuel for travelers within the US in 2014, to cost a total $160 billion. Such impacts are even more severe in various metropolitan areas. For example, Washington D.C. ranked first in terms of delays encountered per commuter. Additionally, the capital region experienced a travel index of 1.34 in 2014, which implies that an hour of travel during normal free-flow conditions would cost rush-hour commuters an additional delay of approximately 20 minutes.

To cope with the recurrent congestion during daily commutes, one popular strategy is to fully utilize the operational capacity at roadway bottlenecks; this includes the deployment of ramp metering (Masher et al., 1975; Papageorgiou, 1991; Smaragdis et al., 2004; Zhang and Ritchie, 1997; Kotsialos et al., 2002; Kotsialos & Papageorgiou, 2004; Kotsialos et al., 2005; Papamichail et al., 2010, etc.), and variable speed limit control (Lin et al., 2004; Hegyi et al., 2004, 2006; Carlson et al., 2011; Hadiuzzaman and Qiu, 2012; Yang et al., 2015, etc.). Both control strategies, which involve no-capacity expansion, have received increasing attention from the traffic research community and highway agencies. Over the past several decades, either ramp metering or variable speed limit (VSL) has been extensively investigated independently in mostly simulation or demonstration studies, and has been

reported to achieve limited improvement. Their integrated operations to achieve the desirable level of effectiveness, however, have not been adequately addressed yet.

In review of related literature, it is notable that only a few studies (Hegyi et al., 2005; Carlson et al., 2010; Lu et al., 2010; Li et al., 2014, etc.) have focused on design of the integrated control, and most were developed primarily under simulation environments. To be a viable strategy in practice, however, the proposed integrated control system should be capable of offering effective mechanisms to address the following critical issues:

- How to identify control boundaries, optimal system activation time, and proper control objectives.
- How to model the response of drivers to VSL under different traffic conditions.
- How to predict the evolution of traffic dynamics when both VSL-complying and non-complying vehicles are in the traffic flows.
- How to develop an operationally efficient strategy to coordinate the ramp metering and VSL control for local bottleneck control.
- How to achieve the optimal control results under different traffic scenarios with different control objectives.
- How to distribute the reduction in traffic volume under different control scenarios, considering both the operational efficiency and equity, so as to achieve a system-wide optimal state.

1.2 Research Objectives

The primary objective of this research is to develop an integrated control system, using both ramp metering and variable speed limit to improve a roadway's operational efficiency, and to keep the traffic flow moving stably near its capacity. To accomplish the above objectives, this study has developed an integrated corridor control system that is capable of offering the following vital functions:

- A dynamic monitoring function to provide essential information for embedded traffic models to update key parameters.
- An algorithm to predict traffic breakdown, to identify the control boundaries, to select the optimal activation time, and to select the proper control objective.
- A statistical module to model drivers' responses to VSL to determine their compliance rates under different traffic conditions.
- A mixed-flow module to capture the traffic evolution with both VSL-complying and non-complying vehicles to reliably predict traffic conditions and to implement efficient optimal control strategies.
- An operationally efficient control strategy to address both the efficiency and equity issues by distributing the target volume reduction optimally to ramps and VSL segments in a local control model.
- An optimal control model that is capable of dynamically selecting the appropriate control objectives, and effectively coordinating the operations between variable speed limit and multiple ramp meters.

1.3 Organization

This dissertation, intending to address the aforementioned critical issues, comprises six primary tasks. Figure 1 illustrates the interrelations between those key tasks.

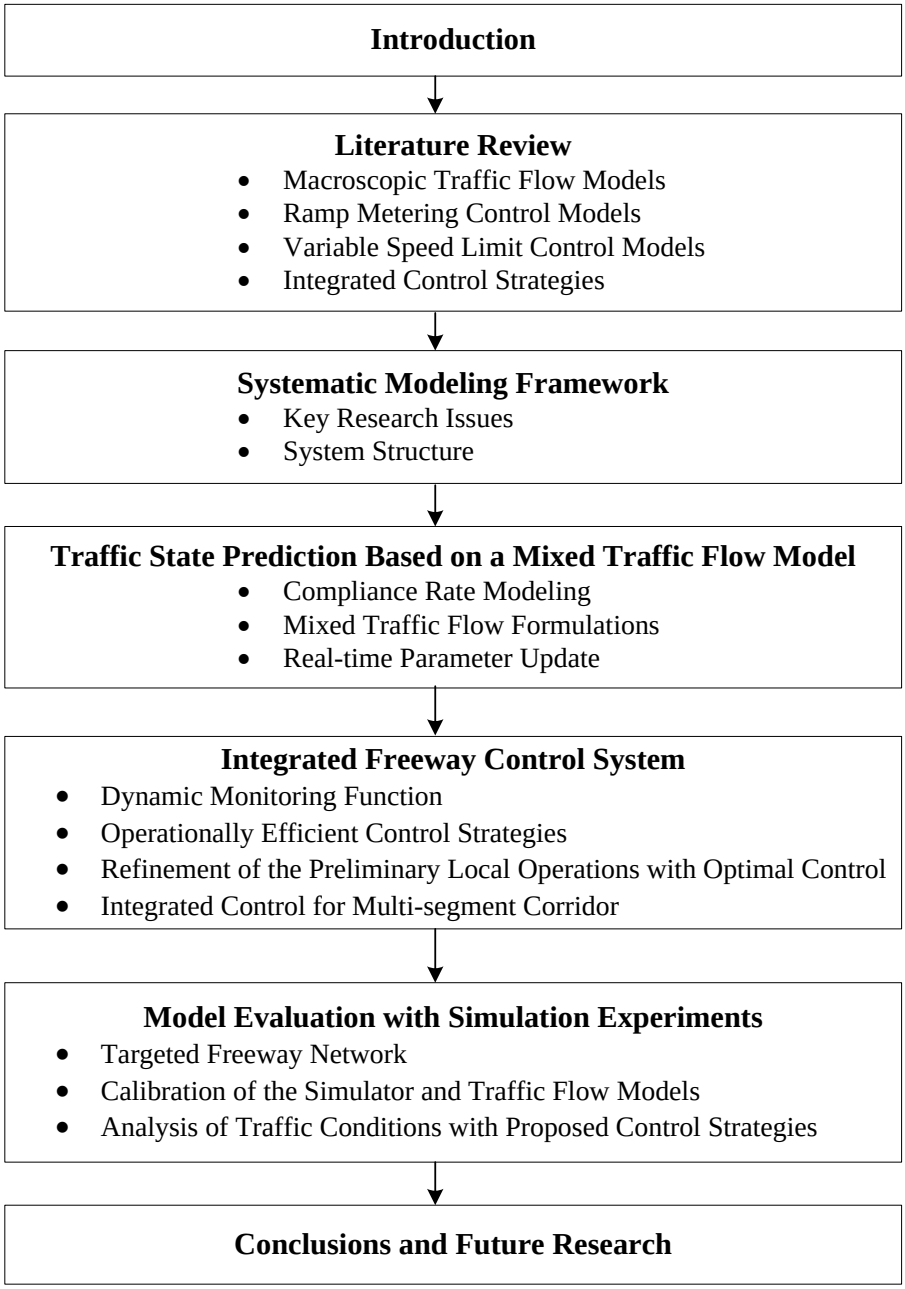

Figure 1.1 Dissertation Organization

The remainder of this dissertation is organized as follows:

- Chapter 2 summarizes the results of the related literature review over the past decades on various aspects of freeway control, including macroscopic traffic flow models, ramp metering control models, variable speed limit control models, and integrated control strategies.

- Chapter 3 presents the core components and their interrelationships in the proposed integrated freeway control system for managing the recurrent congestion from the perspective of both equity and operational efficiency.

- Chapter 4 introduces the traffic state prediction model that includes an estimation of the compliance rate of drivers under advisory variable speed limit (VSL) messages, formulations of traffic flow dynamics involving two vehicle classes, and a mechanism for adjusting model parameters in real time based on the on-line detected traffic data. The primary objective of the prediction model is to accurately predict the evolution of traffic conditions under the integrated operations of VSL and ramp metering. The predicted results will in turn serve as the basis for a local integrated control system to execute the control decisions.

- Chapter 5 introduces the integrated control module, using both ramp metering and variable speed limit to tackle the recurrent bottleneck. This module is capable of selecting the activation time for each available control strategy based on the predicted traffic information, and determining the number of VSLs needed for speed control to control the flow rate at the bottleneck segment not to exceed its capacity. The local control system can also activate ramp metering in a timely manner to support VSL operations within the control segment. The system also has the flexibility to select different control objectives based on the monitored traffic patterns. When the local

control is not sufficient to prevent a breakdown, the system has the functions to extend additional controls to further upstream segments so as to maintain the flow rate within the bottleneck capacity.

- Chapter 6 illustrates a numerical case study on MD-100 with calibrated microscopic simulation to evaluate the effectiveness of those developed strategies. The experimental comparison includes four different scenarios: base case, VSL only, local control and corridor control. The Measures of Effectiveness (MOEs) for performance comparison includes: travel time, densities at critical locations, total time spent in the network, queue lengths at controlled on-ramps, etc.

- Chapter 7 concludes the dissertation with key research findings and future research directions, including the development of an integrated corridor control system, the modeling of the on-ramp and off-ramp capacities, the potential improvement with the emerging connected vehicle technology, etc.

Chapter 2: Literature Review

2.1 Introduction

This chapter summarizes the results of related literature over the past decades on various aspects of freeway control, including macroscopic traffic flow models, ramp metering models, variable speed limit models, and integrated control strategies. A brief description of key studies in each of these areas is presented in sequence below.

2.2 Macroscopic Traffic Flow Models

The core objective of macroscopic models is to view traffic flows on roadway segments as moving streams, rather than focus on the behavior of individual vehicles. Most existing macroscopic models in the literature intend to group all vehicles in a highway segment into one homogeneous class with a first-order differential equation to reflect vital traffic phenomena, such as the formation and propagation of shockwaves, and stop-and-go congestion patterns. To improve computing accuracy, some researchers have explored the potential of extending the first-order single-class model to a high-order level (Payne, 1971; Papageorgiou, 1983; Zhang, 1998; and Michalopoulos et al., 1993).

Since highway traffic flows generally consist of multiple vehicle classes, most single-class models in the literature are insufficient for replicating actual traffic flow dynamics. For example, trucks, which often travel at speeds that differ from passenger cars, may behave like a "moving bottleneck" during congested conditions. This critical issue has motivated some traffic researchers to extend single-class to multi-class macroscopic models (Daganzo, 1997; Chanut & Buisson, 2003; Logghe & Immers, 2008; and Jiang & Wu, 2004).

Single-class Models

One of the pioneering macroscopic models in this category was proposed by Lighthill and Whitham (1955a, 1955b), and Richards (1956), known as the LWR model. The LWR model was developed on the law of flow conservation, as shown in Eq. (2.1):

$$\frac{\partial \rho}{\partial t} + \frac{\partial q}{\partial x} = s \tag{2.1}$$

where ρ is the segment density, v is the space mean speed, and q is the flow rate, which equals ρv. Eq. (2.1) shows that density change within a segment equals the difference between the outflows and inflows divided by the segment length, if the external source, s, is zero. Eq. (2.1) contains two unknown variables and thus cannot be solved directly. It is assumed in the literature (Greenshields, 1935; Greenburg, 1959; Underwood, 1961; Drake et al., 1967; Edie et al, 1963; etc.) that there exists an equilibrium relationship between the speed and density, as defined in Eq. (2.2):

$$v = V_e(\rho) \tag{2.2}$$

Due to discrepancies in the observed empirical data, some researchers have proposed different forms of the equilibrium speed-density relationship and the resulting fundamental diagrams. Examples of those include: the Greenshields Model (Greenshields, 1935), the Greenburg Model (Greenburg, 1959), the Underwood Model (Underwood, 1961), the Drake Model (Drake et al., 1967), and the Edie Model (Edie et al, 1963), etc.

Using the triangular fundamental diagram and discretizing the kinematic wave equation with the Godunov scheme (Godunov, 1959), Daganzo (1994, 1995) proposed the cell transmission model (CTM) that divides the roadway segment into several cells and describes the traffic evolution by the number of vehicles flowing out of each cell. Eq. (2.3) and (2.4) show the core concept of the CTM:

$$n_i(t+1) = n_i(t) + q_i(t) - q_{i+1}(t) \tag{2.3}$$

$$q_i(t) = \min\left\{n_{i-1}(t), Q_i(t), N_i(t) - n_i(t)\right\} \tag{2.4}$$

where $n_i(t)$ is the number of vehicles in cell i at time t; $q_i(t)$ is the number of vehicles entering cell i at time t which takes the minimum of the following three terms: the number of vehicles in its upstream cell, each cell's capacity, $Q_i(t)$, and its remaining space. Over the past two decades, several researchers have made various modifications and extensions of the CTM model. Examples of those enhancements include a lagged cell transmission model (LCTM, see: Daganzo, 1999), an asymmetric cell transmission model (ACTM, see: Gomes and Horowitz, 2006), and an enhanced lagged cell transmission model (ELCTM, see: Szeto, 2008).

Considering the deficiencies of the first-order models in reflecting the non-equilibrium state, Payne (1971) proposed a high-order model that allows the speed to deviate from its equilibrium value, where the static speed-density relationship is replaced with the dynamic speed-density equation under the following two assumptions:

1) The resulting speed does not change instantaneously with the density. Instead, it will start to respond after some delays;

2) The resulting speed also depends on the density of the downstream segment, which reflects a driver's anticipation on adjusting the speed.

Eq. (2.5) is used to reflect the above two assumptions:

$$v(x, t+\tau) = V_e\left[\rho(x+\Delta x, t)\right] \tag{2.5}$$

where τ is the response delay and Δx is the distance to the downstream segment. Eq. (2.5) can further be structured as follows after having been expanded in the Tayler series and re-arranged:

$$\frac{\partial v}{\partial t} + v\frac{\partial v}{\partial x} = \frac{V_e(\rho) - v}{\tau} - \frac{\gamma}{\rho\tau}\frac{\partial \rho}{\partial x} \tag{2.6}$$

where $\gamma = -0.5\partial V_e(\rho)/\partial\rho$. The speed change with time $\partial v/\partial t$ is dependent on three terms:

1) Convection term (the second term on the left): Since vehicles do not adjust their speeds instantaneously, the speed on the upstream segment may affect the current segment's traffic conditions.

2) Relaxation term (the first term on the right): The segment speed is allowed to deviate from its equilibrium value.

3) Anticipation term (the second term on the right): The speed in the current segment is affected by the downstream traffic conditions.

Similar models are also available in these studies by Kuhne (1984), Kerner and Konhauser (1993), and Zhang (1998).

Along the same line, Papageorgiou (1989) discretized Payne's model and added one parameter, κ, to the denominator of the density gradient term to prevent unrealistic results for a very small density. The dynamic speed equation (Eq. 2.9), together with the flow conversation equation (Eq. 2.7), static speed-density relationship (Eq. 2.8), and the flow equation (Eq. 2.10), comprise the basic METANET model that has been widely used for model-based freeway control. Notations used in the METANET model are listed in Table 2.1.

$$\rho_i(k+1) = \rho_i(k) + \frac{\Delta T}{L_i \lambda_i}[q_{i-1}(k) - q_i(k) + r_i(k) - s_i(k)] \tag{2.7}$$

$$V[\rho_i(k)] = v_{f,i} \exp\left[-\frac{1}{a_i}\left(\frac{\rho_i(k)}{\rho_{cr,i}} \right)^{a_i} \right] \tag{2.8}$$

$$\begin{aligned} v_i(k+1) = v_i(k) &+ \frac{\Delta T}{\tau_i}[V(\rho_i(k)) - v_i(k)] \\ &+ \frac{\Delta T}{L_i} v_i(k)[v_{i-1}(k) - v_i(k)] - \frac{\gamma_i \Delta T}{\tau_i L_i} \frac{[\rho_{i+1}(k) - \rho_i(k)]}{\rho_i(k) + \kappa_i} \end{aligned} \tag{2.9}$$

$$q_i(k) = \rho_i(k) v_i(k) \lambda_i \tag{2.10}$$

Table 2.1 Notations of Variables and Parameters Used in the METANET Model

Variables and parameters	Definition
$\rho_i(k)$ (veh/mi/lane)	Number of vehicles per mile per lane for segment i at time step k
$v_i(k)$ (mph)	The space mean speed for segment i at time step k
$V[]$	The equilibrium speed function
$q_i(k)$ (veh/h)	The flow rate leaving segment i to downstream segment i+1 between steps (k, k+1)
$r_i(k)$ (veh/h)	The flow rate entering segment i from on-ramps between steps (k, k+1)
$s_i(k)$ (veh/h)	The flow rate leaving segment i from off-ramps between steps (k, k+1)
L_i (mi)	The length of segment i
λ_i	The number of lanes of segment i
ΔT (hr)	The length of update time interval
$v_{f,i}$ (mph)	The free-flow speed of segment i
$\rho_{cr,i}$ (veh/mi/lane)	The critical density of segment i
a_i	The Speed exponent term of segment i
τ_i (hr), γ_i (mi^2/h), and κ_i (veh/mi/lane)	Parameters in the dynamic speed equations of segment i

If the segment contains an on-ramp, an additional term $-\frac{\delta v r}{\rho}$ should be added to Payne's speed equation to include the negative merging effect caused by the on-ramp volume.

Multi-class Models

Based on the law of flow conservation for a separated class, the multi-class LWR model defines the traffic state evolution for each vehicle class. The core challenge is to define the equilibrium speed-density relationship for each vehicle class, given the presence of another class of vehicles. Some researchers (Chanut and Buisson, 2003; Logghe and Immers, 2008) proposed the "same-speed" concept, suggesting that the speeds of different vehicle classes will be identical after reaching some thresholds. For example, a critical density is defined to be proportional to the jam density in Chanut and Buisson (2003)'s model. If the

summation of densities of two vehicle classes is larger than the critical density, these two vehicle classes will share the same equilibrium speed; they will otherwise follow their own speeds. Logghe and Immers (2008) expanded on the aforementioned work by introducing the concept of a "semi-congested" region, arguing that both the fast and slow vehicles in the free-flow region should follow their respective desired speeds. However, in semi-congested region, vehicles traveling at higher speeds need to reduce their speeds, while vehicles traveling at lower speeds can remain at the same speeds as in the free-flow region. Both types of vehicles in the congested region will travel at the same speed that is decreasing with an increase in density.

Other related studies (e.g., Wong and Wong, 2002) assume that, under the isotropic condition, the equilibrium speed is only the function of the total density with a different free-flow speed for each vehicle class m, as defined below:

$$\begin{aligned} &v_m(x,t) = V_{e,m}(\rho), \ \ \forall m = 1:M \\ &where: \ \rho = \rho_1 + \rho_2 + ... + \rho_M \end{aligned} \tag{2.11}$$

Although the model form is very simple, the authors claimed that it is capable of capturing the two-capacity phenomenon, the hysteresis phenomenon, and the platoon dispersion.

Applying the same idea to model the equilibrium speed, Jiang and Wu (2004) proposed a high-order traffic flow model for traffic streams comprising two classes of vehicles. An additional term, F_k, is added to the dynamic speed equation of class k to model the interaction between different classes (k=1 for fast vehicles; otherwise, k=2). F_2=0 means that faster vehicles do not have any impact on slower vehicles, while F_1 is proportional to both the speed difference between those two classes of vehicles and the density of slower vehicles.

2.3 Ramp Metering Control Models

Ramp metering is a control strategy that uses signals located at the on-ramp to regulate the vehicle flows onto the freeway mainline. Such a control system generally includes signals, mainline detectors (upstream detectors and downstream detectors), on-ramp detectors (check-in detector and check-out detector), queue detectors, and other optional components, as shown in Figure 2.1 (Pearson et al., 2001).

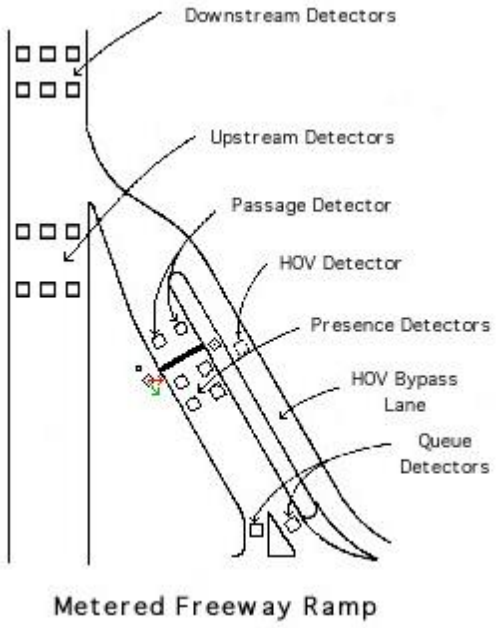

Figure 2.1 A typical ramp metering system (Pearson et al., 2001)

The first pre-timed ramp metering system was implemented in Chicago, IL in 1963 (Piotrowicz & Robinson, 1995). Since then, such a system has been widely tested in many metropolitan areas (Los Angeles, CA, 1968; Minneapolis-St. Paul, MN, 1970; Seattle, WA, 1981; Denver, CO, 1981; Portland, OR, 1981; Detroit, MI, 1984, etc.). Depending on whether or not the real-time detector information is available, the system can be operated under either pre-timed or responsive control. The former control aims mainly to improve the safety near the merging area by reducing traffic merging conflicts, but often results in the underuse of the freeway mainline capacity and excessive queues at the on-ramps if traffic demands deviate

from historical patterns. Thus, the following reviews focus on responsive controls, including local and coordinated ramp metering strategies.

Local Ramp Metering

The earliest algorithm for local ramp metering implemented in the field is the demand-capacity strategy (Masher et al., 1975), where the metering rate, r(k), is computed as follows:

$$r(k) = \begin{cases} q_{cap} - q_{in}(k-1), & if\ o_{out}(k) \le o_{cr} \\ r_{\min}, & else \end{cases} \tag{2.12}$$

The metering rate is the difference between the downstream capacity and the upstream flow measurements from the last interval, when the downstream occupancy is either below its critical level or a preset minimum value if the downstream is already congested. This is an "open-loop" type of control strategy that has no feedback mechanism.

As an alternative, ALINEA (Papageorgiou, 1991) adopts a "closed-loop" feedback algorithm to determine the metering rate, where the selection of output for the current interval is adjusted with the data from the previous interval, as shown in Eq. (2.13):

$$r(k) = r(k-1) + K_R[\hat{o} - o_{out}(k)] \tag{2.13}$$

where r(k) is the metering rate for interval k; K_R is a regulator parameter (e.g., 50-200 veh/hr); and $\hat{o}$ is the targeted occupancy value that is often chosen to be the critical occupancy value. The objective is to maintain the downstream occupancy near its critical value so that the traffic streams are to flow at the capacity level. ALINEA is reported to work better than the demand-capacity strategy and can generate a much smoother metering rate. It has been evaluated in several field tests and some key results are available elsewhere (Papageorgiou et al., 1997).

Some researchers have extended the concept of ALINEA to various levels, including: a flow-based version of ALINEA, an upstream-occupancy-based version of ALINEA, and an

upstream-flow-based version of ALINEA (See: Smaragdis & Papageorgiou, 2003), an adaptive version of ALINEA (AD-ALINEA, see: Smaragdis et al., 2004) and X-ALINEA/Q (any preceding algorithm with ramp queue control). For example, the critical occupancy in AD-ALINEA can be estimated in real time to maximize the mainline throughput. In X-ALINEA/Q, the metering rate will be the maximum between the results calculated from X-ALINEA and the embedded queue control model.

To improve the control effectiveness, Taylor et al. (1998) applied fuzzy logic to local ramp metering. This centers on three major components: fuzzification, rule evaluation, and defuzzification. The numerical input variables are first converted to descriptive variables based on the fuzzy sets. The "if-then" rules are then applied on those descriptive variables to yield the control strategies. Compared with existing ramp metering methods, fuzzy logic control allows users to incorporate expert knowledge in the design process and demand less accuracy on available data. However, selection of the key parameters and fuzzy rules remains quite a challenging task (Bogenberger and Keller, 2001; and Bogenberger et al., 2001).

To tackle the nonlinearity in the fundamental diagram, Zhang and Ritchie (1997) proposed a nonlinear feedback control framework with neural networks to compute the metering rate. For the same research needs, some recent studies apply an iterative learning approach (Hou, et al., 2008) and approximate dynamic programming (Xu, et al., 2006) to optimize the local metering rate.

Coordinated Ramp Metering

As local ramp metering is only responsive to local traffic conditions, it is not sufficient for preventing a system-wide formation of congestion. Hence, for a congested corridor necessitating a coordinated ramp metering control, one should consider both local and system-wide information in computing a metering rate for each ramp within the control boundaries. Both field and simulation evaluations have shown the effectiveness of

coordinated ramp metering on reducing the travel time and increasing the total throughput (Bogenberger & May, 1999; Chu et al., 2005; Papamichail et al, 2010b).

Among a large body of literature on coordinated ramp metering, most of those systems adopt the optimal control and the rolling horizon concepts under predicted traffic conditions (Zhang & Recker, 1999; Chang & Li, 2002; Kotsialos et al., 2002; Kotsialos & Papageorgiou, 2004; Kotsialos et al., 2005; and Papamichail et al., 2010a). In view of the complex and large-scale computing process, other researchers propose simplified but operationally efficient strategies to implement coordinated ramp metering control (Jacobson et al., 1989; Stephanedes, 1994; Paesani et al., 1997; Xin et al., 2004; Papamichail & Papageorgiou, 2008; Papamichail et al., 2010b).

For example, Kotsialos et al. (2002) proposed the Advanced Motorway Optimal Control (AMOC) model to compute coordinated metering rates with the given network topology. Based on the extended METANET model, the control aims to minimize the total network-wide travel time and the waiting time. The formulated discrete, nonlinear optimal control problem can be solved numerically with a feasible direction algorithm (Papageorgiou & Marinaki, 1995), which was reported to achieve a reduction of more than 15 percent on the total travel time in some simulation studies. Kotsialos and Papageorgiou (2004) further applied the same strategy to the ring-road in Amsterdam, focusing on the relationship between efficiency and equity under different constraints and traffic scenarios.

To overcome the inevitable errors associated with the estimation of initial traffic states, model parameters, and future demands for different Origin-Destinations (O-Ds), Kotsialos et al. (2005) modified the original AMOC strategy to a hierarchical control strategy that also incorporates the ALINEA local control model. The output from AMOC is not directly implemented, but set as the reference point for the local ramp metering model.

Other than the optimal and model predictive control (MPC), some researchers also developed various coordinated control strategies, including a competitive ramp metering

strategy (BOTTLENECK (Jacobson et al., 1989) & SWARM (Paesani et al., 1997)), a zone control strategy (Stephanedes, 1994), and coordinated ALINEA (Papamichail & Papageorgiou, 2008), etc.

Under the control of competitive ramp metering, the system will compute two metering rates: one from the local condition and the other from system-wide information, where the more restrictive one will be used for executing the control. In the BOTTLENECK algorithm (Jacobson et al., 1989), the local metering rate will be obtained from the demand-capacity feed forward control. The System Wide Adaptive Ramp Metering (SWARM) algorithm (Paesani et al., 1997) was developed by CALTRANS, and comprises two modules: SWARM-1 and SWARM-2. The former algorithm is used first to compute the required reduction in density, based on the predicted bottleneck density and the saturation density. The required reduction in volume is then assigned to each upstream metered on-ramp. The SWARM-2 algorithm is then applied to determine the local metering rate, based on either the headway theory or the storage model. The actual metering rate to be implemented is based on the current on-ramp volumes and the required reduction in volume, and is subjected to the constraints produced from the SWARM-2 module.

Under the ZONE metering strategy (Stephanedes, 1994), which was initially developed for the MnDOT in the early 1970s, the freeway segment will be divided into several zones, each containing only one ramp. For each zone, the control logic is shown in Eq. (2.14),

$$M + F + A + U = X + B + S \tag{2.14}$$

where M, F, A, U, X, B, and S represent the local ramp volume, the freeway-freeway ramp volume to be controlled, the upstream mainline volume, the non-metered ramp volume, the exit ramp volume, the bottleneck capacity, and the space available in the zone, respectively. The control objective is to keep the traffic volume in each zone at the capacity level by regulating the on-ramp volumes. After suspending the ramp metering control in 2000,

MnDOT (Xin et al., 2004) revised the original algorithm to a stratified zone strategy, where the minimal releasing rate is updated according to the ramp queue size. The main purpose of this revised model is to address public concerns about on-ramp waiting times (equity issue) while maintaining an acceptable level of efficiency.

Another example of such a control is a coordinated ALINEA, known as HEuristic Ramp-metering coOrdination (HERO, e.g., Papamichail & Papageorgiou, 2008; and Papamichcil et al., 2010b). Instead of applying only the local ALIENA control at the bottleneck on-ramp (i.e., master), the metering of the upstream on-ramps (i.e., slave) will be activated to maintain a minimal queue (w_{min}), when the corresponding queue length at the bottleneck on-ramp has reached the threshold. The value of w_{min} is updated for each control interval to balance the queue length at each metered on-ramp.

2.4 Variable Speed Limit Control Models

The purpose of variable speed control is to use the mandatory or advisory speed message to smooth traffic flows and to prevent shockwave impacts. The displayed speed can be adjusted manually or dynamically based on the weather and/or detected traffic conditions. A typical VSL system comprises five modules: sensors, variable message signs, control algorithms, the associated database, and communication systems. Sensors are used to monitor traffic conditions and adjust the displayed speed in response to traffic conditions.

The focus of VSL is to reduce the speed discrepancy among vehicles on some hazardous highway segments to decrease rear-end collisions and improve traffic safety (Steel et al., 2005; and Ulfarsson et al. 2005). Recently, it was recognized that VSL may also offer the potential to mitigate traffic congestion and improve traffic efficiency on work zones and freeway bottlenecks. By dynamically changing the speed limits along a highway segment, VSL can smooth the speed transition between the upstream and congested downstream flows to minimize the impact of shockwaves due to recurrent bottlenecks. The mitigation of traffic

speed variance can also facilitate traffic flows to better use the available roadway capacity during peak periods. Such studies, focusing on safety and mobility improvement, are summarized separately hereafter and are also available elsewhere (Lu and Shladover, 2014).

VSL for Safety Improvement

Most safety-related VSL systems deployed in practice were designed to contend with adverse weather (Katz et al., 2012). For example, in Mobile County, AL, VSLs were installed in a seven-mile section of I-10, which often experienced a high frequency of accidents due to inclement weather. On I-495 in Delaware, VSLs were manually varied by DelDOT operators at the transportation management center (TMC), so that the displayed speed could be dynamically adjusted in response to incidents, extreme weather, and poor surface conditions. In South Carolina, VSLs were placed along a two-mile rural segment of US-25 in Greenville County, where speeding and wet weather were primary contributing factors to about 85 percent of total crashes. In Cheyenne, WY, along the 140 miles of I-80, VSL speeds were determined based on visibility, surface conditions, and detected speeds by State Highway Patrol, maintenance foremen, and TMC operators. In Flagstaff, AZ (Placer, 2001), a fuzzy variable speed limit system was installed on the I-40 corridor in rural northern Arizona. The inputs to the fuzzy system include: the surface condition, average wind speed, wind gust speed, visibility, and precipitation intensity obtained from the Road Weather Information System (RWIS). The deployed system will display different speed limits based on the selected fuzzy rules.

While applying VSL in a work zone, especially in an urban environment, field studies were conducted to evaluate effectiveness on traffic safety and efficiency (Michigan DOT, 2003; Kwon et al., 2007; and Fudala and Fontaine, 2010), where the speed variance was typically selected as the surrogate measure for safety assessment. In the field evaluation along I-96 (Michigan DOT, 2003), it was reported that no obvious changes on the speed

variance were detected but marginal improvement was observed on the average speed. Kwon et al. (2007) reported the field test results on I-494, indicating the effectiveness in reducing the speed variance and increasing throughput as well as the average speed. Based on simulation results for work zones on I-495, Fudala and Fontaine (2010) concluded that appropriate VSL control could postpone the start of congestion if demand does not exceed roadway capacity.

With respect to improving safety under recurrent congestion, Abdel-Aty et al. (2006, 2008) developed a VSL system for I-4 in Orlando, FL, where a relatively simple control strategy was adopted to minimize the difference between the speed limit and the current average speed. However, given that the main control objective is to improve safety measurement, the reduction in travel time was marginal.

Despite the potential benefits of VSL, most such systems are exploratory in nature, and use relatively primitive methods. Hence, the design of reliable algorithms to ensure the benefits of VSL under recurrent congestion or work-zone operations remains a challenging issue.

Mobility-focused Studies

Primarily focusing on work-zone efficiency, Lin et al. (2004) proposed two VSL control algorithms with the objective of reducing queue length and maximizing throughput. The effectiveness of their proposed algorithms was demonstrated through a well-calibrated CORSIM simulation. Kang (2006) proposed an integrated dynamic late merge (DLM) and a VSL control system, and reported an increase in the work zone throughput and a decrease in speed variance compared with the single DLM system.

With respect to the effectiveness of VSL for recurrent congestion, most existing studies were conducted in simulated environments. For example, Hegyi et al. (2004, 2006) modified the METANET traffic flow model and incorporated the VSL effect into the model

predictive control (MPC) approach to determine the optimal speed limit. They reported a nearly 20 percent reduction in travel time, where the incoming flow rates were assumed to be constant during the simulation period.

Allaby et al. (2007) proposed a VSL control strategy that is consistent with the state-of-practice in Europe, and applied it to a Canada freeway under recurrent congestion in a simulation environment. The algorithm works by pre-defining the thresholds for detected volume, occupancy, and speed to display a VSL message, and it uses the rule-based method to implement the decision. Safety improvement was observed but at the cost of having negative impacts on travel time during the experimental period. The authors also conducted a sensitivity analysis with respect to key model parameters used, but they were unable to identify the parameter set that can concurrently improve both safety and operational efficiency.

Papageorgiou et al. (2008) analyzed the impact of VSL on aggregated traffic flow behavior from the theoretical perspective and explored the potential for incorporating a VSL into traffic flow models. For field applications, Carlson et al. (2011) developed a cascade controller that consists of two nested local feedback loops to decide the VSL speed for the main stream traffic control. An approximate 15 percent reduction in total travel time was reported in a simulation environment with METANET.

Using a modified CTM model, Hadiuzzaman and Qiu (2012) proposed a VSL control along with the MPC method to dynamically change the speed limit during operations. Their VISSIM simulation experiments assumed that detectors are placed at every cell to obtain the initial traffic state for the input for MPC, and they showed a reduction of 15 percent in total travel time.

More recently, Talebpour et al. (2013) proposed a reactive rule-based speed harmonization strategy to delay or even prevent traffic breakdown; they conducted a simulation experiment to support the algorithm's effectiveness in terms of improving both

safety and efficiency. Their study assumed that connected vehicle technologies are available to obtain each vehicle's trajectory and to facilitate the early detection of shockwaves. To contend with the uncertainties in driving behaviors, Yang et al. (2015) incorporated a Kalman filter into the traffic flow model to improve the accuracy of state estimation. Their extensive VISSIM simulation results showed a reduction of more than 10 percent on the average travel time. Considering the transient effect when changing the speed of VSL, Wang and Ioannou (2011) introduced a dynamic tracking mode, where drivers tend to track the VSL when certain conditions are satisfied. Rather than modify the original fundamental diagram or replace the steady-state speed with a lower speed generated by VSL, the speed in the dynamic tracking mode is to be updated in a feed-back control mode.

With respect to the field deployment of VSL, most such systems were tested in Europe and the resulting performances varied with each VSL system's embedded algorithm. For example, the VSL experiment in the Netherlands (Smulders, 1990) showed no improvement with regards to capacity, and this may be attributed to its advisory nature. However, the author claimed that traffic stability was significantly improved due to a decrease in small headways in the left lane; this improvement can also be observed in the delay of the congestion starting time. Field implementation in A5 between Friedberg and Frankfurt in Germany (Sparmann, 2006) and an M42 pilot study between J3A and J7 in England (MacDonald Ltd., 2008) both showed an increase of less than 10 percent in freeway capacity. Hegyi and Hoogendoorn (2010) developed the SPECIALIST algorithm to operate the variable speed limit, which was designed explicitly to resolve the shockwaves based on a reactive control logic. A field evaluation conducted on the Dutch A12 freeway showed that such a function can significantly mitigate the impact of shockwaves, but it cannot reduce the total travel time. Weikl et al. (2013) analyzed the data obtained from the German Autobahn A99 near Munich and concluded that VSL could reduce the shockwave speed and balance the lane distribution at the cost of slightly reduced capacity.

In the U.S., Bham et al. (2010) evaluated the VSL system deployed on I-270/I-255 in St. Louis and reported a reduced crash rate and a marginal benefit achieved on mobility. Chang et al. (2011) reported a successful demonstration of an integrated VSL and travel time information system on MD 100 near Coca-Cola Drive. They found that pairing VSL with a system for predicting travel time can significantly reduce the total travel time and increase the throughput over the bottleneck segment.

2.5 Integrated Control Strategies

An integrated control strategy combines both ramp metering and variable speed limit controls to cope with recurrent congestion. Depending on the logic of integration, most existing studies can be classified into the following three categories:

- Determine the ramp metering rate first, and then adjust the VSL;
- Determine the ramp metering rate and VSL speed concurrently;
- Determine the VSL speed first, and then compute the metering rate.

In developing the VSL system, most of those freeways under the first category of studies are assumed to be equipped with ramp metering control. Thus, it is straightforward to apply the VSL as a supplemental component on top of the computed metering rate. Those systems developed by Lu et al. (2010) and Li et al. (2014a) belong to this category. For example, Lu et al. proposed to determine the metering rates independently before optimizing the VSL on the basis of a METANET model in an MPC framework. In Li et al.'s control system, the VSL will not be activated until the ramp queue override mechanism is about to start. Thus, in the authors' models, ramp metering is the primary control strategy to prevent traffic breakdown, and VSL plays as a supplemental role to tackle excessive high demand conditions.

Most such systems, which concurrently determine the metering rate and the displayed speed, are based on the concept of optimal control or on model predictive control. Examples

of studies along this line include: Alessandri et al. (1998), Hegyi et al. (2005), Carlson et al. (2010), and Li et al. (2014b). They share some common features, but they also have their own unique contributions as listed below:

1) Different macroscopic traffic flow models are adopted to predict the traffic dynamics, which are also used as evaluation tools to assess the performance of each of the control strategies. For example, Alessandri et al. (1998), Hegyi et al. (2005), Carlson et al. (2010) use the second-order model (i.e., METANET), while Li et al. (2014b) select the first-order model (i.e., CTM).

2) Various ways are proposed to modify the original traffic flow model to include the VSL effect. For example, Alessandri et al. (1998) adopted Eq. (2.15) to represent the speed-density relationship when VSL is involved:

$$V[\rho_i(t), b_i(t)] = v_{free} b_i(t) \left\{ 1 - \left[\frac{\rho_i(t)}{\rho_{\max}} \right]^{L[3-2b_i(t)]} \right\}^M \tag{2.15}$$

where $\rho_i(t)$ is the density of segment i at time t, $b_i(t)$ is the speed ratio between the VSL and posted speed limit, L and M are positive constant. The above equation suggests that VSL will not only adjust the free-flow speed, but will also strengthen the effect of density on speed. In the work of Hegyi et al. (2005), the speed is chosen as the minimum of the desired speed based on the density and the one based on the displayed speed, as shown in Eq. (2.16):

$$V[\rho_{m,i}(k)] = \min \left\{ v_{free,m} \cdot \exp \left[-\frac{1}{a_m} \left(\frac{\rho_{m,i}(k)}{\rho_{crit,m}} \right)^{a_m} \right], (1+\alpha) v_{control,m,i}(k) \right\} \tag{2.16}$$

where α is the parameter to quantify the effect of the compliance rate. Based on the analysis results of VSL field data, Carlson et al. (2010) modeled the effect of VSL on aggregated traffic flow behavior as follows:

- The free-flow speed is replaced by the displayed speed;
- The critical density increases linearly with a decrease in the displayed speed;

- The parameter a_m increases linearly with a decrease in the displayed speed.

The above three VSL effects can be represented with Eq. (2.17) to Eq. (2.19):

$$v_{f,m}[b_m(k)] = v_{f,m}^{*} b_m(k) \tag{2.17}$$

$$\rho_{cr,m}[b_m(k)] = \rho_{cr,m}^{*} \{1 + A_m[1 - b_m(k)]\} \tag{2.18}$$

$$a_m[b_m(k)] = a_m^{*} \{E_m - (E_m - 1) b_m(k)\} \tag{2.19}$$

where the parameters with asteroid as the superscript denote its original value without VSL; A_m and E_m are parameters calibrated with field data.

3) Different objective functions were adopted to perform the optimal control or the model predictive control. Some studies aimed to minimize total travel time while subjected to several operational constraints; others proposed the multi-objective function that can concurrently minimize total travel time and maximize throughput.

4) Due to the complexity of field implementation, the proposed control strategies were only evaluated in simulation environments. Their simulation results demonstrated that the combined control strategy can outperform individual strategies in terms of reducing network travel time. For example, in Hegyi et al. (2005)'s study, about a 5 percent reduction on total time spent was achieved in the ramp metering only case, but the coordinated VSL and RM control reached up to a 14 percent improvement.

Lu et al. (2011) proposed a coordinated VSL and ramp metering strategy to contend with recurrent congestion at bottlenecks. In their paper, VSL is determined first and then the metering rate. The VSL sub-task is divided into three major parts: 1) design VSL from the most upstream to the critical VSL point to harmonize traffic; 2) design the critical VSL to maximize the bottleneck flow; 3) determine the speed in the storage section. After VSL is selected, the ramp metering rate will be obtained by solving the optimization formulations with its objective function of minimizing the weighted summation of total time spent and maximizing the total travel distance. Their study reported achieving a significant

improvement in both TTS and TTD under a simulation experiment with a coordinated strategy.

2.6 Discussion

In summary, this chapter has reviewed key studies on freeway controls including: macroscopic traffic flow models, ramp metering control strategies, variable speed limit control models, and integrated freeway control. Existing macroscopic traffic flow models are classified as single-class or multi-class, based on the vehicle composition. Each type of model could be further divided into first-order and high-order models based on the assumption of the equilibrium speed. Such models are important components in a freeway control system for capturing the dynamics of traffic evolution.

Ramp metering has been demonstrated in both field tests and simulation evaluations to be effective in enhancing freeway mobility. Compared with the local metering algorithm, coordinated ramp metering often leads to a favorable performance when contending with more severe congestion. Initially designed to improve safety metrics, variable speed limit control has also shown significant potential to improve traffic mobility. Various algorithms, either rule-based or model-based, have been developed to operate the VSL to reach optimal (sub-optimal) control results. Grounded on the above two control strategies, integrated freeway control takes advantage of both controls' strengths to better the system-wide performance in simulation platforms. It may also offer the potential to prevent a traffic breakdown during recurrent congestion.

Despite the success of integrated control reported under simulation environments, the following critical issues remain to be addressed prior to their field deployment:

- The needs to determine the system's activation time and the control scope have not been adequately discussed in the simulation studies but are critical in the design of an operational system. Activating the system control ahead of its

needed time may decrease the compliance rate of the driving population and cause some unnecessary traffic delay, but not taking the control action in a timely manner may lead to inevitable traffic breakdown at recurrent bottleneck areas. How to make the decision sufficiently robust is a critical issue to be addressed.

- Drivers' compliance rate with the VSL system plays a key role in its resulting performance. However, most existing studies focus only on drivers' responses to the speed signs in work-zone scenarios (See: Kwon et al., 2007; Finley et al., 2015), but not under recurrent congestion where the compliance rate of drivers with VSL is mostly assumed to be 100 percent.
- The underlying operational mechanism to coordinate the VSL and ramp metering remains to be enhanced. The metering rate and displayed speed are directly given by the optimization model in most studies. The operational logic to coordinate these two strategies and to consider the compliance rate is extremely imperative, especially for real-time adjustment of control strategies.
- The equity issue in ramp metering control has been extensively discussed, and criticized by the general public. For example, widespread dissatisfaction was discovered and resulted in the metering closure experiment in Minneapolis-St. Paul (Cambridge Systematics, Inc., 2001). Thus, how to address the equity issue in the system design and deployment is critical to the success of any ramp or integrated control.

In view of the above issues, this study aims to propose an optimal and operationally effective integrated freeway control system, capable of incorporating compliance rate into the model and of addressing the equity issue in the system control process.

Chapter 3: An Integrated System Control Structure

3.1 Introduction

This chapter presents the core components -- and their interrelationships -- in the proposed integrated freeway control system for managing recurrent congestion. The rest of this chapter is organized as follows: Section 3.2 presents several key research issues associated with developing both ramp metering and variable speed limits in an integrated control system; Section 3.3 discusses the operational structure of the integrated control system, which includes key system input and output, the function of each principal component, and their interrelations in a real-time operational process.

3.2 Key Research Issues

The objective of the integrated control system is to improve the roadway operational efficiency by preventing a breakdown and keeping the traffic flows moving stably near roadway capacity. To achieve the above goals, the proposed system should be capable of providing the following functions:

- Monitor the real-time roadway conditions to provide information essential for the embedded traffic prediction models to update key parameters, and in order for the integrated system to identify control boundaries, activation time, and selection of the proper control objectives.

- Accurately model drivers' responses to VSL messages to better predict their compliance rates under different traffic conditions.

- Formulate the traffic evolutions process under mixed-flow conditions to provide the foundation for implementing the model-based optimal control.

- Develop algorithms to identify the control boundaries in real time to assist the system in selecting the most effective control strategy among local bottleneck control, coordinated corridor control between multiple on-ramps and VSLs, and integrated control between on-ramps, VSLs and off-ramps.

- Execute the optimal traffic control model to select the appropriate control objectives and coordinate the operations between variable speed limit and multiple ramp meters.

3.3 System Structure

Figure 3.1 depicts the framework of the proposed integrated control system, including the required system input and the generated output, its principal control components, and the operational relations between these control modules.

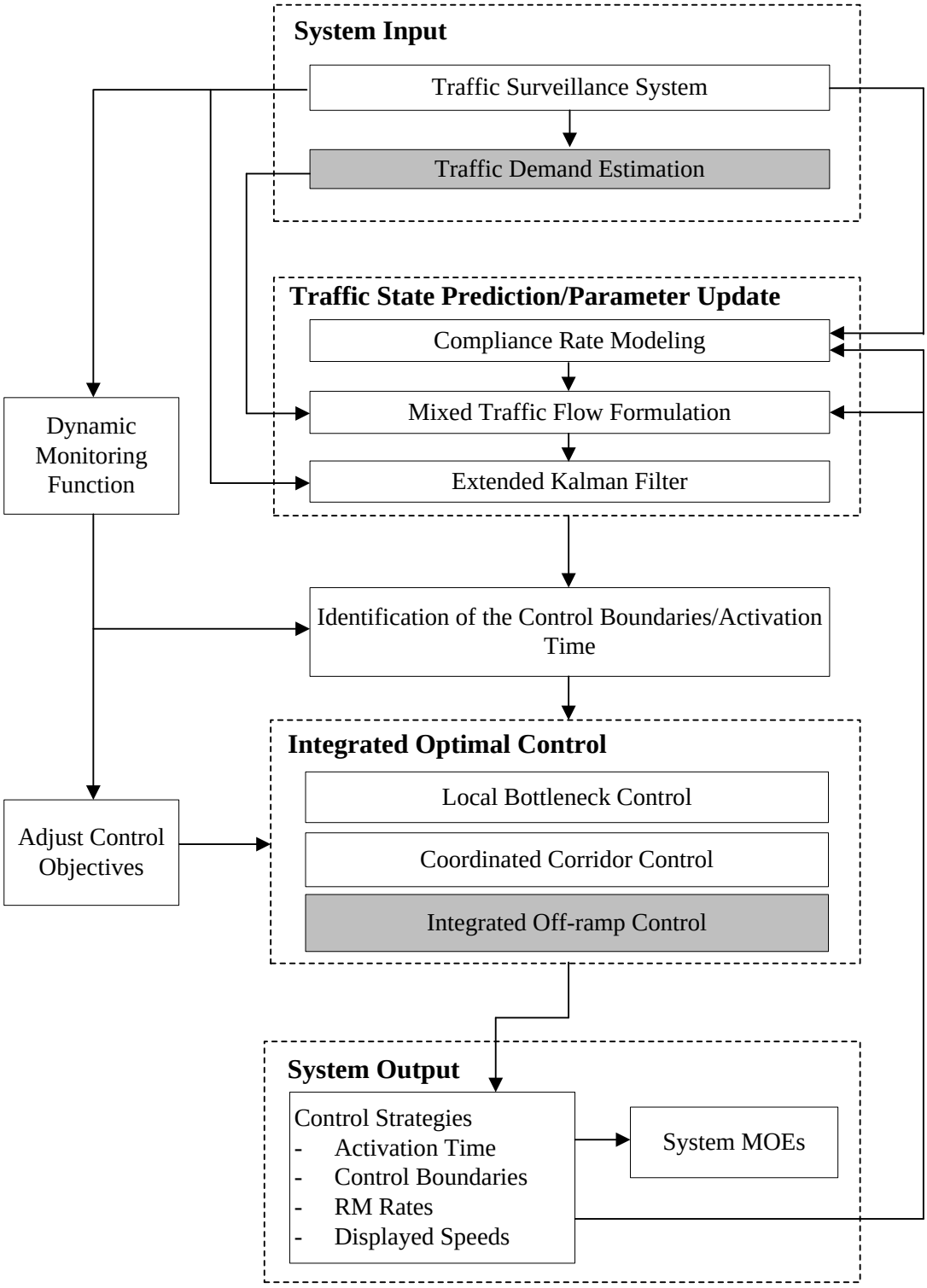

Figure 3.1 The System Structure of the Developed Integrated Control System

A brief description of the key function to be provided in each primary system component is presented below:

- Dynamic Monitoring Module: This component aims to provide continuous monitoring of traffic conditions for the entire freeway corridor. Taking the traffic surveillance data as input, this module will identify the current traffic condition as one of those five predicted states, ranging from free-flow to stagnant congestion. The boundaries between those states will be estimated from field data using a clustering method. The identified traffic information is essential for the system to determine: 1) the control boundaries and activation time; and 2) the control objective adopted in the optimal control module. Section 5.2 will discuss this component in detail, where the definition of each state will be described, along with the algorithm to perform the clustering analysis.

- Traffic state prediction/parameter update: This component includes three models to predict the evolution of traffic conditions over the freeway corridor, which serves as the foundation for all control modules. The first module for compliance rate estimation aims to describe the response of drivers to variable speed limit messages. Instead of using a pre-selected constant as in the literature (Hegyi, 2004), the compliance rate is modeled as a function of the display speed, the difference between the prevailing and displayed speeds, and the interaction between these two values. The proposed model has been validated with field data of several months from one VSL field deployment site. The second module is the mixed traffic flow model, which adopts the second-order macroscopic formulations calibrated with field data to represent the evolution of traffic dynamics along the freeway corridor. Those vehicles, complying with the

VSL message and following the regular speed limit, are divided into two classes in the macroscopic formulations, where the effect of the slow-moving vehicles on other vehicles with higher speeds is explicitly modeled in the speed equations. To best reflect the time-varying traffic conditions, especially during the transition state, this model further contains an updating mechanism with the extended Kalman filtering to dynamically adjust the key model parameters, based on the available real-time surveillance data. Figure 3.2 shows the interrelations between those three primary models.

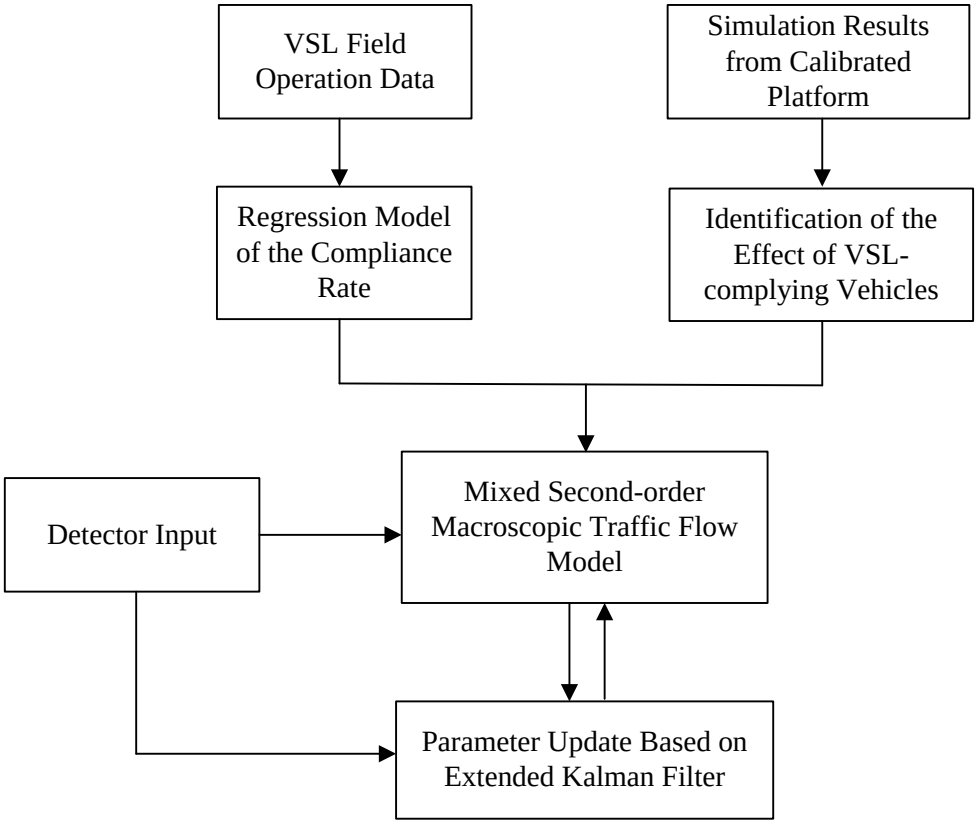

Figure 3.2 Components of the Mixed Traffic Flow Model

- Identification of the control boundaries and activation time: This component is responsible for computing the system activation time and the control boundaries.

The proposed integrated system will activate the control operations if the predicted congestion formation may occur within the prediction horizon. The operational flowchart to determine the activation time, based on the dynamic traffic monitoring system, is shown in Figure 3.3. The number of VSLs to be activated in the local control mode will then be determined based on the targeted flow rate reduction and the VSL operational constraints with information regarding activation time and control boundaries. The proposed integrated system can then proceed to assess whether the local control is sufficient for preventing an increase in traffic from a breakdown or whether the coordinated control is needed.

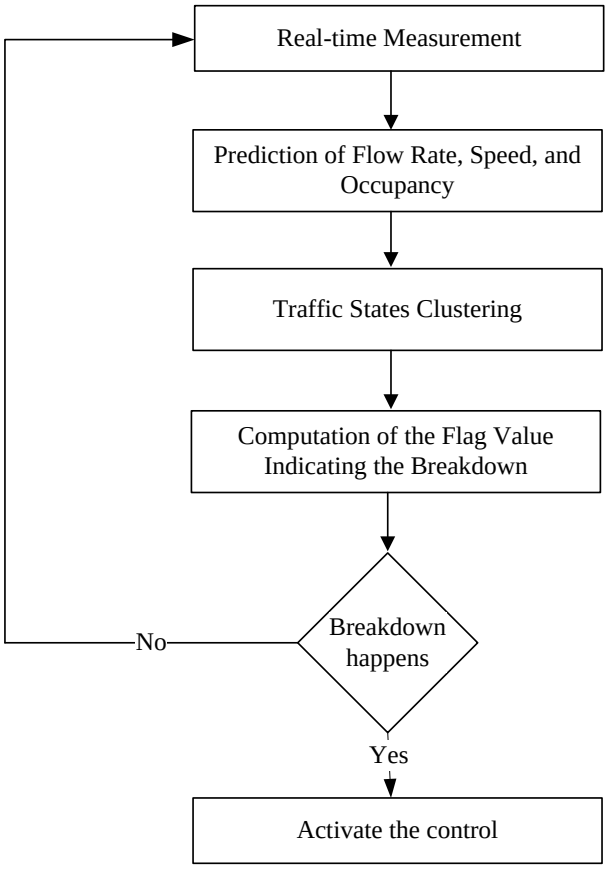

Figure 3.3 Flowchart of Determining the Activation Time

- Adjust control objectives: This module offers the function to dynamically switch the control objective between maximizing the throughput and minimizing the total travel time. In principle, to account for the equity of vehicles from the metered on-ramps, the control objective is always set to maximize the total throughput unless the traffic breakdown is inevitable. Section 5.4 will illustrate the detailed logic of the module and the underlying rationales.

- Integrated optimal control: this component functions to incorporate the above traffic state prediction module into a model-based optimization process to determine the optimal distribution of flow rate reduction between on-ramps and the mainline segments with VSLs. The core information for such flow distribution will be based on the results predicted by the mixed-flow traffic module and the bottleneck's capacity. To minimize the disruption to the on-ramps while preventing mainline breakdown, more traffic volume reductions, if needed, are generally distributed in sequence to the VSL-controlled mainline segments. Sections 5.3 and 5.4 will discuss the logic used to distribute the required flow rate reduction between on-ramps and freeway mainline segments. An extension of such local control to multiple freeway ramps and VSL operations will be presented in Section 5.5. The flowchart of the developed integrated control system is shown in Figure 3.4.

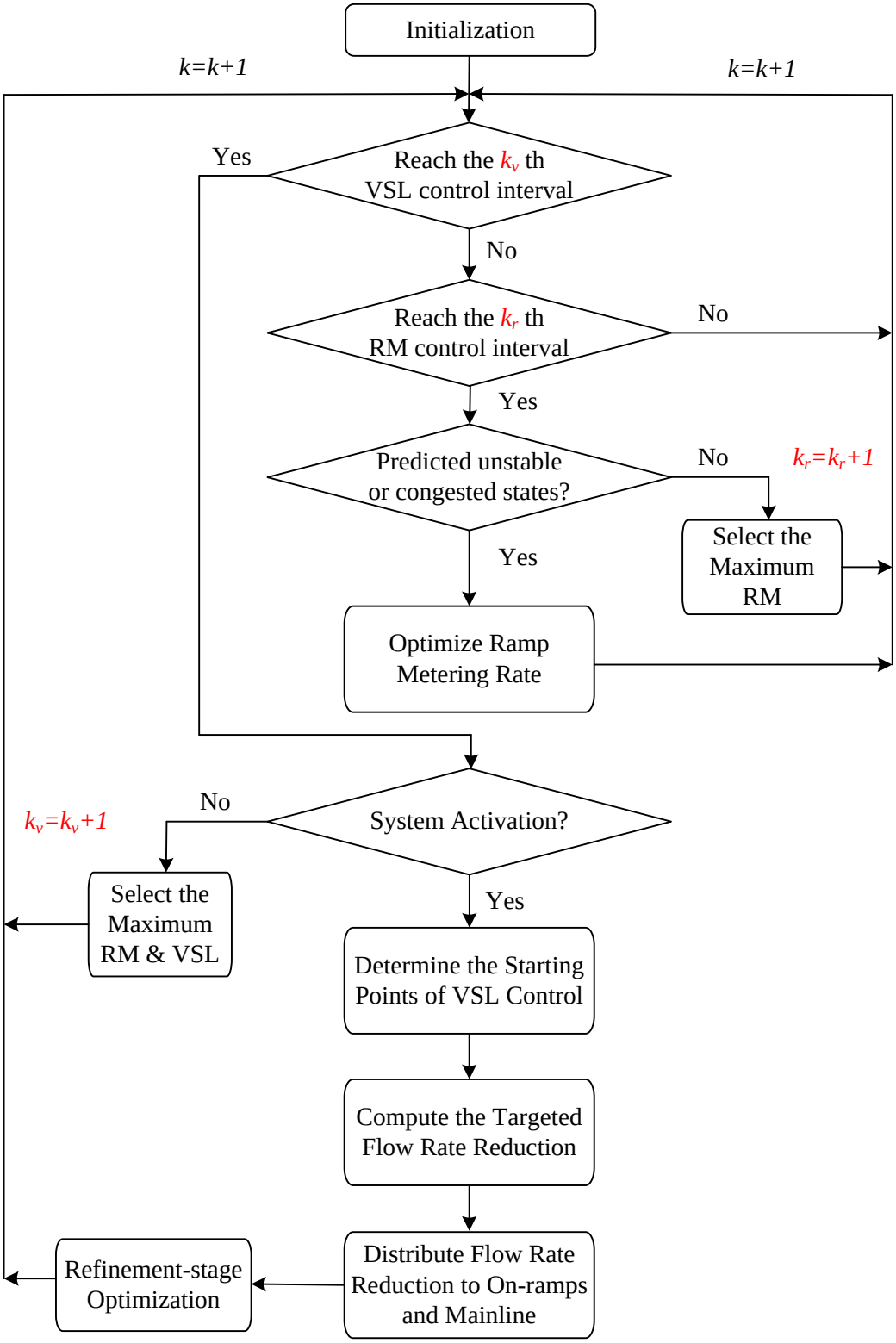

Figure 3.4 Flowchart of the Entire Integrated Corridor Control

Chapter 4: Traffic State Prediction Based on a Mixed Traffic Flow Model

4.1 Introduction

This chapter introduces the traffic state prediction model that includes three major components. The first is to estimate the compliance rate of drivers with an advisory variable speed limit (VSL) sign. Taking the compliance rate as the input, the second model formulates the evolution of traffic flow dynamics involving two vehicle classes. The third component presents the mechanism for adjusting model parameters in real time, based on the real-time traffic data. The primary objective of this prediction model is to accurately predict the evolution of traffic conditions under the integrated control of VSL and ramp metering. The predicted results will in turn serve as the basis for the integrated system to make an effective control decision.

4.2 Compliance Rate Modeling

Different from those used in Europe and other countries, most VSLs within the United States are operated in the advisory but not mandatory mode. Hence, the compliance rate of drivers with displayed VSL messages may have significant impacts on the operational effectiveness and the resulting outflow rate from each segment under control.

Most existing studies on this topic either assume a compliance rate of 100 percent in their simulation evaluations or add an adjustment factor to reflect the non-compliance effect (Hegyi, 2004). To further consider the impact of the compliance rate on the control effectiveness, some researchers (e.g., Franz, 2015) conducted sensitivity analysis with respect to different compliance rates (e.g. 25 percent, 50 percent, 75 percent, etc.), and computed the resulting differences with predefined Measures of Effectiveness (MOEs), such as travel time

and throughput. Another class of researchers promoted the use of a feedback mechanism to adjust the displayed speed limit if significant non-compliance patterns were detected (Lin et al., 2004).

Noticeably, the sensitivity analysis cannot fully capture driver responses to VSL because the compliance rate may vary with traffic conditions. On the other hand, the feedback mechanism can only be regarded as reactive in nature, lacking the proactive ability to prevent resulting traffic from breakdown. Hence, modeling the compliance rate with VSL under different traffic conditions remains an imperative issue in the proposed integrated control system.

With the above issues in mind, this section first presents the analysis results of the VSL field data from MD-100, followed by statistical expressions of research findings.

Experimental Design

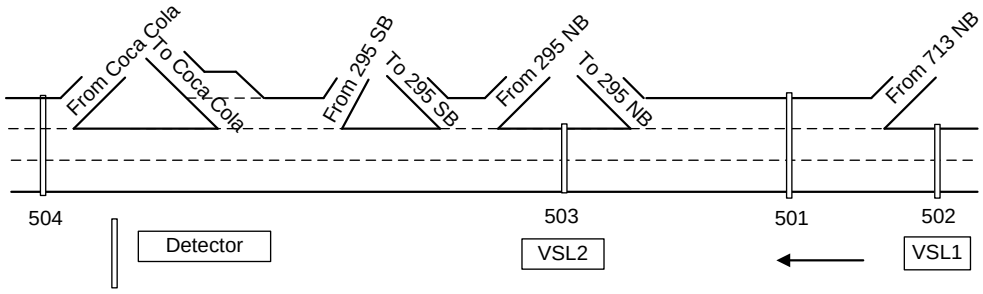

Figure 4.1 The Network Settings of the Data Analysis

Figure 4.1 illustrates the field site on the roadway segment of MD-100 WB between MD-170 and US-1. This roadway segment regularly experiences congestion during the PM peak hours, and the bottleneck often occurs at the downstream of Coca-Cola Drive. Four detectors were installed on the roadside to detect occupancy, speed and volume, along with two VSL signs to display advisory speed limits.

Note that Detector 504 was used to monitor traffic conditions at the bottleneck location. If congestion is detected, VSL-2 will be activated. The displayed speed is determined by the flow rate difference between detectors 503 and 504. VSL-1 was operated with the same algorithm and the information from detectors 503 and 502.

To observe a driver's willingness to reduce their speed when observing VSL messages, this study employs the data from January 4th to January 25th in 2010, during which the VSL demonstration had been implemented for more than two weeks. The speed data from detector 502 is regarded in the analysis as the upstream speed, and the data from detector 501 is denoted as the downstream speed. To avoid speed reduction caused by congestion, the occupancy data from detector 501 was also observed, and those above the critical occupancy were excluded from this study.

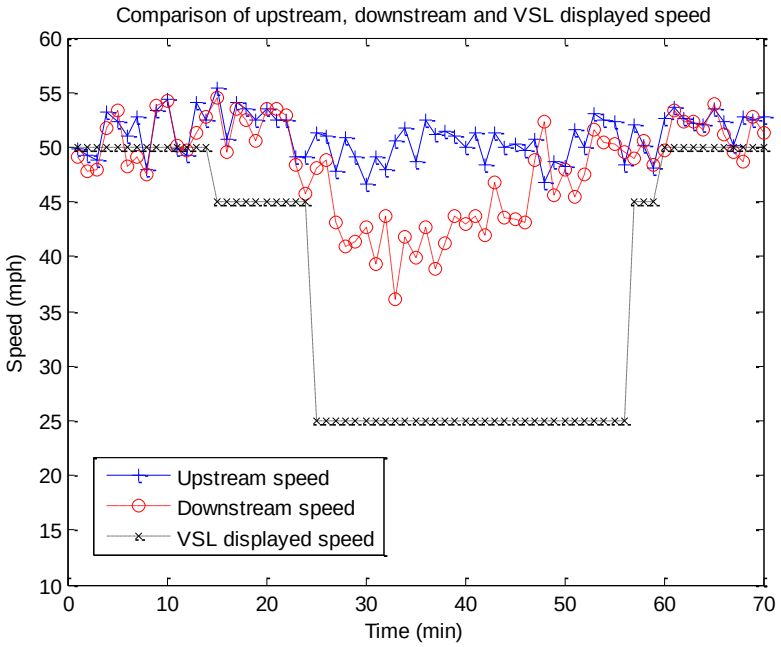

Figure 4.2 Comparisons of the Upstream, Downstream, and VSL Speed

Computing the Compliance Rate

As shown in Figure 4.2, the upstream speed was approximately equal to the posted speed limit (i.e., 50 mph). When the downstream speed was approximately equal to the VSL speed, driver compliance was nearly 100 percent. When the downstream speed was between the upstream speed and the VSL displayed speed, the compliance rate generally laid between 0 and 1.

The methodology to compute the compliance rate is straightforward. Let v_{vsl} denote the speed of compliant drivers (i.e., α friction) and v_u be the speed of those non-compliant drivers. Thus, the downstream speed v_d can be expressed as follows:

$$v_d = (1-\alpha)v_u + \alpha v_{vsl} \tag{4.1}$$

Then, one can approximate the compliance rate as follows:

$$\alpha = \frac{v_d - v_u}{v_{vsl} - v_u} \tag{4.2}$$

Statistical Modeling

Based on the analysis of field data, it seems that the following variables may potentially affect the compliance rate:

- Speed difference between the prevailing speed and the displayed speed;
- VSL displayed speed;
- Upstream speed; and
- Downstream density.

As shown in Figure 4.3, it seems that the upstream speed of the target segment and its downstream density have no obvious effect on the compliance rate and thus have been excluded from further studies.

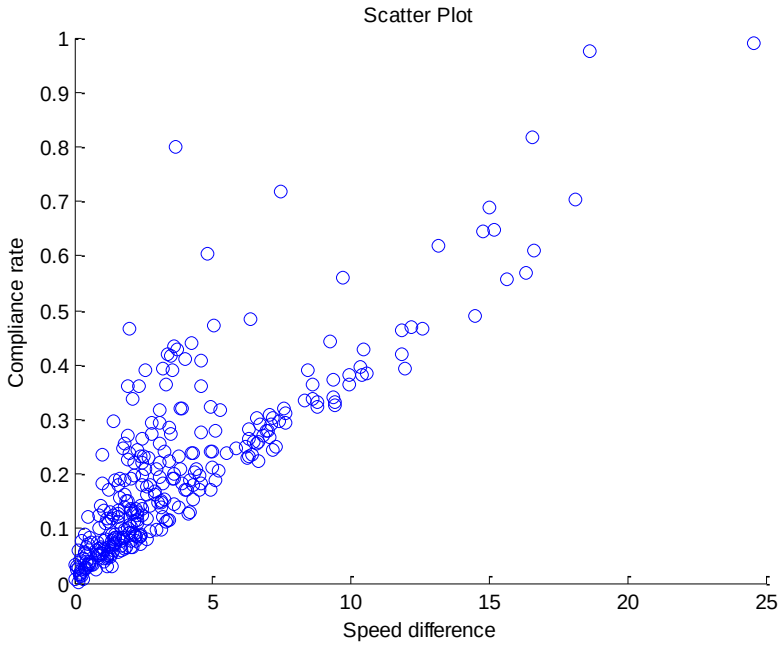

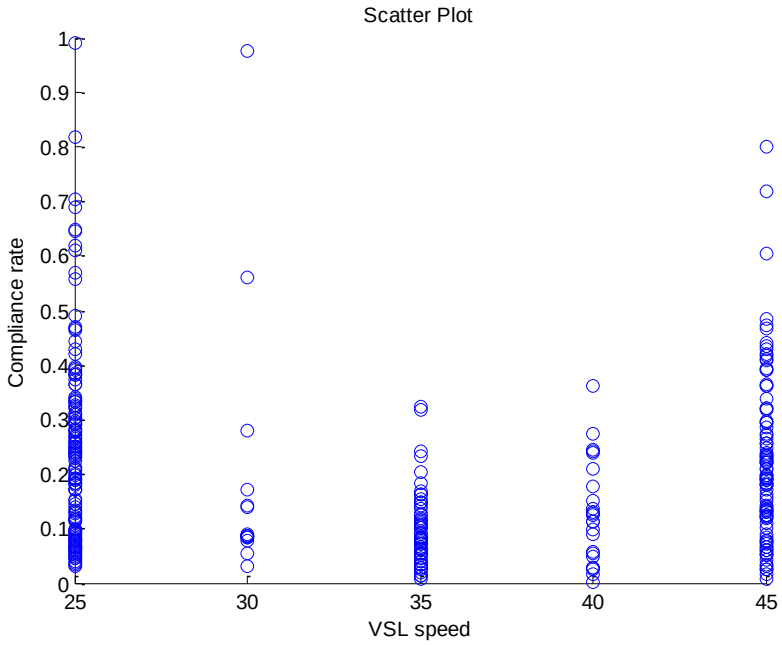

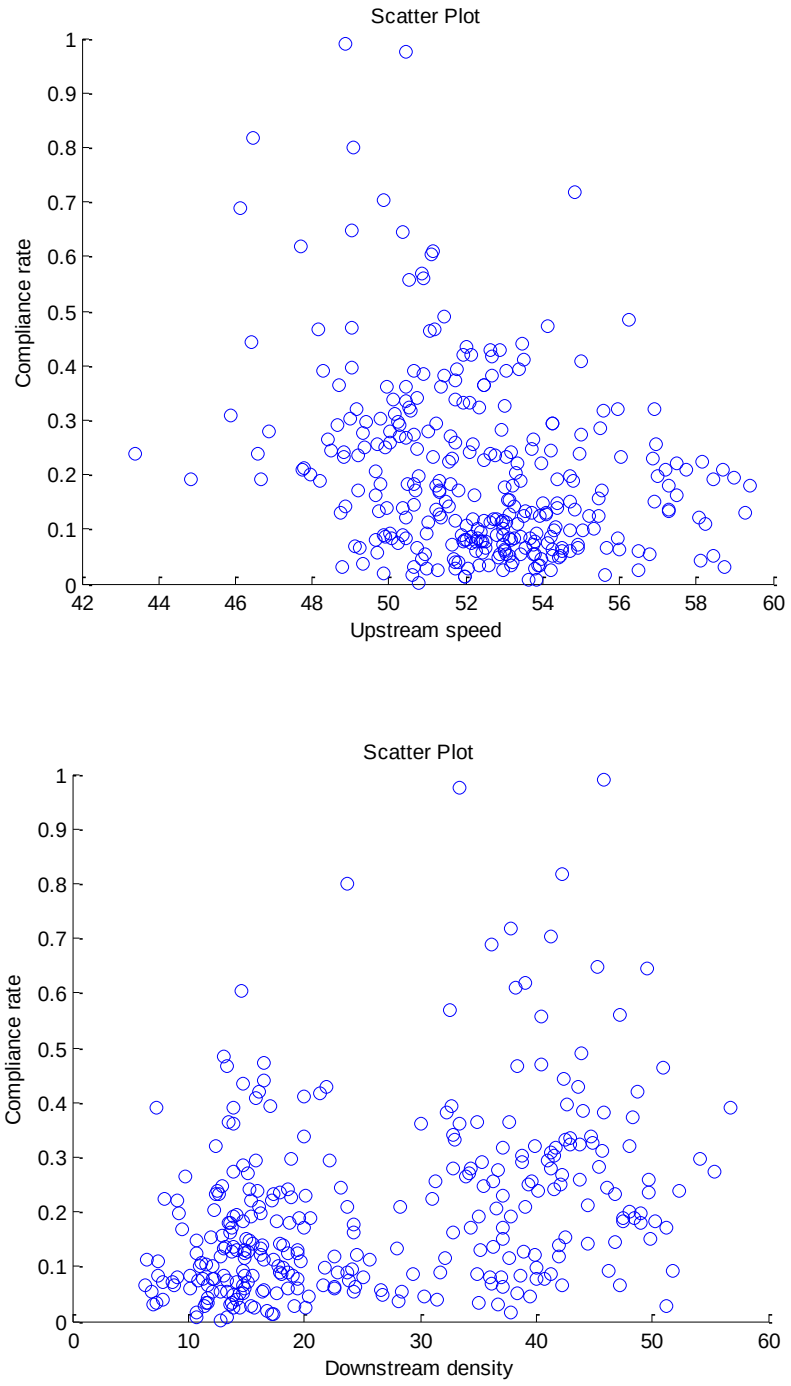

Figure 4.3 Scatter Plot of Potential Independent Variables and Compliance Rate

When applying the speed difference (x_{spd}) as the independent variable, one can express its relation with the compliance rate (CL) as in Eq. (4.3) and Figure 4.4, respectively.

$$\begin{array}{l} CL \quad = 0.064 + \ 0.037 \ x_{spd} \\ (t-value) \quad (8.957) \quad (27.389) \\ R^2 = 0.708 \end{array} \tag{4.3}$$

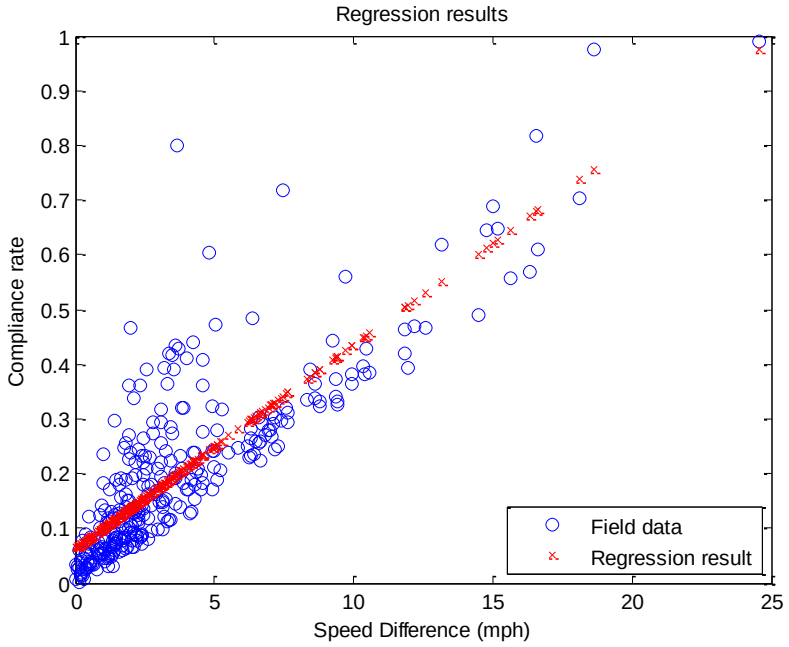

Figure 4.4 Regression Results with Speed Difference as Independent Variable

As shown in Figure 4.4, the compliance rate of drivers seems to increase with the prevailing and displayed speeds. However, the speed difference alone is not sufficient to account for some cases where the speed difference lies within a small range.

Assuming that drivers are reluctant to abide by a lowered speed limit, the compliance rate should be positively related to the displayed speed (x_{vsl}), as shown in Eq. (4.4) and Figure 4.5. Although both variables are significant and the R^2 is improved, the two-slope pattern in scenarios with a small speed difference cannot fully be reflected with Eq. (4.4).

$$\begin{array}{l} CL \quad = -0.240 + \ 0.046 \ x_{spd} + \ 0.008 \ x_{vsl} \\ (t-value) \quad (-11.658) \quad (39.131) \quad (15.31) \\ R^2 = 0.834 \end{array} \tag{4.4}$$

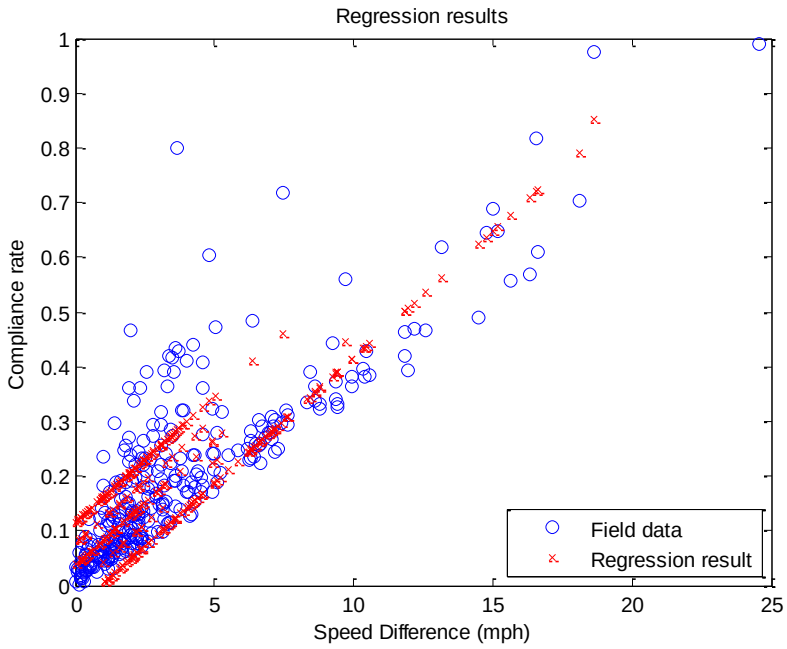

Figure 4.5 Regression Results with Speed Difference and VSL Displayed Speed as Independent Variables

The patterns in the above figure exhibit a nonlinearity when the speed difference is small. This could be solved potentially by introducing the interaction term, $x_{spd} \cdot d_{vsl}$, where x_{spd} denotes the speed difference and d_{vsl} is a dummy variable defined as follows:

$$d_{vsl} = \begin{cases} 1, x_{vsl} \le 40 \\ 0, x_{vsl} > 40 \end{cases} \tag{4.5}$$

The interaction term suggests that the effect of the speed difference on the compliance rate also varies with the displayed speed. The results of the regression model with three variables are shown in Eq. (4.6) and Figure 4.6, respectively.

$$\begin{array}{lcccccc} CL & = & -0.074 + & 0.087 & x_{spd} + & 0.003 & x_{vsl} - & 0.045 & x_{spd} \cdot d_{vsl} \\ (t-value) & & (-3.512) & (26.247) & & (4.665) & & (-12.882) & \end{array} \tag{4.6}$$
$$R^2 = 0.8925$$

where x_{spd} is the difference between the prevailing and displayed speeds in mph, x_{vsl} is the displayed speed in mph, and $d_{vsl} = \begin{cases} 1, x_{vsl} \le 40 \\ 0, x_{vsl} > 40 \end{cases}$.

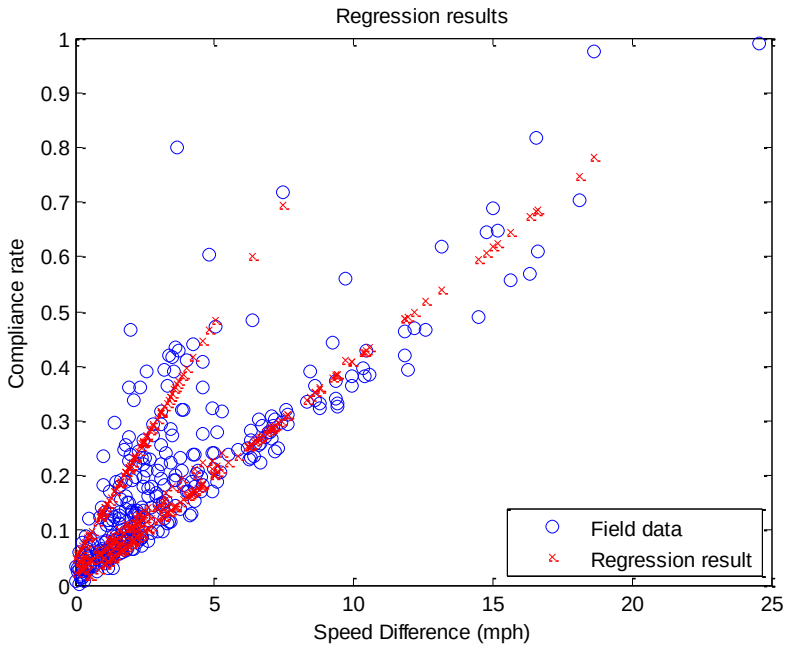

Figure 4.6 Regression Results with Speed Difference, VSL Displayed Speed, and the Interaction Term as Independent Variables

The estimation results suggest that when the displayed speed is higher than 40 mph, the coefficient of the speed difference is 0.087. However, when the displayed speed is reduced to less than or equal to 40 mph, the coefficient is reduced by 0.045 to less than half of its original value.

A refined model is further proposed to account for the obvious structural change, which occurs when the speed difference is about 7.5 mph. For the data points of $x_{spd} < 7.5$, the speed difference, the displayed speed, and the interaction term of the previous two variables are selected as independent variables for developing the prediction model. For those

cases satisfying $x_{spd} \geq 7.5$, only the speed difference and the displayed speed are chosen instead. The final regression results are shown in Eq. (4.7) and Figure 4.7, respectively.

$$\underset{(t-value)}{CL} = \begin{cases} \underset{(-3.517)}{-0.088} + \underset{(27.71)}{0.088} x_{spd} + \underset{(4.587)}{0.003} x_{vsl} - \underset{(-11.26)}{0.043} x_{spd} \cdot d_{vsl}, \; x_{spd} < 7.5; R^2 = 0.816 \\ \underset{(-5.3309)}{-1.0462} + \underset{(17.633)}{0.041} x_{spd} + \underset{(5.230)}{0.041} x_{vsl}, \; x_{spd} \geq 7.5; R^2 = 0.914 \end{cases} \tag{4.7}$$

where x_{spd} is the difference between the prevailing and the displayed speeds in mph, x_{vsl} is the displayed speed in mph, and $d_{vsl} = \begin{cases} 1, x_{vsl} \leq 40 \\ 0, x_{vsl} > 40 \end{cases}$.

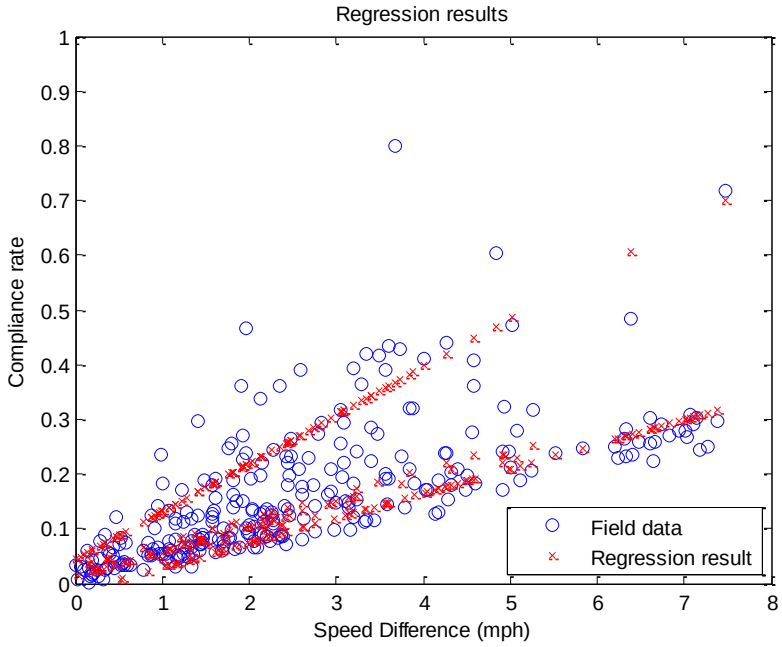

(a) When the Speed Differences are less than 7.5 mph

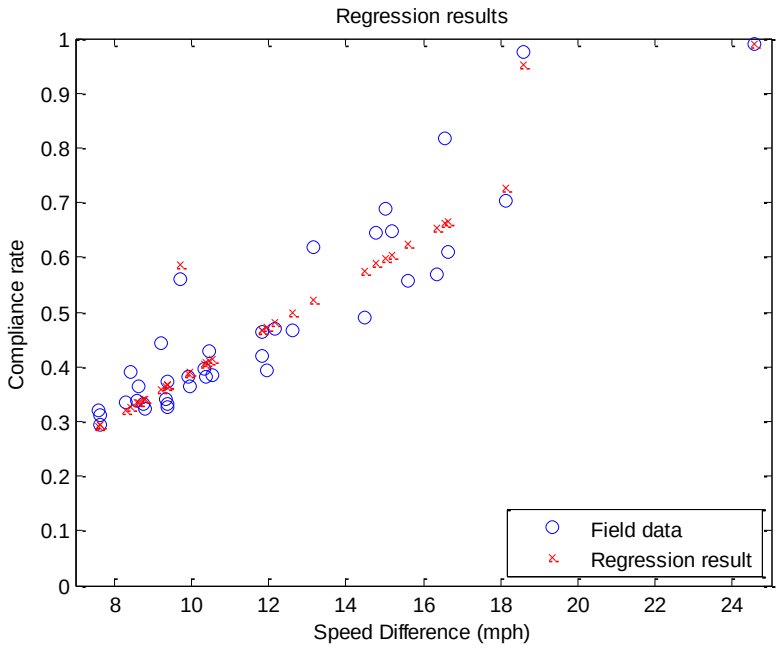

(b) When the Speed Differences are Larger than or Equal to 7.5 mph

Figure 4.7 Final Regression Results

4.3 Mixed Traffic Flow Formulations

Due to the advisory nature of VSL, some drivers in the field study were observed to reduce their speeds in accordance with the displayed speed; but, others chose to continue at their original speeds. As a result, there are actually two types of vehicles constituting the traffic flows: one class that follows the reduced speed and another that stays with the posted speed limit. Thus, the macroscopic traffic flow model developed for the homogeneous condition cannot fully reflect the actual traffic dynamics.

Prediction Model under Heterogeneous Conditions

As in most studies, the second-order macroscopic traffic flow model, METANET (Papageorgiou, 1989), is selected as the base model, where the freeway segment and notations used in this study are shown in Figure 4.8 and Table 4.1, respectively.

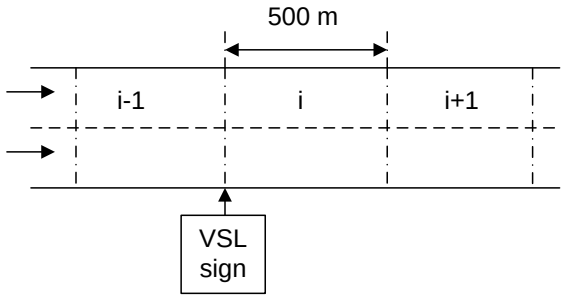

Figure 4.8 Typical freeway sketch with three segments

Table 4.1 Definitions of Variables used in the Mixed Traffic Flow Models

Variables and parameters	Definition
$\rho_{j,i}(k)$ (veh/mi/lane)	The number of class j vehicles per mile per lane for segment i at time step k
$v_{j,i}(k)$ (mph)	The space mean speed of class j vehicles for segment i at time step k
$V_j[]$	The equilibrium speed function of class j vehicles
$q_{j,i,out}(k)$ (veh/h)	The flow rate of class j vehicles leaving segment i to downstream segment i+1 between steps (k, k+1)
$q_{j,i,in}(k)$ (veh/h)	The flow rate of class j vehicles entering segment i from upstream segment i-1 between steps (k, k+1)
$r_{j,i}(k)$ (veh/h)	The flow rate of class j vehicles entering segment i from on-ramps between steps (k, k+1)
$s_{j,i}(k)$ (veh/h)	The flow rate of class j vehicles leaving segment i from off-ramps between steps (k, k+1)
L_i (mi)	The length of segment i
λ_i	The number of lanes of segment i
ΔT (hr)	The length of update time interval
$v_{f,ji}$ (mph)	The free-flow speed of segment i for class j vehicles
$\rho_{cr,ji}$ (veh/mi/lane)	The critical density of segment i for class j vehicles
a_{ji}	The speed exponent term of segment i for class j vehicles
τ_i (hr), γ_i (mi^2/h), and κ_i (veh/mi/lane), β_i	The parameters in the dynamic speed equations of segment i

While the VSL is not activated, the traffic flow dynamics for segment i can be formulated as follow.

$$\rho_i(k+1) = \rho_i(k) + \frac{\Delta T}{L_i \lambda_i}[q_{i,in}(k) - q_{i,out}(k) + r_i(k) - s_i(k)] \tag{4.8}$$

$$q_{i,in}(k) = q_{i-1,out}(k) \tag{4.9}$$

$$V[\rho_i(k)] = v_{f,i} \exp\left[-\frac{1}{a_i}\left(\frac{\rho_i(k)}{\rho_{cr,i}}\right)^{a_i}\right] \tag{4.10}$$

$$\begin{aligned} v_i(k+1) = v_i(k) &+ \frac{\Delta T}{\tau_i}[V(\rho_i(k)) - v_i(k)] \\ &+ \frac{\Delta T}{L_i} v_i(k)[v_{i-1}(k) - v_i(k)] - \frac{\gamma_i \Delta T}{\tau_i L_i} \frac{[\rho_{i+1}(k) - \rho_i(k)]}{\rho_i(k) + \kappa_i} \end{aligned} \tag{4.11}$$

$$q_{i,out}(k) = \lambda_i \rho_i(k) v_i(k) \tag{4.12}$$

The dynamic speed is computed based on the static speed-density relationship, the convection from upstream, and the anticipation of drivers to the downstream condition. METANET has been widely used to model the freeway traffic evolution during the past several decades.

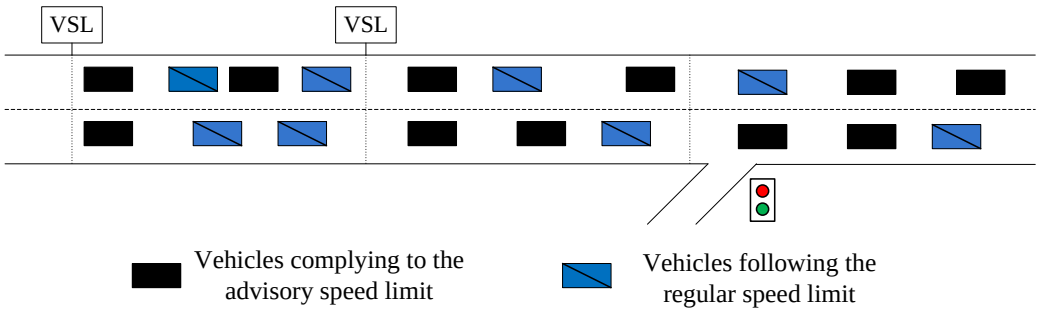

Figure 4.9 Vehicles with Different Speeds and Same Length

To account for two possible vehicle classes during the VSL operational period, one can restructure METANET as follows for the segment without VSL messages, where subscripts 2 and 1 represent those vehicles that will and will not follow VSL messages.

$$\rho_{j,i}(k+1) = \rho_{j,i}(k) + \frac{\Delta T}{L_i \lambda_i}[q_{j,i,in}(k) - q_{j,i,out}(k) + r_{j,i}(k) - s_{j,i}(k)] \text{ , j= 1, 2} \quad (4.13)$$

$$q_{j,i,in}(k) = q_{j,i-1,out}(k) \quad (4.14)$$

$$V_{j,i}(k) = V_j\left[\rho_{1,i}(k), \rho_{2,i}(k)\right] = v_{f,ji} \exp\left[-\frac{1}{a_{ji}}\left(\frac{\rho_{1,i}(k) + \rho_{2,i}(k)}{\rho_{cr,ji}}\right)^{a_{ji}}\right] \text{ , j= 1, 2} \quad (4.15)$$

$$\begin{aligned} v_{1,i}(k+1) = {} & v_{1,i}(k) + \frac{\Delta T}{\tau_i}[V_{1,i}(k) - v_{1,i}(k)] + \frac{\Delta T}{L_i} v_{1,i}(k)[v_{1,i-1}(k) - v_{1,i}(k)] \\ & - \frac{\gamma_i \Delta T}{\tau_i L_i} \frac{[\rho_{1,i+1}(k) + \rho_{2,i+1}(k) - \rho_{1,i}(k) - \rho_{2,i}(k)]}{\left[\rho_{1,i}(k) + \rho_{2,i}(k) + \kappa_i\right]} - \frac{\beta_i \Delta T}{\tau_i}\left[V_{1,i}(k) - V_{2,i}(k)\right] \end{aligned} \quad (4.16)$$

$$\begin{aligned} v_{2,i}(k+1) = {} & v_{2,i}(k) + \frac{\Delta T}{\tau_i}[V_{2,i}(k) - v_{2,i}(k)] + \frac{\Delta T}{L_i} v_{2,i}(k)[v_{2,i-1}(k) - v_{2,i}(k)] \\ & - \frac{\gamma_i \Delta T}{\tau_i L_i} \frac{[\rho_{1,i+1}(k) + \rho_{2,i+1}(k) - \rho_{1,i}(k) - \rho_{2,i}(k)]}{\left[\rho_{1,i}(k) + \rho_{2,i}(k) + \kappa_i\right]} \end{aligned} \quad (4.17)$$

$$q_{j,i,out}(k) = \lambda_i \rho_{j,i}(k) v_{j,i}(k) \text{ , j= 1, 2} \quad (4.18)$$

The speed of those vehicles "not following VSL," affected by the vehicles "following VSL," is formulated in Eq. (4.16), where such impacts, captured with the parameter β, may vary with the speed difference between these two classes of vehicles. Eq. (4.17) suggests that the vehicles "following VSL" are not affected by the vehicles "not following VSL." Noticeably,

the value of parameter β has a significant impact on the final output and deserves a rigorous experimental analysis.

On the segment with VSL, one can restructure Eq. (4.14) as follows to reflect the presence of two different driver types:

$$q_{1,i,in}(k) = (1-\alpha_i)\left[q_{1,i-1,out}(k) + q_{2,i-1,out}(k)\right] \tag{4.19}$$

$$q_{2,i,in}(k) = \alpha_i\left[q_{1,i-1,out}(k) + q_{2,i-1,out}(k)\right] \tag{4.20}$$

Effects of VSL-complying Vehicles

This sub-section presents the impacts of VSL-complying vehicles (parameter β) under different traffic conditions with simulation experiments using the same network of MD-100 WB (see Figure 4.1).

As shown in Table 4.2, the speed limit on the segment in the simulation experiment between Detector 503 and Detector 504 is reduced from 50 mph to 45, 40, 35, 30 and 25 mph, respectively. For each traffic scenario, the corresponding compliance rate is assumed to be 0, 0.1, 0.2, …, 0.9, and 1. For each combination of speed limit and compliance rate, the experimental analyses were conducted for three hours over 10 replications.

Table 4.2 Experimental Designs for Determining the Impact of VSL-complying Vehicles

Design Variables		
Name	Speed limit	Compliance rate
Lower bound	25 mph	0
Upper bound	50 mph	1
Incremental interval	5 mph	0.1
Experimental Duration	3 hours	
Number of Replications	10	
Total Time	1980 hours	

The experimental analysis is intended to investigate the following two key issues: under what kind of situations will VSL-complying vehicles indeed have a negative effect on non-complying vehicles, and how can one quantify such impacts, if they exist, with different traffic variables.

Note that if the impact due to VSL-complying vehicles is insignificant, the speed generated from the simulation with mixed traffic, denoted as "actual speed" hereafter, should be equal to or very close to the weighted average of the resulting speeds from two separate simulations with only one type of vehicle (alpha=0 and alpha=1), denoted as "expected speed" hereafter. Here, the range of 5 mph is used to define the indifference zone. For example, as shown in Figure 4.10, the value of β is zero when the displayed speed is 35 mph and the compliance rate is 0.8.

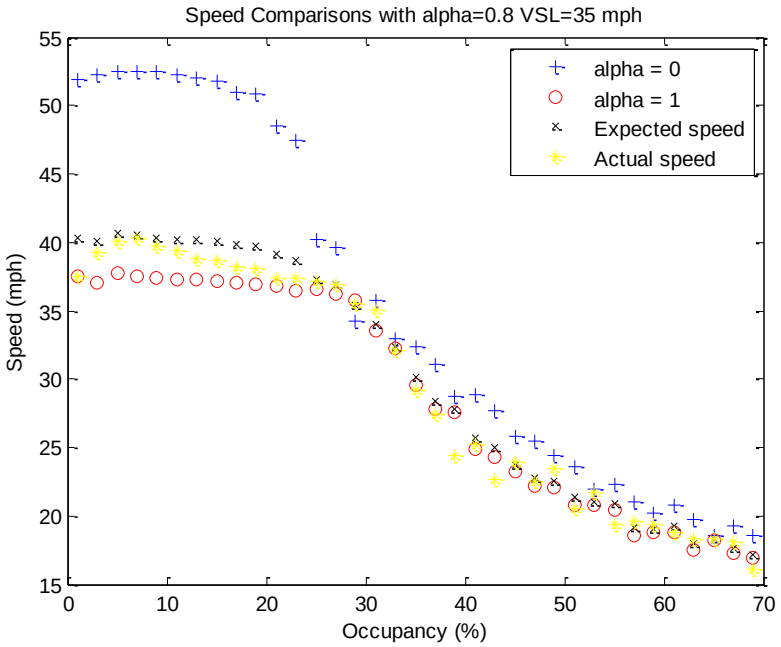

Figure 4.10 Simulation Results where the Effect of a VSL-complying Vehicle is not Substantial

However, the experimental results shown in Figure 4.11 are inconsistent with the presumption. At least, when the occupancy is between 10 percent and 25 percent, the actual speed $v_a(o)$ (yellow asterisk) is much lower than the expected speed $v_e(o)$ (black cross) computed with Eq. (4.21).

$$v_e(o) = (1-\alpha)v_1(o) + \alpha v_2(o) \tag{4.21}$$

where α is the compliance rate, o is the occupancy, $v_1(o)$ and $v_2(o)$ is the average speed when the speed limit is the normal posted speed limit (corresponding to alpha=0) and displayed VSL (corresponding to alpha=1), respectively. It suggests that under these conditions, the movements of those non-complying vehicles are somehow blocked by VSL-complying vehicles.

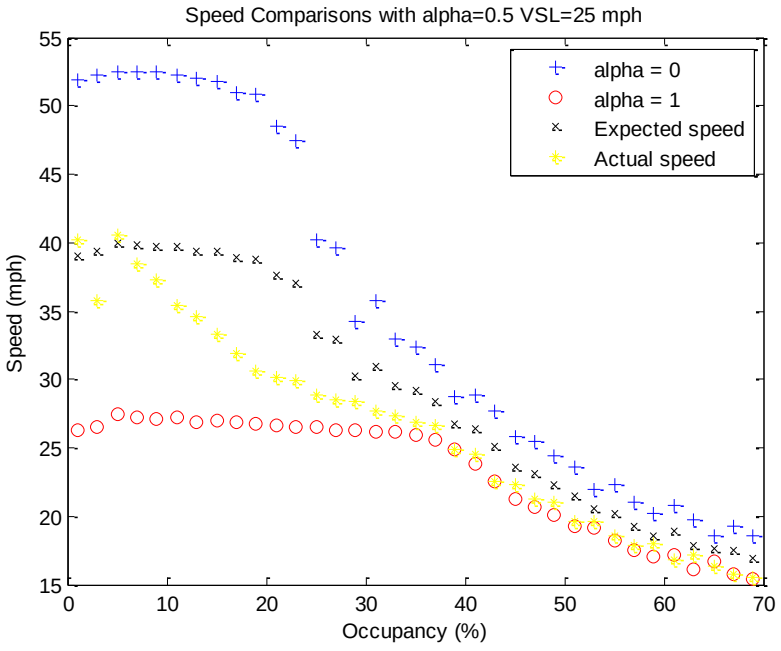

Figure 4.11 Simulation Results where the Effect of a VSL-complying Vehicle is Substantial

The impact of VSL-complying vehicles under different combinations of displayed speed and compliance rate could also be shown directly in these figures, representing the relationship between the expected and actual average speeds such as Figures 4.12 (a) and (b).

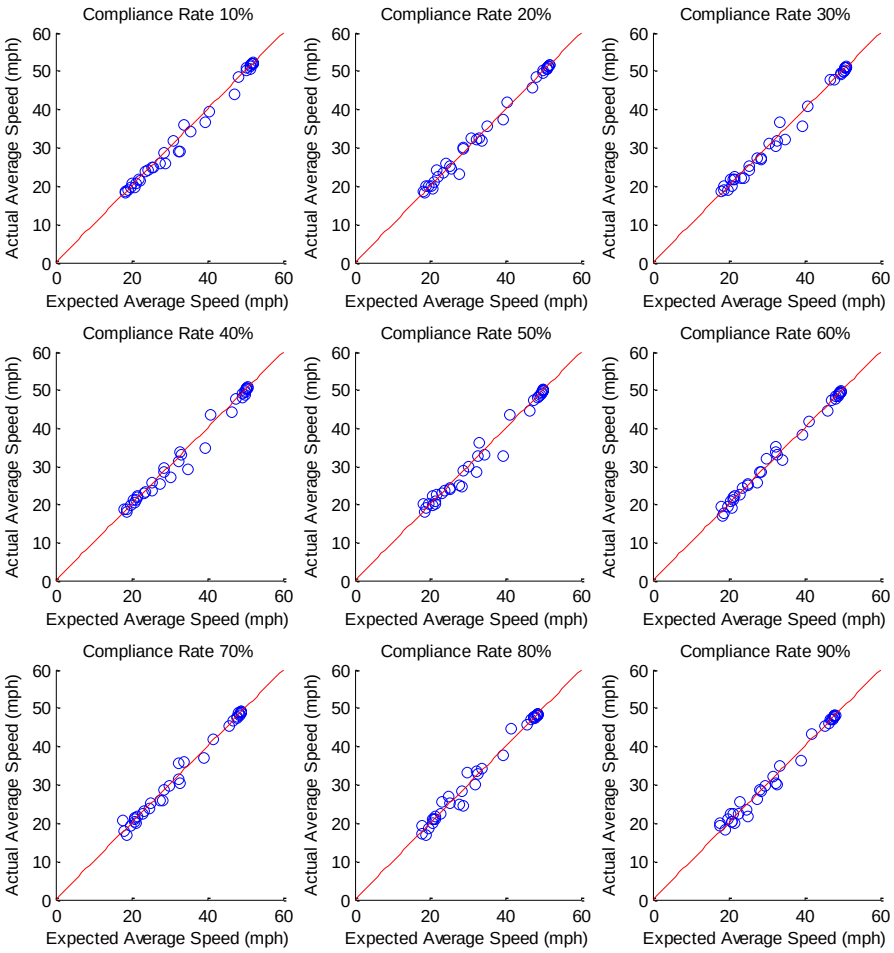

(a) Reduced Speed = 45 mph

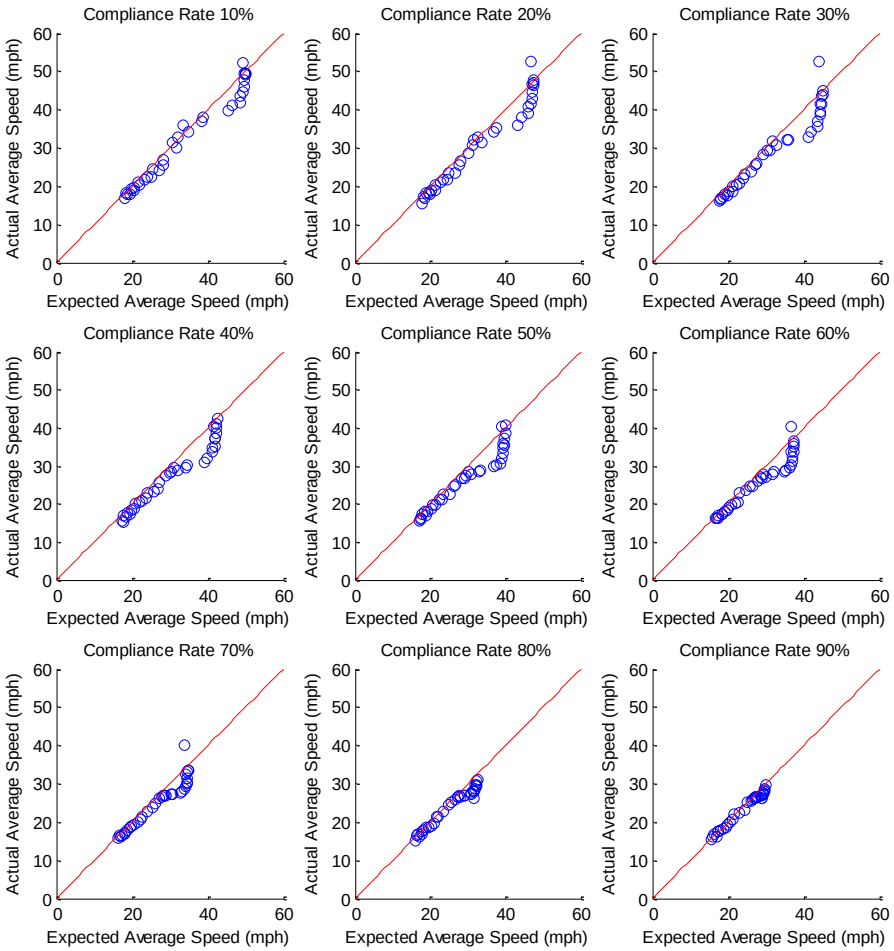

(b) Reduced Speed = 25 mph

Figure 4.12 The Comparison of Expected and Actual Average Speeds

Figures 4.12 (a) suggests that there exists no obvious difference between the expected and actual average speeds when the displayed speeds are 45 mph. However, while the displayed speeds are 25 mph, as shown in Figures 4.12 (b), the actual speed is significantly lower than the expected speed in some cases.

For those cases where the effect of a VSL-complying vehicle does exist, the actual average speed can be shown with the following equation:

$$v_a(o) = (1-\alpha)\left[v_1(o) - \beta\left[v_1(o) - v_2(o)\right]\right] + \alpha v_2(o) \tag{4.22}$$

By incorporating Eq. (4.21) into Eq. (4.22), one can rewrite the equation as follows:

$$\beta = \frac{v_e(o) - v_a(o)}{(1-\alpha)\left[v_1(o) - v_2(o)\right]} \tag{4.23}$$

The values of β for those cases with the speed limits of 30 mph and 25 mph are drawn in Figures 4.13 (a) and (b), respectively. As shown in Figure 4.13 (a), for those cases displaying 30 mph on the VSL, the impact only exists when the occupancy lies approximately between 17 percent and 23 percent, and the compliance rate is between 0.3 and 0.5. The computed β values range from 0.4 to 0.6, increasing with the occupancy and the compliance rate. Any values lower or higher than the above range will result in indifference between the expected and actual average speeds. Similarly, as shown in Figure 4.13 (b), for those cases displaying 25 mph as the VSL, the impact exists only when the occupancy lies approximately between 13 percent and 23 percent, and the compliance rate is between 0.1 and 0.7. The resulting β value ranges from 0.2 to 0.8, which also increases with the occupancy and the compliance rate.

The interval of the compliance rate is set as 0.1 in the experiment. For any compliance rate within that interval observed in the field study, the corresponding β value can be computed by taking interpolation between the nearest two compliance rates. For those cases where the differences are smaller than the defined indifference threshold (i.e., 5 mph), the value of β will be set to zero.

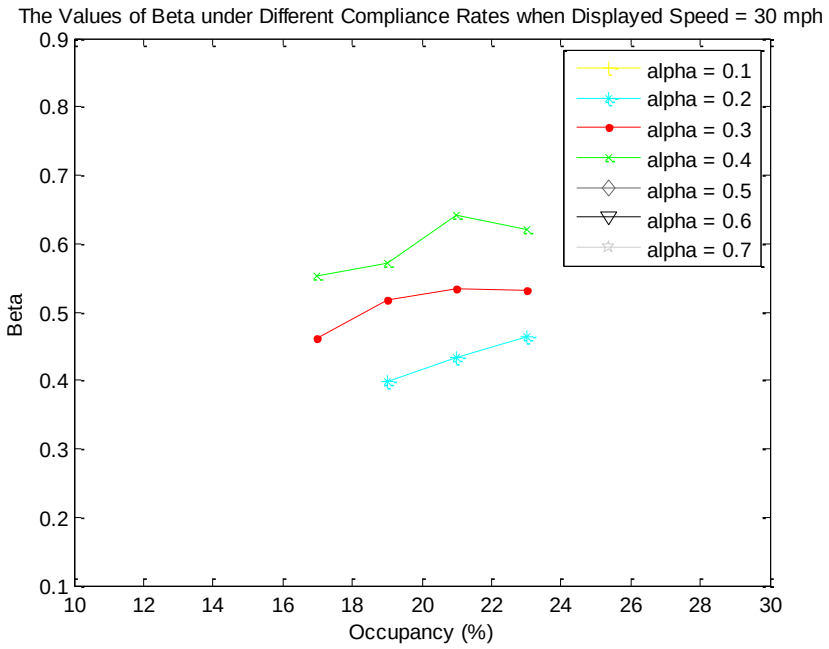

(a) Reduced Speed = 30 mph

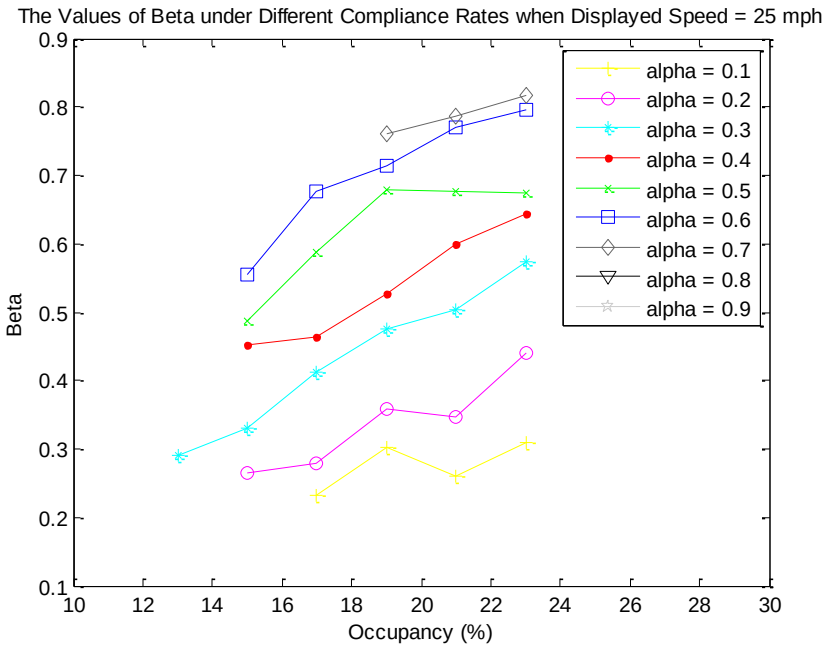

(b) Reduced Speed = 25 mph

Figure 4.13 The Magnitude of the Effect of VSL-complying Vehicles

4.4 Real-time Parameter Update

Note that after rigorously modeling the effect of VSL-complying vehicles and calibrating other key parameters, it is likely that traffic conditions within the congested area are evolving to the breakdown state, and such a complex state transition may not be fully captured with the set of pre-calibrated parameters, especially under certain abnormal conditions (i.e., incident, inclement weather, etc.). Hence, this study proposed the activation of an extended Kalman filter (EKF) to perform the real-time parameter update for all key traffic model parameters.

The general model equation of EKF has been stated as follows:

$$\mathbf{y}(k) = f\left[\mathbf{y}(k-1), \boldsymbol{\xi}(k)\right] \tag{4.24}$$

where f includes the traffic flow model that can be expressed with Eq. 4.10-4.17.

$\mathbf{y} = [\mathbf{x}^T, \mathbf{d}^T, \mathbf{p}^T]^T$ is the state vector, where:

- $\mathbf{x} = [\rho_2, v_2, \rho_3, v_3, ..., \rho_{M-2}, v_{M-2}, \rho_{M-1}, v_{M-1}]^T$, i.e., the density and speed from the second to the second last segments (The first and last segments are regarded as boundaries), respectively; M is the number of segments;
- $\mathbf{d} = [q_1, v_1, \rho_M, ..., r_{on}, ..., ..., s_{off}, ...]^T$, i.e., the upstream flow rate and speed, the downstream density, and all on-ramp and off-ramp flow rates;
- $\mathbf{p} = [v_f, \rho_{cr}, a]^T$, i.e., the free-flow speed, the critical density, and the speed exponent term.

The observation equation is set as follows:

$$\mathbf{z}(k) = h\left[\mathbf{y}(k-1), \boldsymbol{\eta}(k)\right]$$

$$= \begin{bmatrix} q_1(k) \\ v_1(k) \\ \vdots \\ \lambda_d \rho_d(k) v_d(k) \\ v_d(k) \\ \vdots \\ \rho_M(k) g(k) \\ \vdots \\ r_{on}(k) \\ \vdots \\ \vdots \\ s_{off}(k) \\ \vdots \end{bmatrix} + \begin{bmatrix} \eta_1^q(k) \\ \eta_1^v(k) \\ \vdots \\ \eta_d^q(k) \\ \eta_d^v(k) \\ \vdots \\ \eta_M^o(k) \\ \vdots \\ \eta_{on}^r(k) \\ \vdots \\ \vdots \\ \eta_{off}^s(k) \\ \vdots \end{bmatrix} \tag{4.25}$$

where

- $\mathbf{z}(k)$ includes the measured flow rate and the speed at the most upstream and all intermediate detectors; the occupancy measured at the downstream segment; and the measured on-ramp and off-ramp flow rate;
- d denotes the segment where the detector locates;
- M denotes the downstream segment;
- on and off denote the segment where the on-ramp and off-ramp locates, respectively;
- g denotes the conversion factor between occupancy and density;
- $\boldsymbol{\xi}(k)$ and $\boldsymbol{\eta}(k)$ denote the model uncertainty and the measurement noise with zero mean and covariance matrix, $\mathbf{Q}(k)$ and $\mathbf{R}(k)$, respectively;
- $\mathbf{A}$ and $\mathbf{H}$ are the Jacobian matrix of first-order partial derivatives of the function f and h with respect to y, where

$$\mathbf{A}_{ij} = \frac{\partial f_i}{\partial y_j}\left[\mathbf{y}(k-1), 0\right] \tag{4.26}$$

$$\mathbf{H}_{ij} = \frac{\partial h_i}{\partial y_j}\left[\mathbf{y}(k-1), 0\right] \tag{4.27}$$

The core steps for the extended Kalman filter are summarized below:

Step 1: Project the state ahead

$$\hat{\mathbf{y}}(k) = f\left[\mathbf{y}(k-1), 0\right] \tag{4.28}$$

Step 2: Project the error covariance ahead

$$\hat{\mathbf{P}}(k) = \mathbf{A}_{\mathbf{y}(k-1)}\mathbf{P}(k-1)\mathbf{A}^T_{\mathbf{y}(k-1)} + \mathbf{Q}(k-1) \tag{4.29}$$

Step 3: Calculate the Kalman gain

$$\mathbf{K}(k) = \hat{\mathbf{P}}(k)\mathbf{H}^T_{\hat{\mathbf{y}}(k)}\left[\mathbf{H}_{\hat{\mathbf{y}}(k)}\hat{\mathbf{P}}(k)\mathbf{H}^T_{\hat{\mathbf{y}}(k)} + \mathbf{R}(k)\right]^{-1} \tag{4.30}$$

Step 4: Correct the state based on real-time measurement

$$\mathbf{y}(k) = \hat{\mathbf{y}}(k) + \mathbf{K}(k)\left[\mathbf{z}(k) - h\left[\hat{\mathbf{y}}(k), 0\right]\right] \tag{4.31}$$

Step 5: Correct the error-covariance

$$\mathbf{P}(k) = \left[\mathbf{I} - \mathbf{K}(k)\mathbf{H}_{\hat{\mathbf{y}}(k)}\right]\hat{\mathbf{P}}(k) \tag{4.32}$$

Based on the detector input with 1 minute interval, the parameter of the traffic flow model can be updated to achieve more accurate prediction results.

4.5 Closure

This chapter presents the prediction function using the model developed for mixed traffic. The proposed mixed traffic flow model is capable of representing the traffic dynamics when only part of the driving population follows the displayed speed reduction. The compliance rate is found to be a function of several important traffic variables (i.e., the difference between the prevailing speed and the displayed speed, and the displayed speed), from the analysis of field data. The proposed model is calibrated under the assumption that drivers can be categorized into two groups: following the posted speed limit or the reduced speed limit. In the dynamic speed equation, non-complying vehicles are likely to be affected by those vehicles following the reduced speed limit under certain circumstances. These circumstances and the magnitude of such impacts have been quantified with carefully calibrated simulation experiments. An EKF has also been developed to update model parameters to facilitate the real-time applications.

Chapter 5: Integrated Freeway Control System

5.1 Introduction

Grounded on the developed traffic flow model, this chapter introduces an integrated freeway control system, utilizing both ramp metering and variable speed limits to tackle recurrent congestion. The proposed system is capable of selecting the activation time for each available control strategy based on predicted traffic conditions, and can determine the number of VSLs needed for speed control so as to ensure that the flow rate at the bottleneck segment will not exceed its capacity. The integrated local system can also activate the ramp metering in a timely manner to support the VSL operations within the control segment. This operationally efficient control strategy is described in Section 5.3. To better its effectiveness under various congestion scenarios, the system has the flexibility to select different control objectives, as described in Section 5.4, based on the detected traffic patterns. Section 5.5 presents the integrated corridor control system, which can distribute a target level of volume reduction to multiple on-ramps, when the local bottleneck control alone is not sufficient to prevent traffic from breakdown.

5.2 Dynamic Monitoring Function

As is well recognized, traffic flows at highway bottlenecks often evolve from the unstable state to the breakdown or jam condition within a short time frame. This is likely due to the complex weaving interactions between on-ramp vehicles, off-ramp flows, and mainline traffic.

To contend with congested shockwaves propagated from the bottleneck segment during peak periods, one can certainly apply existing operational strategies, such as ramp

metering and variable speed control. However, due to the capacity difference between the bottleneck and its upstream roadway segments, there are challenges associated with determining when to activate the available control strategies since executing excessive control may result in underuse of available roadway capacity. Hence, development of a robust mechanism to predict the onset of traffic breakdown in the bottleneck highway segment is one essential task.

To do so, any control system shall have an effective prediction module to offer the following key functions: (1) realistically reflect the evolution of traffic flows at the bottleneck and its connected highway segments; (2) effectively capture the transition of traffic conditions from unstable to breakdown states; and (3) efficiently predict the onset of traffic breakdown in advance for the control center to take actions in time. Unfortunately, most existing traffic control systems have not been designed to have the above functions. Hence, this study focused on exploring the potential of integrating the proposed macroscopic model with a dynamic monitoring module to determine the activation time of each available control strategy.

To best reflect the time-varying traffic conditions, especially during the transition state, this study has further incorporated the extended Kalman filtering mechanism in the prediction module to dynamically update the model parameters, based on the available real-time data. The remaining section is organized as follows: definitions of "traffic states" and the monitoring module are presented in the next section, followed by the illustration of the breakdown prediction algorithm.

Clustering of Traffic States

Classification of traffic states for use in the monitoring module is based on the studies of Schönhof and Helbing (2007), which includes: stable free-flow, meta-stable free-

flow, unstable, meta-stable congestion and stable congestion. Basically, no congestion may occur in the first two states, but the meta-stable free-flow state is likely to evolve to the unstable state which is regarded as moving toward the breakdown condition. In general, it is not common that the unstable state will be skipped when the transition takes place. Meta-stable congestion and stable congestion are the two states where traffic breakdown occurs.

Instead of choosing the thresholds between each state arbitrarily, this study has adopted the following k-means clustering (Wagstaff et al., 2001) to identify such key parameters (see Table 5.1), and apply field data to illustrate such a calibration process.

Table 5.1 Constrained K-means Algorithm

Constrained K-means (Data set $d_i = (q_i, o_i, v_i) \in D$, must-line constraints $M(d_i, d_j)$, cannot-link constraints $N(d_i, d_j)$)

1. Pick the initial cluster center, C_j (j=1:5), to represent the five traffic states.

2. For each d_i:

   If $M(d_i, d_j) = 1$ for any d_j in cluster j,

      Assign d_i to cluster j.

   Else,

      Assign d_i to cluster j which has the minimum distance between d_i and its center C_j,

      and satisfies $N(d_i, d_j) = 0$ for every d_j in cluster j.

3. Calculate the new cluster center, C_j, by averaging all d_j currently assigned to cluster j.

4. Repeat Steps 2 & 3 until the cluster center converges.

The occupancy value, which lies in the middle of each region in Figure 5.1a, refers to the occupancy of the initial cluster center. Then, the averaged flow rate and speed of each d_i within the region is used as the first and third components of the center, respectively.

Figure 5.1b shows the clustering results using the k-means algorithm. Note that when comparing these results with those based only on occupancy (Figure 5.1a), the advantage of the former lies in its capability of concurrently considering flow rate, speed, and density in the clustering process.

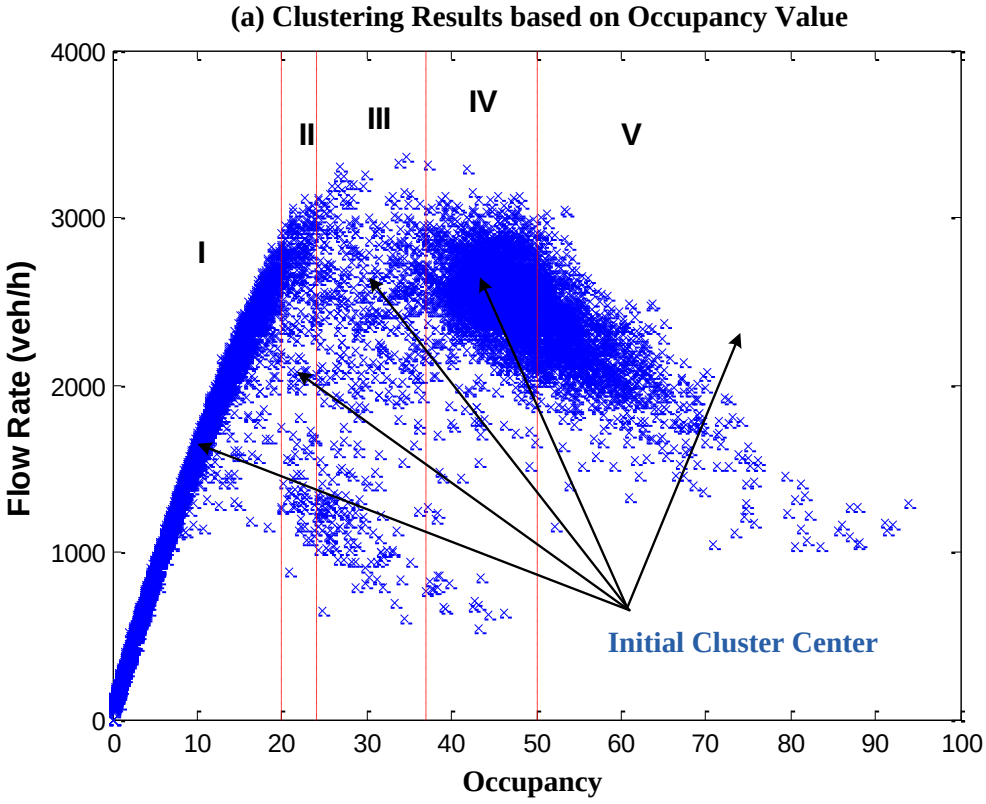

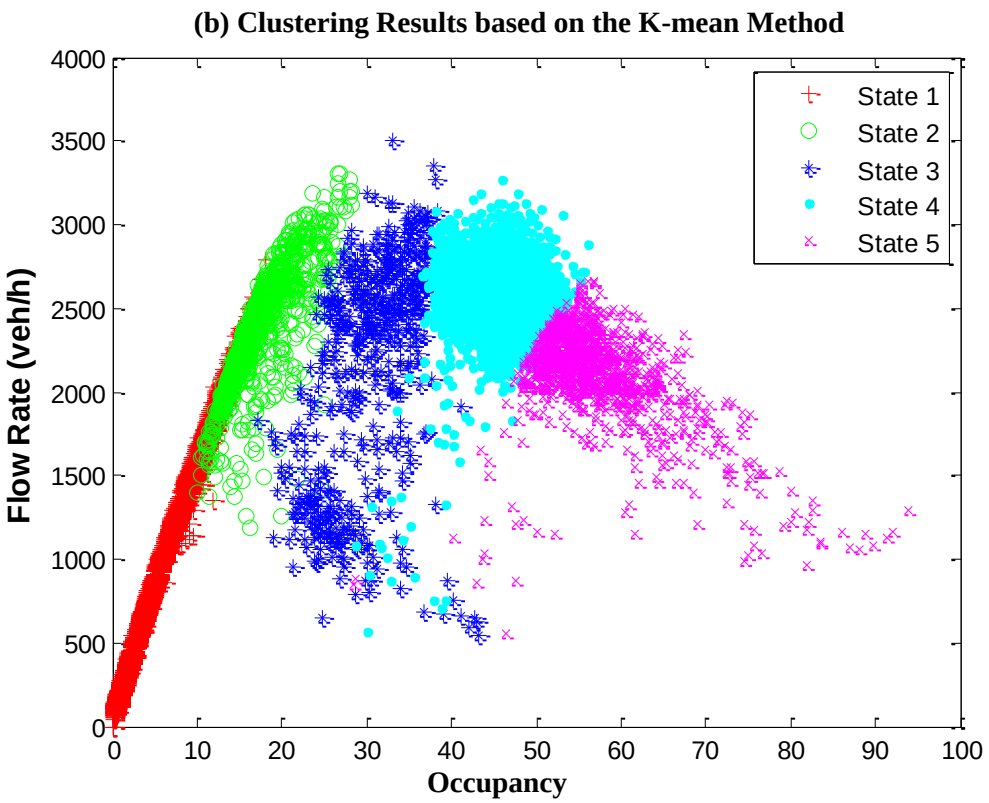

Figure 5.1 Clustering Results

The monitoring function is implemented at every minute when the new detector data becomes available.

Algorithm to Predict Traffic Breakdown

The actual breakdown time is defined as the time point during which the speed drops below 25 mph for over five minutes. The prediction algorithm will be implemented over every minute when any new traffic data becomes available, and the predicted time horizon is 10 minutes ahead of real-time operations. Hence, when the prediction model indicates that the traffic breakdown will occur in the next five minutes, one can have sufficient operation time to activate the proper control strategies. The key steps for executing the prediction algorithm are shown in Table 5.2, and also illustrated in Figure 5.2. The predicted traffic state of time

T_2, which is predicted at time T_1, is denoted as $State(T_1, T_2)$, and the variable Flag is defined to indicate whether or not to activate the control.

Table 5.2 Algorithm to Predict Traffic Breakdown

1. At time T, predict the traffic volume, occupancy, and speed for time T+1, T+2, …, T+9, and T+10.
2. Cluster each predicted data point into one of the five traffic states whose center has the minimum distance to that point. Those predicted states for the next 10 minutes are denoted as: $State(T, T+1)$, $State(T, T+2)$,…, $State(T, T+9)$, and $State(T, T+10)$.
3. If $State(T, T+4) = State\,1$ or $State\,2$,
   Set Flag = -1;
   Elseif $State(T, T+4) = State\,3$,
   Set Flag = 0;
   Else,
   Set Flag = 1.
4. For each $State(t, T+5), where\ t = T-5 : T$
   If $State(t, T+5) = State\,4$ or $State\,5$,
   Flag = Flag+1.
5. If Flag>=3 or $State(T, T+5) = State\,5$,
   Activate the control.
   Else,
   Go the Step 6.
6. Return to Step 1 when clock turns to T+1.

For instance, as shown in Step 3 above, at time T, the state, predicted for four minutes ahead, $State(T, T+4)$, is used to initialize the Flag variable, which is given a larger value to account for the congested condition. At time T, there are a total of six predicted

states for time T+5, which are predicted at times $T-5, T-4, ..., T-1, and\ T$, respectively. If any of these predictions indicates congestion, then the Flag value will be increased by one. The control will be activated if at least half of the predictions (three out of six times) for one time suggest that the traffic condition may evolve toward breakdown, or if the five-minutes-ahead prediction from the current time interval indicates the presence of severe congestion.

For example, as shown in Figure 5.2, the model at 7:05 AM will perform the state prediction for the time period from 7:06 AM till 7:15 AM. And the predicted state at 7:09 AM is used to initialize the Flag. The traffic states of 7:10 AM predicted subsequently by the model at the time from 7:00 AM to 7:05 AM, which are covered by the left vertical dashed line in the figure, are then adopted to change the Flag value. If the condition in Step 5 is satisfied, the control will be activated; otherwise, the time clock is advanced to 7:06 AM.

Note that a safety margin of five minutes is set between the time to activate control strategies and the predicted breakdown time. Thus, even if the predicted breakdown time is two minutes later than its actual onset time, the traffic operation center still has three minutes of advanced notice to take necessary actions.

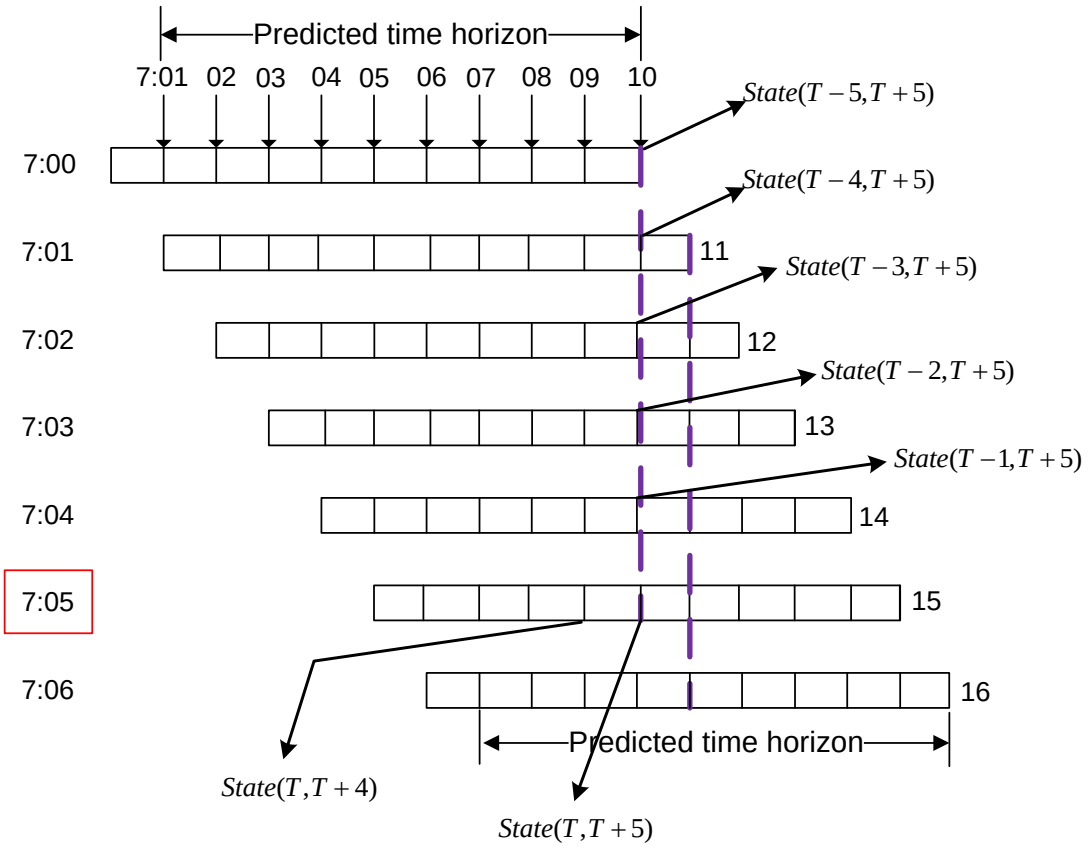

Figure 5.2 Example Illustrating the Breakdown Prediction Algorithm

5.3 Operationally Efficient Local Control Strategies

This section presents the integrated local control strategy, comprising metering control for one on-ramp and variable speed limit control, which could be implemented directly in the field if the optimization model is not available. To facilitate this presentation, the notations used hereafter are summarized below:

Table 5.3 Notations used in the Integrated Local Control

Variables	Explanations
Index Variables	
Δt	Time step for updating traffic conditions (10 s)
n_1	Number of Δt in one VSL control interval (n_1=6)
n_2	Number of Δt in one ramp metering control interval (n_2=3)
n_p	Number of Δt in one prediction horizon (n_p=30)
$t_v = n_1 \Delta t$	Length of one VSL control interval (1 min)
$t_r = n_2 \Delta t$	Length of one ramp metering control interval (30s)
$t_p = n_p \Delta t$	Length of one prediction interval (5 min)
k	Time step index of traffic flow models, where k th interval $= k\Delta t$
k_v	Time step index of VSL control, where k_v th interval $= k_v t_v$
k_r	Time step index of ramp metering control, where k_r th interval $= k_r t_r$
i	Index of freeway segments
b	Index of the bottleneck
d	Index of the most downstream segment in the VSL control area
N	Number of segments in the network
M	A very big number used for penalty purpose
Traffic Flow Variables	
L_i	Length of segment i (mi)
λ_i	Number of lanes on segment i
$\rho_i(k)$	Density of segment i at time step k (veh/mi/ln)
$v_i(k)$	Speed of segment i at time step k (mi/h)
$q_i(k)$	Flow rate out of segment i at time step k (veh/h)
$v_{f,i}(k)$	Free-flow speed limit of segment i at time step k (mph)
$\rho_{c,i}$	Critical density of segment i (veh/mi/ln)
$a_i, \tau_i, u_i, \kappa_i$	Parameters in traffic flow models for segment i
$d(k)$	On-ramp demand at time step k (veh/h)
$r(k)$	On-ramp flow rate at time step k (veh/h)
Control Variables	
$R(k)$	Ramp metering rate at time step k (veh/h)
$w(k)$	On-ramp queue length at time step k (veh)
C_r	On-ramp capacity (veh/h)
$w_{\max}$	Maximum allowed queue length at the on-ramp
$R_q(k)$	Ramp metering rate resulting in the maximum allowed queue at time step k (veh/h)
$\Delta Q_R^j(k_v)$	Flow rate reduction distributed to on-ramps when the j th VSL is activated at the k_v th VSL control interval (veh/h)

$R^j(k)$	Ramp metering rate at time step k when the j th VSL is activated (veh/h)
$V_i(k)$	Posted speed limit of segment i at time step k (mph)
$V^j(k_v)$	Displayed speed of VSL j at the k_v th VSL control interval (mph)
$V_t^j(k_v)$	The t th option for displayed speed of VSL j at the k_v th VSL control interval (mph)
$\Delta Q_b(k_v)$	Targeted reduction on the flow rate from the control area at the k_v th VSL control interval (veh/h)
$Q_b(k_v)$	Estimated average outflow rates from the control area at the k_v th VSL control interval (veh/h)
C_b	Bottleneck capacity (veh/h)
$\rho_b(k)$	Bottleneck density at time step k (veh/mi/ln)
$\rho_{c,b}$	Bottleneck critical density (veh/mi/ln)
K	Gain factor used in the VSL control
Δv	The speed reduction interval for VSL control interval (mph)
Δv_j	The speed reduced from the regular speed limit for VSL j (mph)
v_l	The lowest speed allowed to be displayed (mph)
$S_v(j)$	The set of potential displayed speeds of VSL j
S^j	Segment set controlled by VSL j
$Q_t^j(k_v)$	Estimated average outflow rates from the control area at the k_v th VSL control interval if the j th VSL is activated with the t th option (veh/h)
$\Delta Q_t^j(k_v)$	Reduction on the flow rate from the control area at the k_v th VSL control interval if the j th VSL is activated with the t th option (veh/h)
$Q^j(k_v)$	Estimated average outflow rates from the control area at the k_v th VSL control interval if the j th VSL is activated (veh/h)
$\Delta Q^j(k_v)$	Reduction on the flow rate from the control area at the k_v th VSL control interval if the j th VSL is activated (veh/h)
$\bar{\rho}^j(k)$	The resulting average density over the segments controlled by VSL j at time step k (veh/mi/ln)
$\bar{\rho}_c^j$	Average critical density over the segments controlled by VSL j (veh/km/ln)
$J_{\max}$	Maximum number of VSLs to be activated
$\delta(k)$	Penalty added to the solution at time step k

As illustrated in Section 5.2, if breakdown is predicted to occur within the prediction horizon, one shall activate the control system. The local control includes a ramp meter at the nearest upstream on-ramp from the bottleneck and several variable speed limit signs within the impacted boundaries of the bottleneck. The process of executing the entire local control shall take the following sequential steps:

Step 1: Determine the Starting Point of the VSL Control

Due to the nature of VSL, such control on the mainline segment shall start from the upstream segment of the bottleneck, rather than from within the boundaries impacted by the predicted congestion. This is to ensure that drivers receiving the VSL instruction can take necessary actions in time to mitigate the waves of congestion formation.

Step 2: Compute the Targeted Flow Rate Reduction

The purpose of the local bottleneck control is to maintain the bottleneck flow rate at its capacity level. The targeted flow rate reduction for the entire control area at the k_v-th VSL control interval can be determined from the following two components, shown in Eq. (5.1) and Figure 5.3:

$$\Delta Q_b(k_v) = \underbrace{Q_b(k_v) - C_b}_{Module\ 1} + \underbrace{K\{\rho_b(n_1(k_v - 1)) - \rho_{c,b}\}}_{Module\ 2} \tag{5.1}$$

where:

$\Delta Q_b(k_v)$ is the targeted reduction on the flow rate from the control area at the k_v-th VSL control interval (veh/h);

$Q_b(k_v)$ is the estimated average outflow rate from the control area at the k_v-th VSL control interval (veh/h);

C_b is the bottleneck capacity (veh/h);

K is the gain factor used in the VSL control;

$\rho_b(n_1(k_v - 1))$ is the bottleneck density at the (k_v-1)-th VSL control interval (veh/mi/ln);

$\rho_{c,b}$ is the bottleneck critical density (veh/mi/ln).

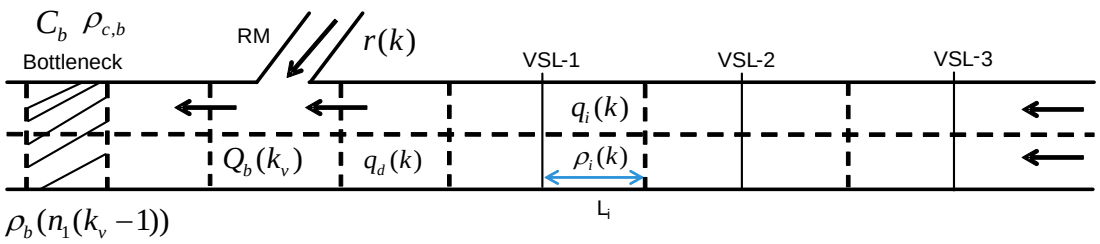

Figure 5.3 Settings of the Study Site when No VSLs are Activated

Module 1 in Eq. (5.1) equals the difference between the estimated flow rates from the control area and bottleneck capacity. Due to the potential difference between the predicted and actual bottleneck conditions,

2 is added to Eq. (5.1) to adjust the control objective, based on the occupancy data fed back from the previous interval. If the computed $\Delta Q_b(k_v)$ is larger than zero (i.e., the predicted flow rate exceeds the bottleneck capacity), the speed of VSLs shall be reduced at the next VSL control interval, and vice versa.

If the speeds of VSL-1, VSL-2, and VSL-3 from intervals k_v -1 to k_v remain unchanged, the posted speeds for all segments in the control boundaries are set to be unchanged:

$$V_i(k) = V^j(k_v - 1),\ for\ i \in S^j,\ j = 1:3, k = n_1(k_v - 1) + 1 : n_1 k_v \tag{5.2}$$

where, $V_i(k)$ is posted speed limit of segment i at time step k, and $V^j(k_v - 1)$ is the displayed speed of VSL j at the interval k_v-1. The free-flow speeds for all steps in the corresponding control interval shall be updated correspondingly:

$$v_{f,i}(k) = V_i(k), k = n_1(k_v - 1) + 1 : n_1 k_v \tag{5.3}$$

Based on the proposed traffic flow model shown in Eq. (4.10) – Eq. (4.17), the system can compute the flow rate $q_i(k)$, density $\rho_i(k)$, and speed $v_i(k)$ of each segment at time step k, and also use Eq. (5.4) to compute the average outflow rate (veh/h) from the control area at interval k_v.

$$Q_b(k_v) = \frac{1}{n_1} \sum_{k=n_1(k_v-1)+1}^{n_1 k_v} \left[q_d(k) + r(k) \right], d \in S^1 \tag{5.4}$$

where, $q_d(k)$ is flow rate from the most downstream segment in the VSL control area at step k, and $r(k)$ is the flow rate from the metered on-ramp at step k. Substituting Eq. (5.4) into Eq. (5.1), one can obtain the targeted flow rate reduction of $\Delta Q_b(k_v)$.

Step 3: Coordination between the Mainline and its On-ramps

To address equity among drivers, the proposed control system is designed to allocate the flow rate reduction to the mainline segment, and then decide if it is necessary to further activate the on-ramp control and other upstream VSLs to reduce the flow rate to the target level. Figure 5.3 illustrates an example of such control on a highway segment which has three VSLs in the control area. Then, the operational process for speed control can be summarized in Table 5.4.

Table 5.4 Operational Process to Distribute the Flow Rate Reduction

1. Set $V^1(k_v) \in S_v(1) = \{v_l, v_l + \Delta v, ..., V^1(k_v - 1) - \Delta v, V^1(k_v - 1)\}$ (5.5)

2. For each element $V_t^1(k_v)$ in $S_v(1)$, compute $Q_t^1(k_v)$

3. For each obtained $Q_t^1(k_v)$, set $\Delta Q_t^1(k_v) = Q_b(k_v) - Q_t^1(k_v)$ (5.6)

4. Select $V^1(k_v)$, whose $\Delta Q^1(k_v) = \max\{\Delta Q_t^1(k_v) : \Delta Q_t^1(k_v) \le \Delta Q_b(k_v)\}$, *for all t* (5.7)

5. Set $R^1(k) = \max\{R(n_1(k_v - 1)) - \Delta Q_R^1(k_v), R_q(k)\}$ (5.8)

6. If $R^1(k) = R_q(k)$ or $\bar{\rho}^1(k) > \bar{\rho}_c^1$

   Go to Step 7;

   Else,

   Stop.

7. Set $V^2(k_v) \in S_v(2) = \{V^1(k_v), V^1(k_v) + \Delta v, ..., V^2(k_v - 1) - \Delta v, V^2(k_v - 1)\}$ (5.9)

8. Repeat Step 2 to Step 5 for VSL-2

9. If $R^2(k) = R_q(k)$ or $\bar{\rho}^{1,2}(k) > \bar{\rho}_c^{1,2}$

   Go to Step 10

   Else,

   Stop.

10. Repeat Step 7 and Step 8 for VSL-3 and end the algorithm.

As shown in Eq. (5.5), the speed of VSL-1 is set to be between v_l (i.e., the lowest allowed displayed speed) and $V^1(k_v - 1)$ (i.e., currently displayed speed) with Δv as the incremental interval. For each potential choice $V_t^1(k_v)$, the corresponding compliance rate and the resulting flow rate $Q_t^1(k_v)$ is computed by Eq. (4.4) and Eq. (5.4), respectively. For each obtained $Q_t^1(k_v)$ in Step 2, the resulted flow rate reduction $\Delta Q_t^1(k_v)$ is obtained by Eq. (5.6), and the displayed speed $V^1(k_v)$ is selected to satisfy Eq. (5.7).

With the selected displayed speed for VSL-1 obtained in Step 4, the required ramp metering rate is computed by Eq. (5.8), which should be larger than or equal to the minimum allowed metering rate, where:

$$\Delta Q_R^1(k_v) = \Delta Q_b(k_v) - \Delta Q^1(k_v) \tag{5.10}$$

$$R_q(k) = d(k) - \frac{w_{\max} - w(k)}{\Delta t} \tag{5.11}$$

$$w(k+1) = w(k) + \Delta t[d(k) - r(k)] \tag{5.12}$$

$$0 \le r(k) = \min\left\{d(k) + w(k)/\Delta t, C_r, R(k)\right\} \tag{5.13}$$

Eq. (5.10) computes the remaining flow rate to be reduced when VSL-1 is activated; Eq. (5.11) computes the minimum allowed metering rate which could prevent spillback onto the surface street; Eq. (5.12) and Eq. (5.13) updates the on-ramp queue length as in Carlson et al. (2010). If spillback may occur at the on-ramp or $\overline{\rho}^1(k)$ (i.e., average density within the area controlled by VSL-1) is larger than $\overline{\rho}_c^1$ (i.e., the average critical density), the VSL-2 will be activated, where:

$$\overline{\rho}^1(k) = \sum_{i \in S^1} \rho_i(k) L_i \Big/ \sum_{i \in S^1} L_i \tag{5.14}$$

$$\overline{\rho}_c^1 = \sum_{i \in S^1} \rho_{c,i} L_i \Big/ \sum_{i \in S^1} L_i \tag{5.15}$$

The choice set of the displayed speed with VSL-2 is determined similarly by Eq. (5.9), and Step 2 to Step 5 should be repeated for VSL-2. If either condition in Step 9 is satisfied, VSL-3 shall be activated. Otherwise, the process for executing this algorithm will be terminated. The flowchart to determine the number of VSLs to be activated is summarized in Figure 5.4.

If all available VSLs and the on-ramp control have been activated, and still either mainline breakdown or ramp queue spillback is inevitable, this indicates that the local bottleneck control alone is not sufficient to maintain the target highway segment operated at the capacity level. Hence, the entire corridor, even the segments which do not experience recurrent congestion, should also be included in the control boundaries. For example, metering control should be implemented at more upstream on-ramps.

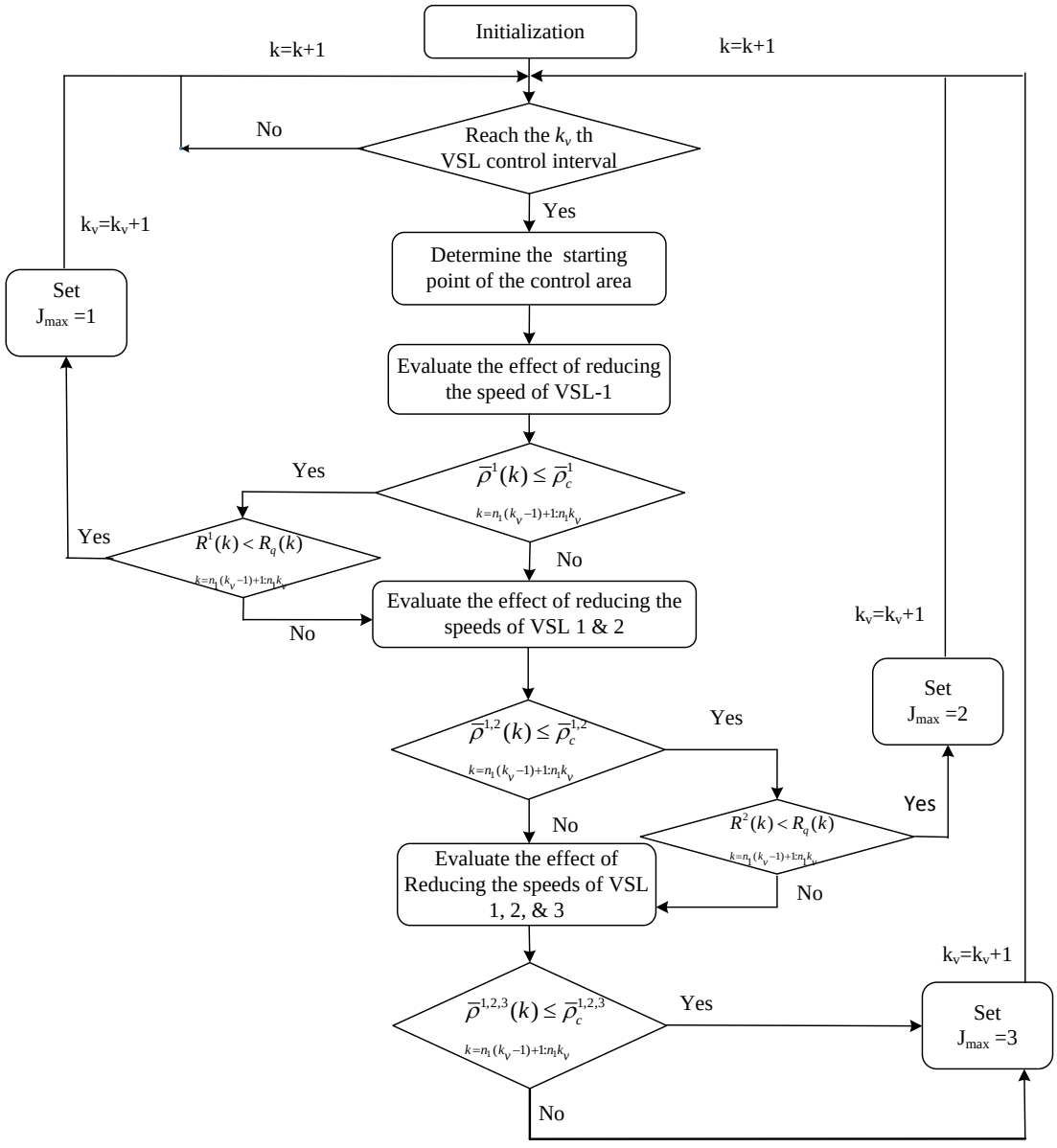

Figure 5.4 Flowchart to Determine the Number of Activated VSLs

5.4 Refinement of the Initial Local Operations with Optimal Control

Taking the control output from the initial local operations, this section presents an optimal control process to further improve the resulting effectiveness. Note that if traffic conditions can be prevented from evolving to the unstable and congested states (State III, IV, and V) during the prediction horizon under the initial local controls, the objective function

shall be set to maximize the total throughput represented by the total travel distance; and also to prevent traffic from breakdown on every roadway segment. However, if unstable and congested states are inevitable under the initial local operations due to either a temporary demand surge or deviation from the prediction volume, the objective function shall be switched to minimizing the total delay (or total travel time) for traffic on the mainline segment and at the on-ramp.

Optimization Formulations

Taking the above two scenarios into consideration, Figure 5.5 shows the process for implementing the optimal control. More specially, Eq. (5.16) shows the objective function of maximizing the throughput:

$$Min\ -TTD = -\Delta t \sum_{k=k_0+1}^{k_0+n_p} \sum_{i=1}^{N} \left[\rho_i(k) v_i(k) \lambda_i L_i \right] + \delta(k_0) \tag{5.16}$$

which is:

$$\begin{aligned} &\text{Eq. (4.10)-(4.17) for traffic flow model formulations} \\ s.t. \quad &\text{Eq. (5.5)-(5.15) for operational constraints for RM and VSLs} \\ \delta(k_0) = &\begin{cases} 0 & if\ all\ \rho_i(k) < \rho_{c,i}, w(k) < w_{\max}, k = k_0+1 : k_0+n_p, i = 1:N \\ \delta(k_0) + M & if\ any\ \rho_i(k) \geq \rho_{c,i}, w(k) \geq w_{\max}, k = k_0+1 : k_0+n_p, i = 1:N \end{cases} \end{aligned} \tag{5.17}$$

At each VSL control interval, the decision variables are the ramp metering rate and the displayed VSL speeds. As shown in Eq. (5.17), starting from k_0 the current time step, the total travel distance for the next n_p steps within the prediction horizon will be computed. For any k within the n_p steps, if traffic breakdown takes place at any segment or ramp queue has reached the maximum value, a large penalty M is added to the penalty term $\delta(k_0)$ to prevent the corresponding control decisions from being selected.

In contrast, if the objective function is switched to minimize the total delay (total travel time) for traffic on both the mainline and the on-ramp, the objective function can be represented with Eq. (5.18).

$$Min\ \ TTT = \Delta t \sum_{k=k_0+1}^{k_0+n_p} \sum_{i=1}^{N} \left[\rho_i(k) \lambda_i L_i + w(k) \right] \tag{5.18}$$

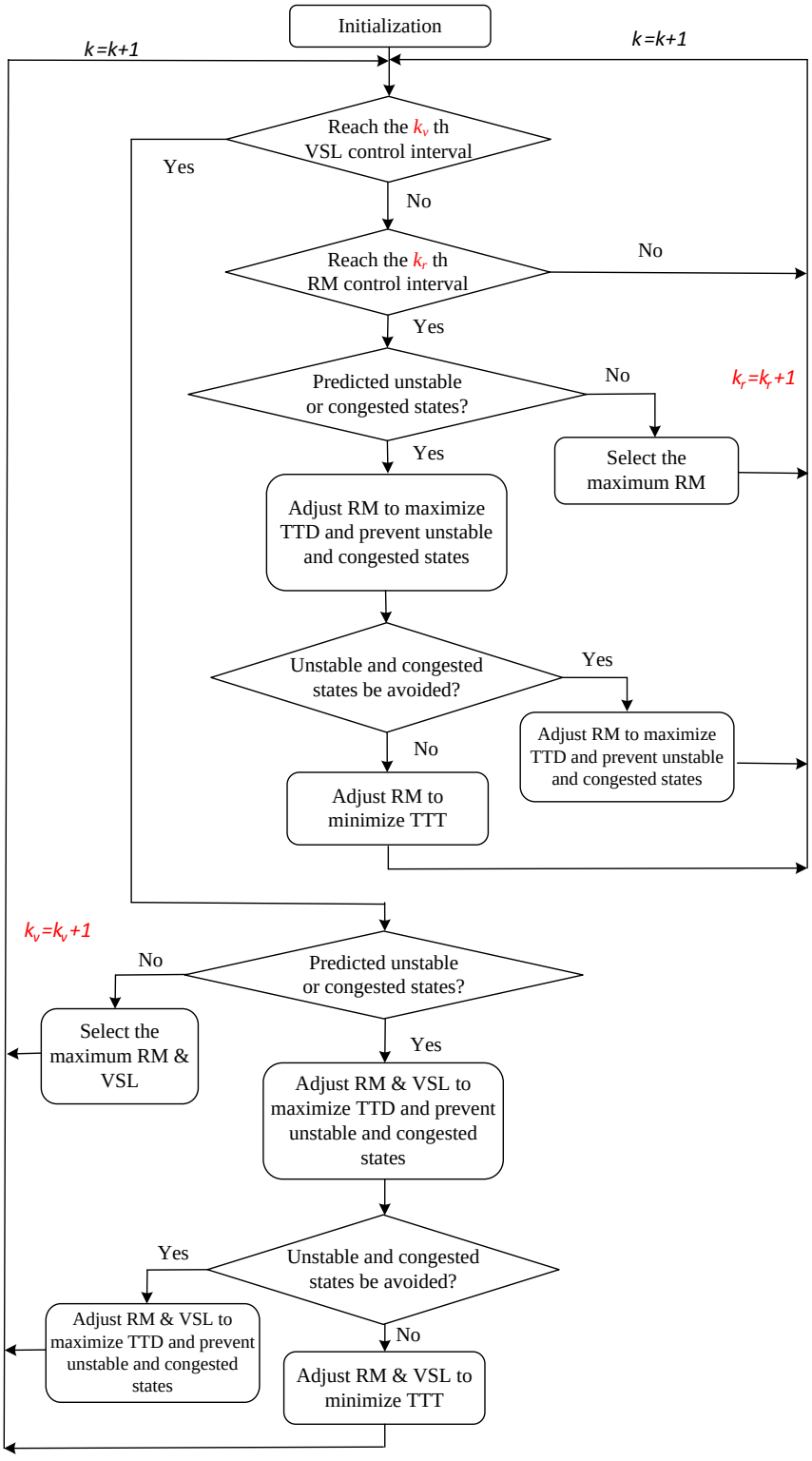

Figure 5.5 Flowchart of the Optimization Framework

5.5 Extended Model: Integrated Control of a Multi-segment Corridor

As stated before, an integrated corridor control is necessary when the local bottleneck control alone is not sufficient to prevent breakdown when the traffic volumes increase consistently on more than one highway segments. To design such a system-wide integrated control, this study has further proposed an extended corridor control model which can: 1) determine the conditions to activate the additional controls for upstream segments; 2) compute the target level of volume reduction to be distributed to upstream segments so as to reach the system-wide optimal state; and 3) execute the deactivation mechanism for the corridor control system.

In the integrated corridor control, the models used to predict the traffic dynamics are similar to those in the local integrated control; but, the control zone is pre-determined, based on the historical congestion pattern. Differing from the local control, all on-ramps within the control zone could be activated sequentially to mitigate the congestion level. The entire control zone is divided into sub-zones, each including at most one ramp. If a sub-zone is activated based on the predicted conditions, the system will begin to use a VSL display to show the reduced speed limit and activate the on-ramp signal metering. If multiple sub-zones are activated, then the system's control module shall coordinate all displayed speeds and metering rates.

Determine the Activation Conditions

The control action for the upstream segment could be activated under two conditions: temporary local demand surge at upstream on-ramps and insufficient control capability of the local bottleneck control. Hereafter, the bottleneck congestion and local congestion is denoted as Type-1 and Type 2 congestion, respectively.

An example of networks with multiple segments is shown in Figure 5.6 to illustrate integrated control process. Additional key variables are presented in Table 5.5. The big dot at the most downstream point represents the bottleneck location, where the index of sub-zone starts from the bottleneck and there are four sub-zones in the control zone.

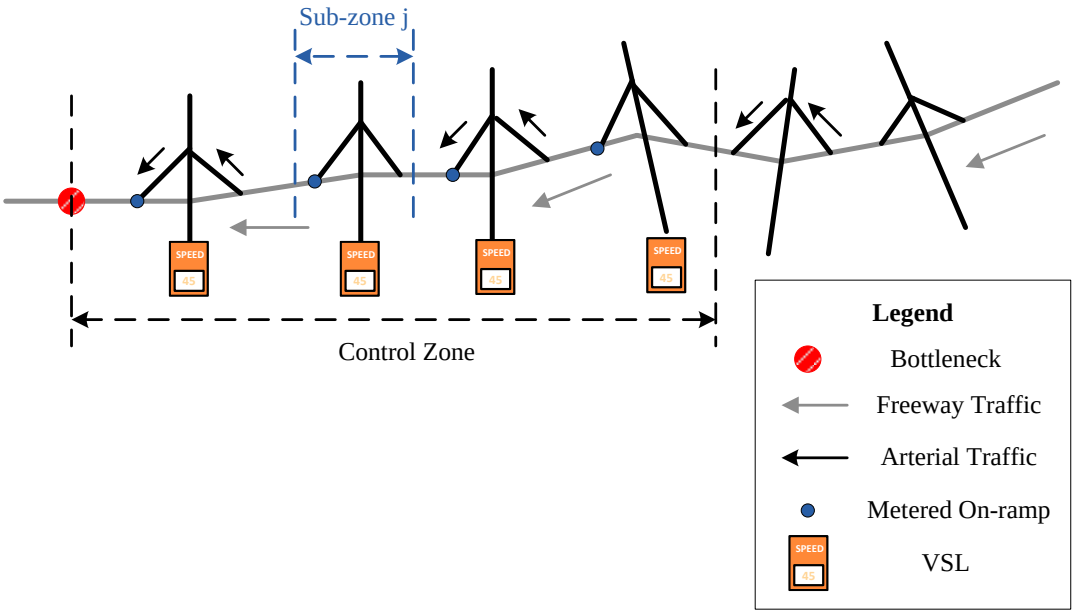

Figure 5.6 Settings of the Integrated Corridor Control

Table 5.5 Additional Key Variables for the Corridor Control

Variables	Explanations
k	Time step index of traffic flow models, where k th interval $= k\Delta t$
k_0	Current interval
k_p	Prediction interval of traffic flow models
j	Index of sub-zones
b	Index of the bottleneck
$\rho_j(k)$	Density of sub-zone j at time step k (veh/mi/ln)
$v_j(k)$	Speed of sub-zone j at time step k (mi/h)
$q_j(k)$	Flow rate out of sub-zone j at time step k (veh/h)
$R_{j,b}(k)$	Ramp metering rate in sub-zone j decided by corridor control starting at the bottleneck at time step k (veh/h)
$R_{j,l}(k)$	Ramp metering rate in sub-zone j decided by corridor control starting at the sub-zone l at time step k (veh/h)
$w_j(k)$	On-ramp queue length in sub-zone j at time step k (veh)
$V_{j,b}(k)$	Displayed speed of VSL in sub-zone j decided by corridor control starting at the bottleneck at time step k (mph)
$V_{j,l}(k)$	Displayed speed of VSL decided in sub-zone j by corridor control starting at the sub-zone l at time step k (mph)
$\Phi(s)$	Objective function within feasible region s

The developed algorithm embedded in the center of the control system will be activated to monitor the traffic conditions at the bottleneck location, and to decide whether or not the control operations should be activated. Steps to activate such an algorithm are listed below:

Step 1: Prediction of the Bottleneck's Traffic Conditions

As shown in Figure 5.7, with the information of the current condition at time k_0 and the estimated demand, the traffic conditions over the prediction horizon ($\rho_b(k)$, $v_b(k)$, and $q_b(k)$, where $k = k_0 + 1 : k_0 + k_p$) at the bottleneck can be predicted with the embedded traffic flow model.

Step 2: Check the Activation Conditions of Sub-zone 1 (due to the Type-1 Congestion)

The prediction model for traffic breakdown will then take these results as additional input, and project the potential breakdown intervals in the prediction horizon. If traffic breakdown is predicted to take place in the target time horizon, the control system will activate all controls in sub-zone 1. Details of the breakdown prediction model could be found in Section 5.2.

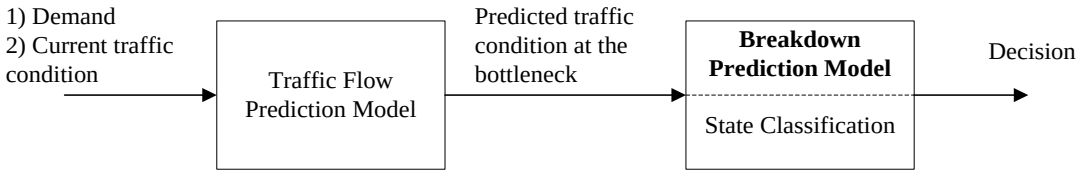

Figure 5.7 Flowchart to Activate the Control System

Step 3: Activation of Upstream Sub-zones (due to Type-1 Congestion)

If the activation of all controls in sub-zone 1 is not able to prevent breakdown, the integrated corridor control system shall activate all control strategies available in sub-zone 2. The same process can be activated sequentially for more sub-zones in the upstream.

Step 4: Activation of Upstream Sub-zones (due to Type-2 Congestion)

Assuming that sub-zone j was not activated to contend the bottleneck congestion but the local density at sub-zone j was predicted to increase over the critical density, the integrated control system shall activate separate control starting from sub-zone j, and then evaluate if controls for its upstream segments shall be included.

As illustrated in Figure 5.8, for instance, the breakdown at the bottleneck could be well controlled by the activation of sub-zone 1, the displayed speed and metering rate

determined by the corridor control, starting from the bottleneck were $V_{1,b}(k)$ and $R_{1,b}(k)$. In the meantime, since the density at sub-zone 3 was predicted to rise over the threshold, the control system needs to activate controls in both sub-zones 3 and 4. The displayed speeds and metering rates at these two segments determined by the corridor control starting from sub-zone 3 were denoted as $V_{3,3}(k)$, $R_{3,3}(k)$, and $V_{4,3}(k)$, $R_{4,3}(k)$, respectively.

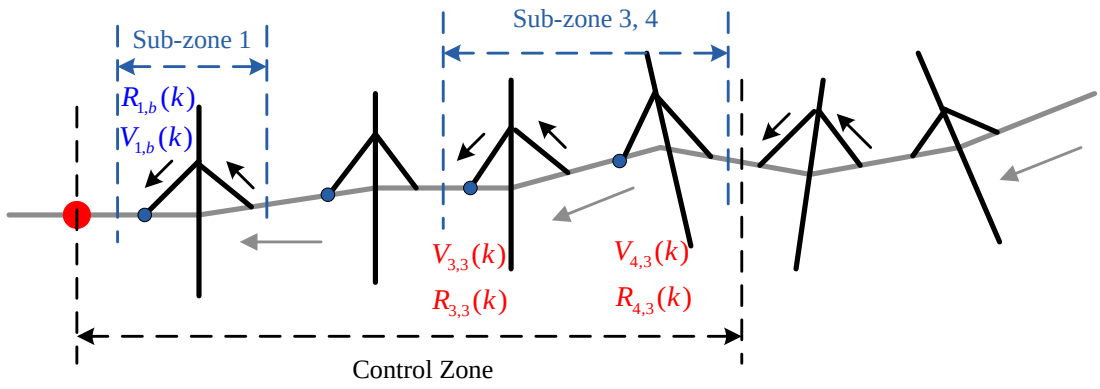

Figure 5.8 Scenarios with Separate Control Zones

Step 5: Determine the Control Outputs under both Type-1 and Type-2 Congestion

As illustrated above, the control system at one segment could be activated either by Type-1 bottleneck congestion or Type-2 local congestion. Thus, it is possible that the control system at one particular segment could be affected by both types of congestion. For example, as shown in Figure 5.9, the output of control system at sub-zone 3 is determined by both the bottleneck control starting from sub-zone 1 (denoted as $V_{3,b}(k)$, $R_{3,b}(k)$) and the local control starting from sub-zone 3 (denoted as $V_{3,3}(k)$, $R_{3,3}(k)$). While multiple values for displayed speed and metering rate exist for the same segment, the conservative one shall be selected, as shown in Eq. (5-19) and Eq. (5-20).

$$R^j(k) = \min\left\{R_{j,b}(k), R_{j,l}(k)\right\} \tag{5-19}$$

$$V^j(k) = \min\left\{V_{j,b}(k), V_{j,l}(k)\right\} \tag{5-20}$$

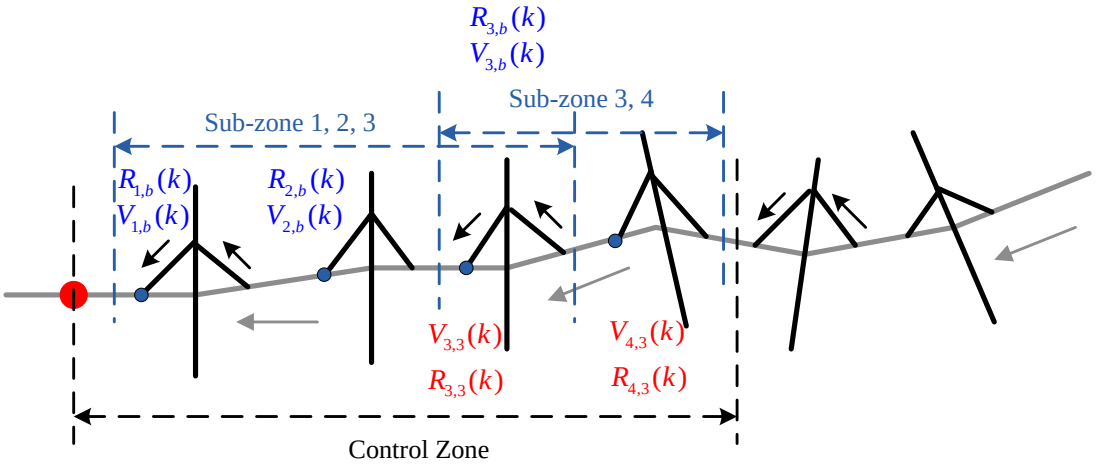

Figure 5.9 Scenarios with Overlapped Control Zones

Coordination among Segments

This section illustrates how the speed and metering rates shown above are computed. Note that the displayed speed, $V_1(k)$, and metering rate, $R_1(k)$, in sub-zone 1 could be determined based on the local integrated control system proposed in Sections 5.3 and 5.4. However, if multiple sub-zone controls are activated, the displayed speeds in these sub-zones need to be coordinated as illustrated in Table 5.4. And the metering rates are to be optimized with the following formulations.

$$\begin{aligned} &\min\ \Phi(s) \\ &s.t.\ \ R_{\min} < R_j(k) < R_{\max} \\ &\qquad w_j(k) < w_{\max} \end{aligned} \tag{5-21}$$

where, $\Phi(s)$ denotes either Eq. (5.16) to minimize total travel time or Eq. (5-18) to optimize the total travel distance. The ramp metering rate should be within the lower and upper bound, and the on-ramp queue length shall not spill back to local arterials; s is the feasible search region determined by the traffic flow models shown in Eq. (4-10) to Eq. (4-17).

Note that selection of the minimal metering rates could affect the equity and the performance. The minimal metering rate of zero may lead to the greatest inequity condition because all target volume reduction will only be assigned to the on-ramp where congestion occurs, unless the ramp queue spills back. However, allowing long waiting time at a target ramp may raise significant public concerns and even violations to the ramp signals.

Control Deactivation

When demand to the bottleneck segment starts to reduce after the peak period, the system should deactivate the control strategies on some upstream segments, or even switch the corridor control mode back to the local control mode. Similar to the activation strategy, the deactivation mechanism should both work in real-time and be robust. The procedures to deactivate the system are shown below.

Step 1: Locate the Potential Segments: The system should keep tracking the number of separate control zones and the most upstream segment in each sub-zone.

Step 2: Check the Deactivation Criterion: For each segment identified in Step 1, the following conditions should be satisfied to justify the deactivation:

1) The control algorithm decides to set the displayed speed and metering rate at the maximum level;
2) The bottleneck that results the sub-zone control is not in the breakdown condition;
3) The segment under the control operations is not in the breakdown condition.

Step 3: Perform the Deactivation Action: If all criteria are satisfied, increase the counter by one. If the counter has reached five, then deactivation should begin. If any criterion is not satisfied before the counter reaches five, then it should be reset to zero.

5.6 Closure

This chapter first presents an integrated local control strategy utilizing both local ramp metering and variable speed limits to mitigate the recurrent freeway congestion. Based on the proposed traffic flow formulations, which include compliance rate of drivers and dynamic monitoring system, the proposed system employs its breakdown prediction system to obtain the optimal system activation time. The operationally efficient control algorithm manages to allocate the targeted reduction on the flow rate to the mainline and the on-ramp, considering both mobility and equity. If the necessary hardware is available, the output generated from the above algorithm could be further incorporated in an optimization framework at the refinement stage to achieve the optimal system performance.

The local bottleneck control alone, which includes single ramp metering and VSL control for upstream segments, may not be sufficient for preventing traffic breakdown when the demand experiences a sudden surge. Under this situation, it is necessary to incorporate those upstream segments into the control boundaries. The methodology to integrate corridor control and distribute the excess volume among different on-ramps is further proposed in this chapter.

Chapter 6: Model Evaluation with Simulation Experiments

6.1 Introduction

To evaluate the effectiveness of all developed models and their potentials for field implementation, this research has conducted simulation experiments on MD-100 WB between MD-170 and US-1. The selection is based on the fact that those highway segments often experience recurrent congestion during the afternoon peak. Additionally, the results of a field demonstration in 2010 showed the potential to use variable speed control to improve mobility. The focus of evaluation in this chapter is to analyze the effectiveness of integrating speed and ramp controls under the 2015 volume level.

As an essential task of simulation evaluation, the experimental work starts with calibration of the driving behaviors in the simulator, using volume and speed data collected in the 2010 field demonstration. The simulation output based on calibrated parameters is then used to compute key variables in the macroscopic control models.

The MOEs adopted for performance evaluation include travel time along the entire segment, densities at the bottleneck and the weaving segments, total time in the network by all vehicles, and queue lengths at all on-ramps.

6.2 Target Freeway Segments

MD-100 is a major east-west highway, connecting US-29 in Ellicott City, Howard County and MD-177 in Pasadena, Anne Arundel County in Maryland via two lanes in each direction on most segments. The highway segments for simulation evaluation cover approximately five miles, starting from MD-170 (Telegraph Rd) to US-1 (Washington Blvd).

The geometric layout of these segments is shown in Figure 6.1. Note that these segments for exercising control operations include a total of four on-ramps, one from each of the following roads: MD-713, MD295, and Coca-Cola Dr. and three off-ramps to MD-295 and Coca-Cola Dr.

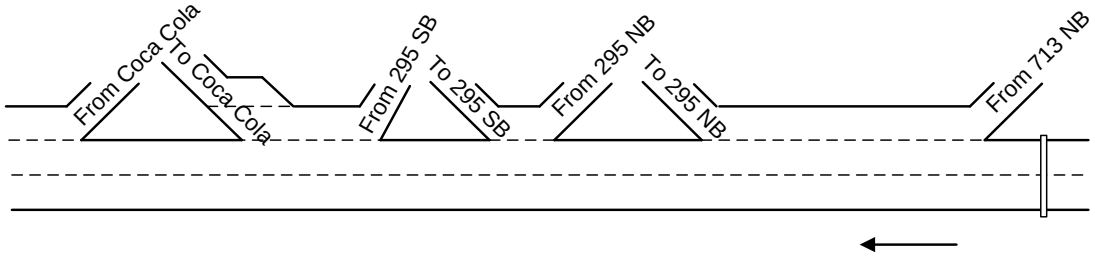

Figure 6.1 Geometric Settings of Study Site

As shown in Figure 6.2, recurrent congestion starts from the bottleneck at the on-ramp for Coca-Cola Rd in the afternoon peak (around 4 PM) every weekday (e.g., data of Dec 14th, 2016 is shown in the figure). The queues usually extend over 1.75 miles to the MD-713 (Arundel Mills Blvd.) on-ramp, and are even longer on rainy and snow days.

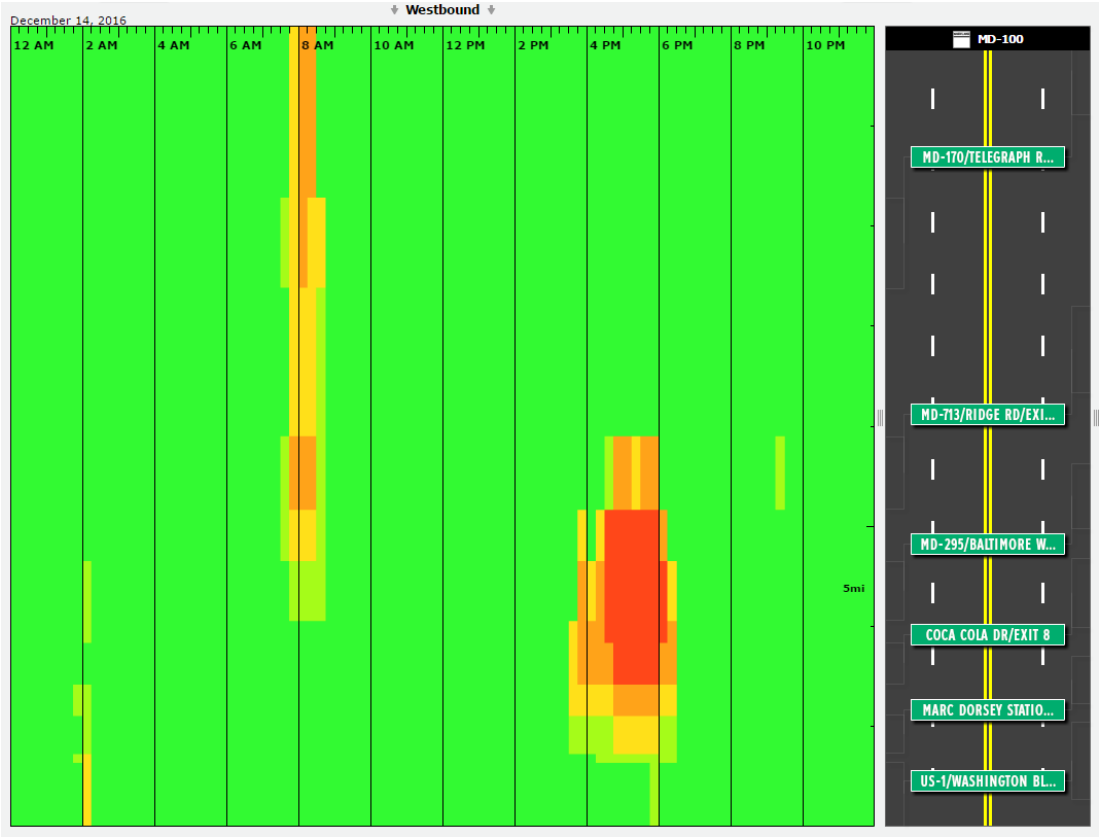

Figure 6.2 Congestion Pattern for MD-100 WB on a Typical Weekday

Additionally, Figure 6.3 shows traffic conditions (i.e., speed and occupancy) for a typical day within the 2010 field demonstration at the downstream of the Coca-Cola Dr. Driver speeds start to drop around 4:30 PM and recover to normal condition after 6 PM. The most severe congestion occurs between 5:00 PM and 5:30 PM, when the average speed drops below 20 mph. The left and middle lanes share similar characteristics, but the right lane serves as an acceleration/deceleration lane.

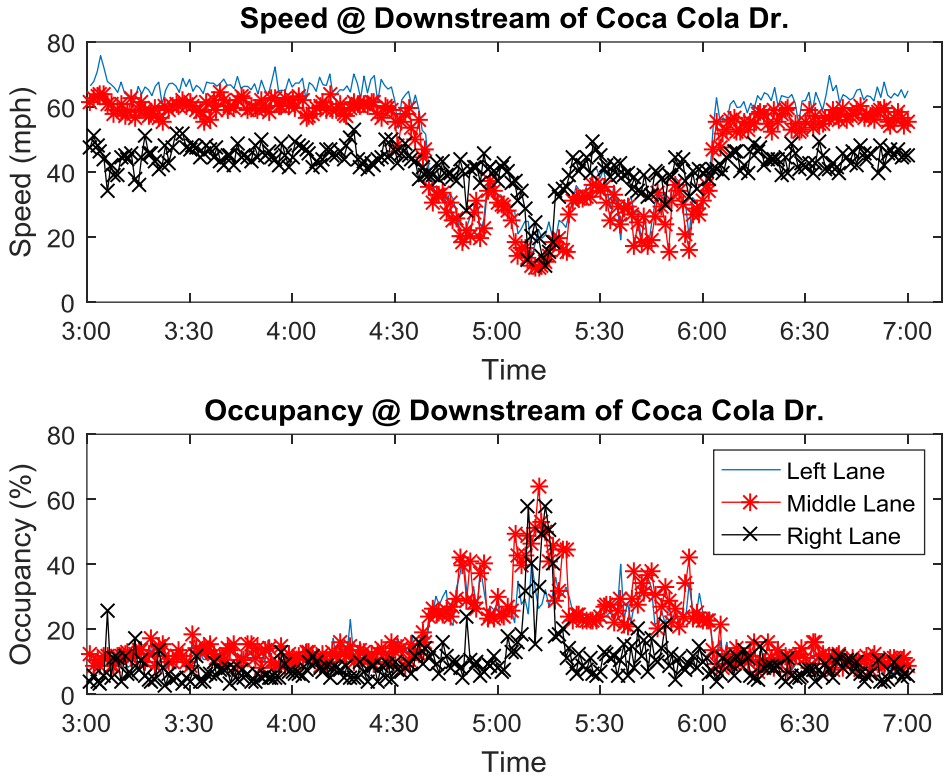

Figure 6.3 Traffic Conditions at the Bottleneck Grouped by Lanes

The MOEs selected to evaluate the system performance are listed below.

- Travel time from MD-170 to Coca-Cola Dr.
- Bottleneck Density downstream of Coca-Cola Dr.
- Density at the weaving segment downstream of MD-295 SB
- Density at the weaving segment downstream of MD-295 NB
- Total time spent in the network on both mainline and on-ramps
- Queue length at MD-295 NB, MD-295 SB, and Coca-Cola Dr.

6.3 Calibration of the Simulator and the Traffic Control Models

As stated above, the microscopic simulator, VISSIM, is first calibrated with field data, obtained from a VSL demonstration conducted between December 2009 and January 2010.

The 2010 demand data in the interval of 15 minutes used in the calibration of the microscopic simulator is shown in Figure 6.4.

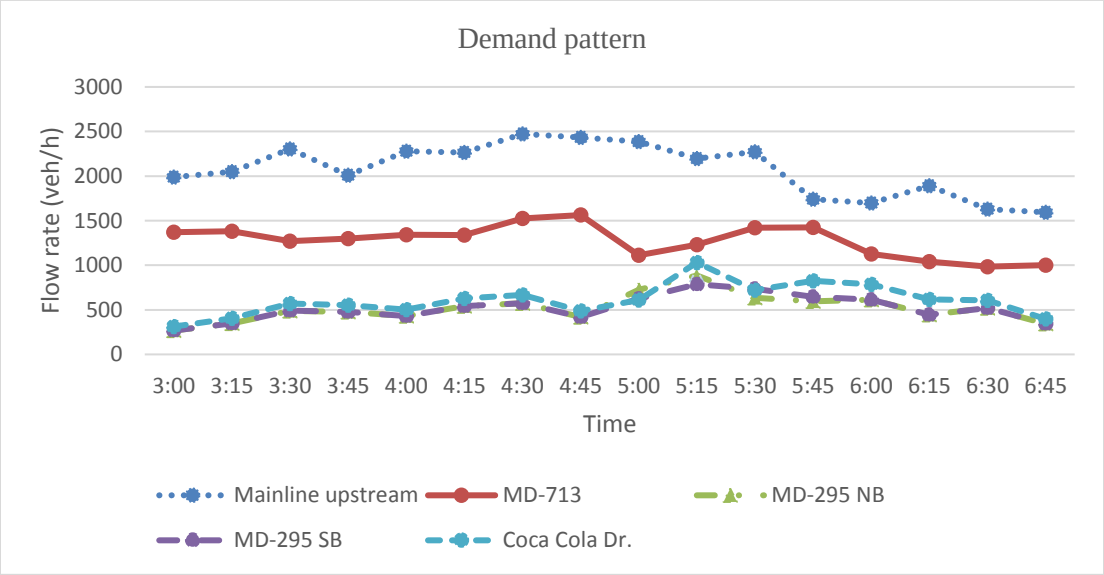

Figure 6.4 Traffic Demand for Calibration of VISSIM Simulation

One set of detectors was installed at each of the following three locations in the 2010 field demonstration and in simulation experiments: the downstream of Coca-Cola Dr., the downstream of MD-295 NB off-ramp, and the downstream of MD-713 on-ramp, during the field demonstration period. A total of four-hour data, including volume and speed on a typical day, were collected and used to calibrate the VISSIM simulator. The commonly-used Genetic Algorithm (GA) was applied to perform the calibration task, focusing on parameters for characterizing the car-following and lane-changing behaviors. The evolution process of GA is

shown in Figure 6.5, where 1,000 populations are generated in each iteration, and a total of 500 iterations are generated for evolution. The selected fitness function is equal to the relative volume plus speed errors averaged over three detectors. Note that due to the large number of populations, only those with relative error less than 20 percent were shown in Figure 6.5. The parameters returned from the best population have reached the relative error of 12.1 percent.

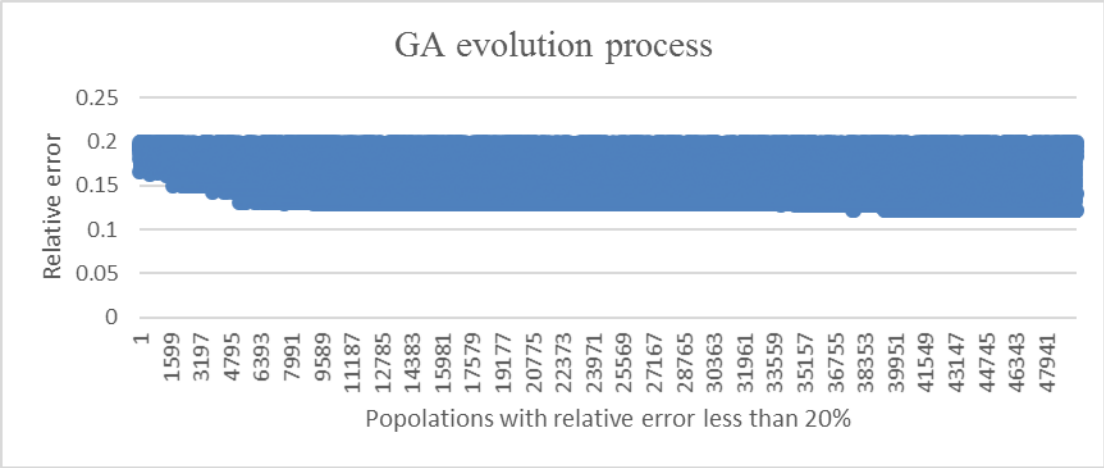

Figure 6.5 Evolution Process of GA when Calibrating VISSIM

To obtain accurate prediction results, the proposed macroscopic traffic flow model for use in control operations is then calibrated to match the traffic data, generated from the simulator with calibrated traffic parameters. There are a total of 13 highway segments in the model, and traffic data are collected from the VISSIM simulator at locations corresponding to those segments. The same GA method was also applied to perform the parameter calibration which has yielded 9.45 percent relative errors from the best population. Evolution of the GA calibration process (only when relative error was less than 15 percent) is shown in Figure 6.6.

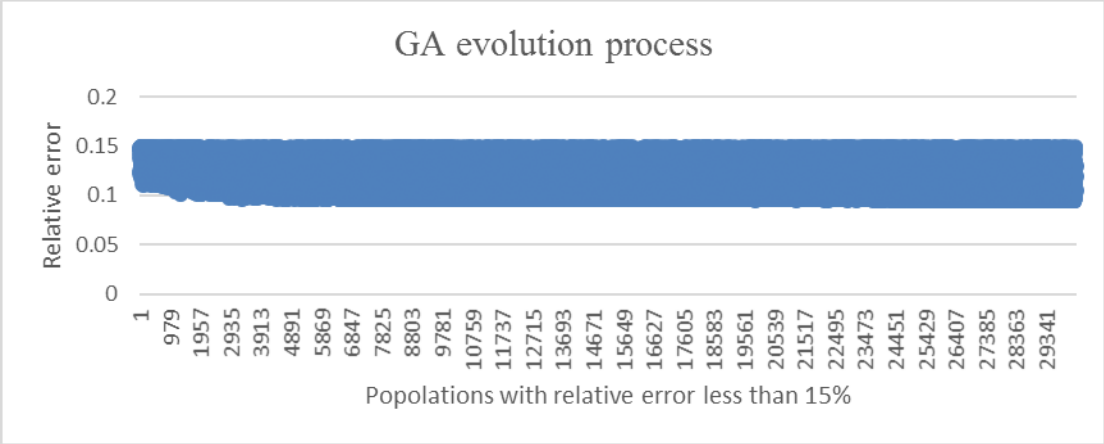

Figure 6.6 Evolution of the GA Calibration Process when Calibrating Traffic Flow Model

Sections 5.4.2 and 5.4.3 in VISSIM 5.20 User Manual (PTV, 2009) illustrate its car-following and lane-changing models, and their parameters calibrated with GA for field data in 2010 are shown in Table 6.1. Key parameters selected for calibration in the traffic flow model are shown in Table 6.2.

Table 6.1 Selected Key Parameters in VISSIM

Class	Parameter	Coca Cola	Weaving Segment	Normal Segment
Car Following	CC0 (Standstill Distance) (m)	0.63	0.48	0.82
	CC1 (Headway Time) (s)	0.51	0.5	0.58
	CC2 (Following Variation) (m)	7.5		
	CC7 (Oscillation Acceleration) (m/s^2)	0.91		
	CC8 (Standstill Acceleration) (m/s^2)	5.65		
Lane Change	Own: Maximum deceleration (m/s^2)	-3.95		
	Own: -1 m/s^2 per distance (m)	47.66		
	Trailing: Maximum Acceleration (m/s^2)	-5.67		
	Trailing: -1 m/s^2 per distance (m)	64.53		

Table 6.2 Selected Key Parameters in the Traffic Flow Model

Parameter	Coca Cola	Weaving Segment	Normal Segment
Free-flow speed (mph)	63.3	61.18	
Critical density (veh/mi/ln)	21.82	27.2	
tau (hr)	0.019	0.010	0.002
nu (mi^2/h)	33.75	114.61	6.80
kai (veh/mi/ln)	116.41	21.17	66.09

6.4 Evaluation Results with the Volumes in 2015

Model Applications

Although the evaluated locations varied, the comparison between 2010 and 2015 data shows an increase of 7-10 percent in the volume. For example, the increase in traffic demand from MD-170 (mainline upstream) and Coca-Cola Dr. (bottleneck) was about 10 percent and 7.5 percent, respectively (See Figures 6.7 and 6.8).

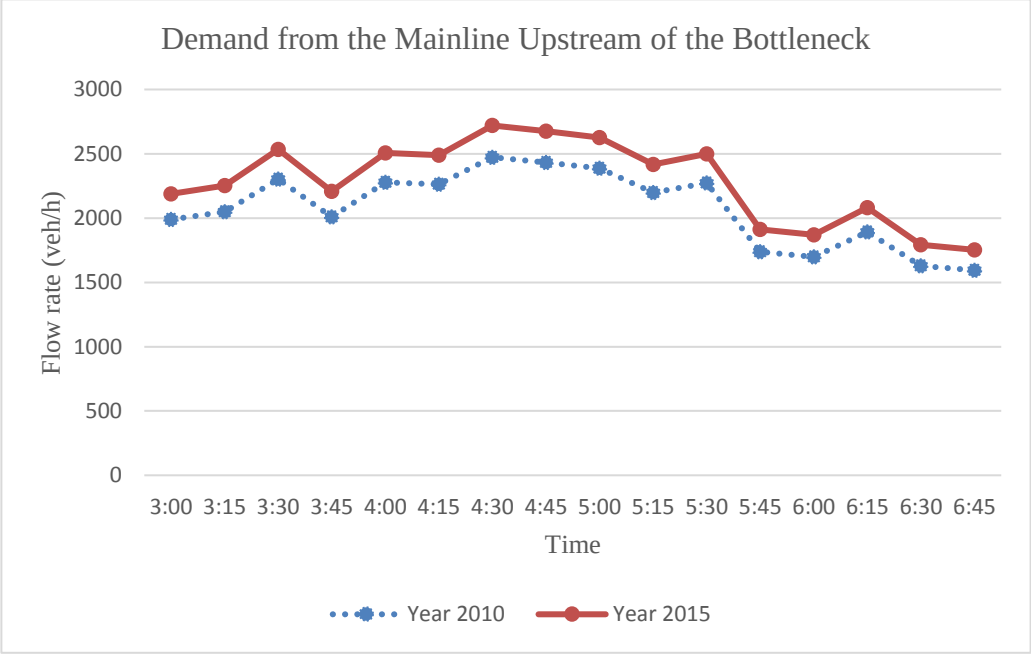

Figure 6.7 Comparison of 2010 and 2015 Flow Rates on the Mainline Upstream of the Bottleneck

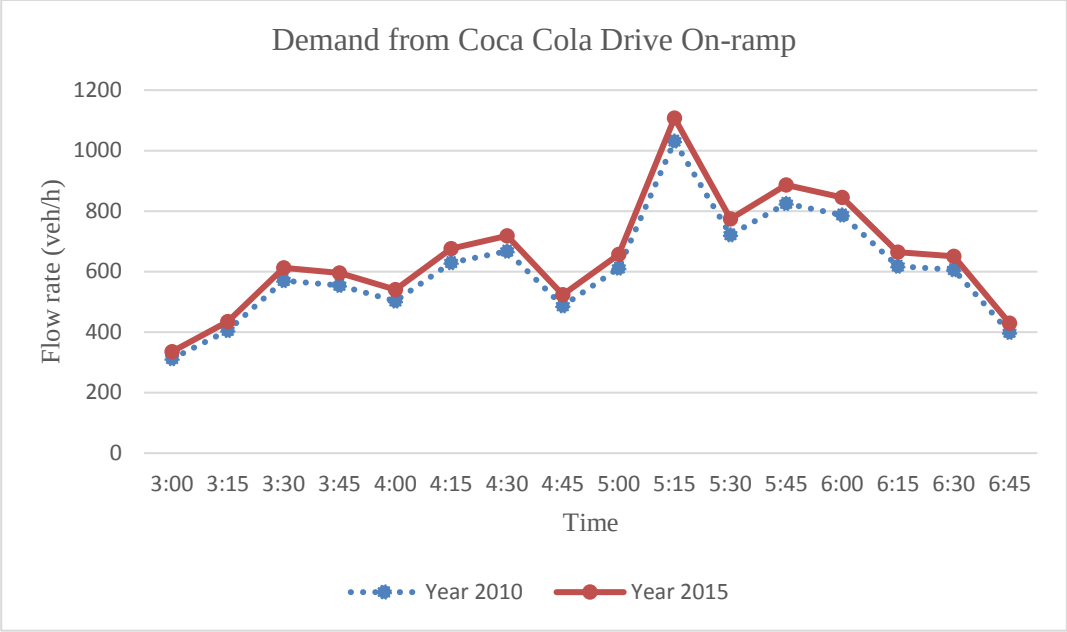

Figure 6.8 Comparison of 2010 and 2015 Flow Rates at the Bottleneck On-ramp (Coca-Cola)

All scenarios for model evaluation are listed in Table 6.3. The VSL-only scenario adopts the same control logic -- proposed in the local integrated control -- but excludes ramp metering. The purpose is to evaluate the effectiveness of VSL control under different demand levels and the necessity of including ramp metering. In the local integrated control, due to insufficient capacity of the target segment near Coca-Cola Dr., the on-ramp at MD-295 SB -- the closest upstream on-ramp -- is selected to execute ramp metering. The corridor control includes VSL and all three on-ramp meterings within the congested area. As stated in Section 6.2, the performance evaluation will focus on travel time for the entire corridor, density profiles at critical segments, total time spent in the network, and queue lengths at metered on-ramps.

Table 6.3 Description of the Selected Scenarios

Scenario No.	Description
1	Base: no control
2	VSL-only
3	Local integrated control
4	Corridor integrated control

Locations of VSLs and ramp meters for the target control segments are shown in Figure 6.9. The storage room for the on-ramp at Coca Cola Dr., MD-295 SB, and MD-295 NB was 40, 80, and 50 vehicles, respectively.

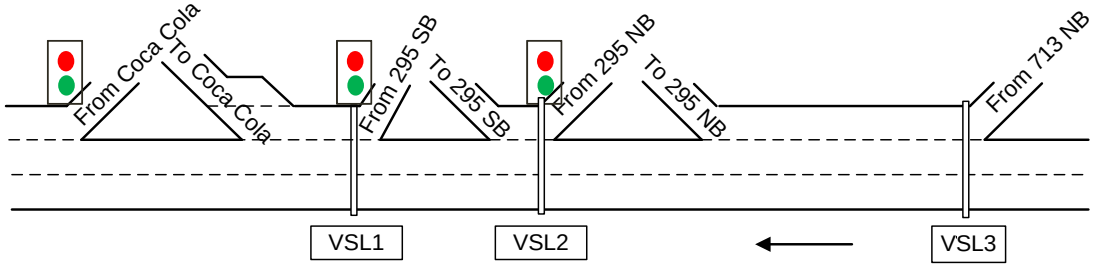

Figure 6.9 Settings of the Control Devices

Compliance Rate to VSL

Note that the compliance rate of drivers to VSL needs to be investigated prior to the performance comparison. Since the compliance rate has been modeled with respect to the combination of different driving populations, the proposed traffic flow model used in the entire control process has adopted the compliance rate to all three VSLs over all experimental scenarios.

Travel Time Comparison

The times needed to travel from MD-170 to Coca-Cola Dr. under different control scenarios are summarized in Table 6.4, where all three control strategies are able to reduce the total travel time over the congested area, and the resulting improvements range from 7.84 percent to 27.99 percent.

Table 6.4 Performance Comparison of Average Travel Time

Scenario	Ave_TT (s)	Percentage Improvement over No Control Scenario
No control	362.18	N/A
VSL	333.80	7.84%
Int Local	287.05	20.74%
Int Corridor	260.81	27.99%

A detailed comparison of travel time evolution is shown in Figure 6.10. Notably, travel time increases significantly in the afternoon peak period (starting from 4:30 PM), and shows that drivers need to take over 13 minutes (800 seconds) to pass the segment that only takes less than four minutes (200 seconds) during off-peak hours. VSL control can reduce the congestion level, but not to a significant degree. Both local and corridor-integrated controls are effective, as shown in the reduced congestion magnitude and duration. Taking the corridor control scenario for example, the congested duration was reduced by approximately 15 minutes, and the longest travel time was shortened by 420 seconds. Notably, some differences in the MOEs are observed between the local integrated and corridor controls, indicating that the former is no longer sufficient to cope with the increased demand.

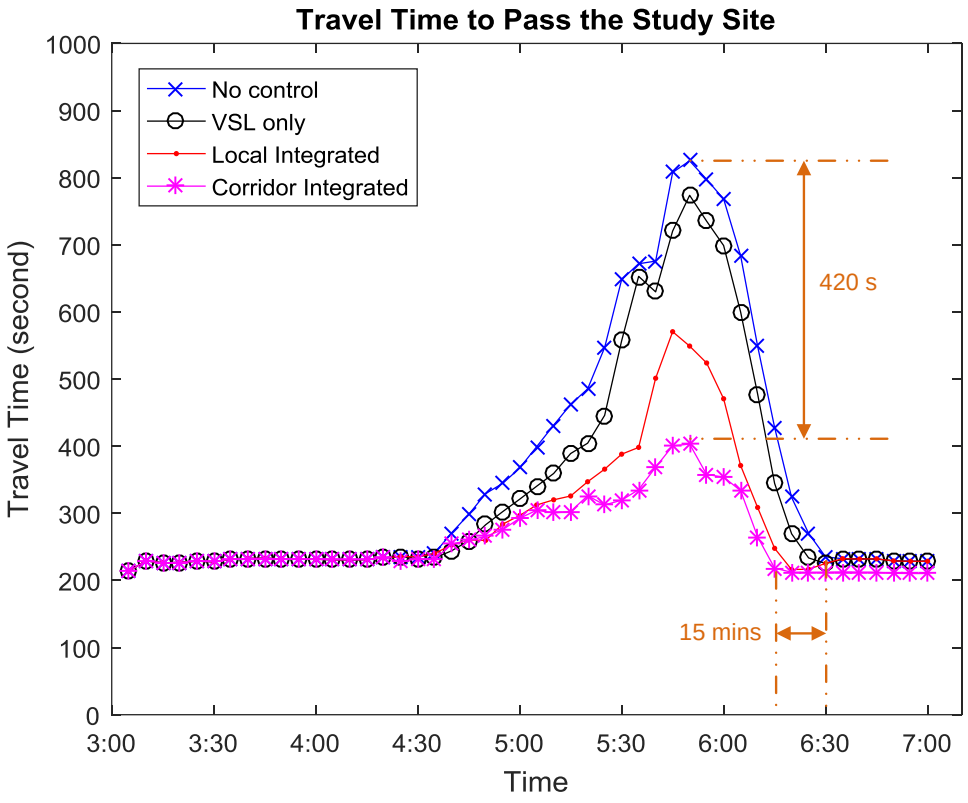

Figure 6.10 Comparison of Travel Time Evolutions

Traffic Conditions at the Bottleneck

The bottleneck density at the downstream of Coca-Cola Dr. is shown in Table 6.5. The improvement from VSL control is not significant, probably due to the relatively low critical density and the uphill slope at the bottleneck. Since ramp metering can reduce the entry volume to the bottleneck, the integrated local and corridor controls have achieved the reduction of 7.59 and 12.11 percent in density. The relatively large demand in 2015 is the primary factor preventing the freeway segment from keeping bottleneck density at an acceptable level.

Table 6.5 Performance Comparison of Average Bottleneck Density

Scenario	Ave_Density (veh/mi/ln)	Percentage Improvement over No Control Scenario
No control	42.90	N/A
VSL	41.40	3.49%
Int Local	39.65	7.59%
Int Corridor	37.70	12.11%

The evolution of bottleneck density is shown in Figure 6.11. Under the no-control scenario, the density in the target segment increases from less than 20 veh/mi/ln to near 80 veh/mi/ln. The VSL-only control does not exhibit significant impacts, except for the period when congestion is about to end (around 6:30 PM). The local integrated control, however, yielded better performance during the congestion dissipation period (between 6:15 and 6:30 PM), but not in the congestion formation period. The corridor control can outperform the other three strategies by reducing the maximum density from about 80 veh/mi/ln to about 70 veh/mi/ln, and by shortening the severe congestion period by 20 minutes, during which the density dropped to around 30 veh/mi/ln over the shortest time periods among all control scenarios.

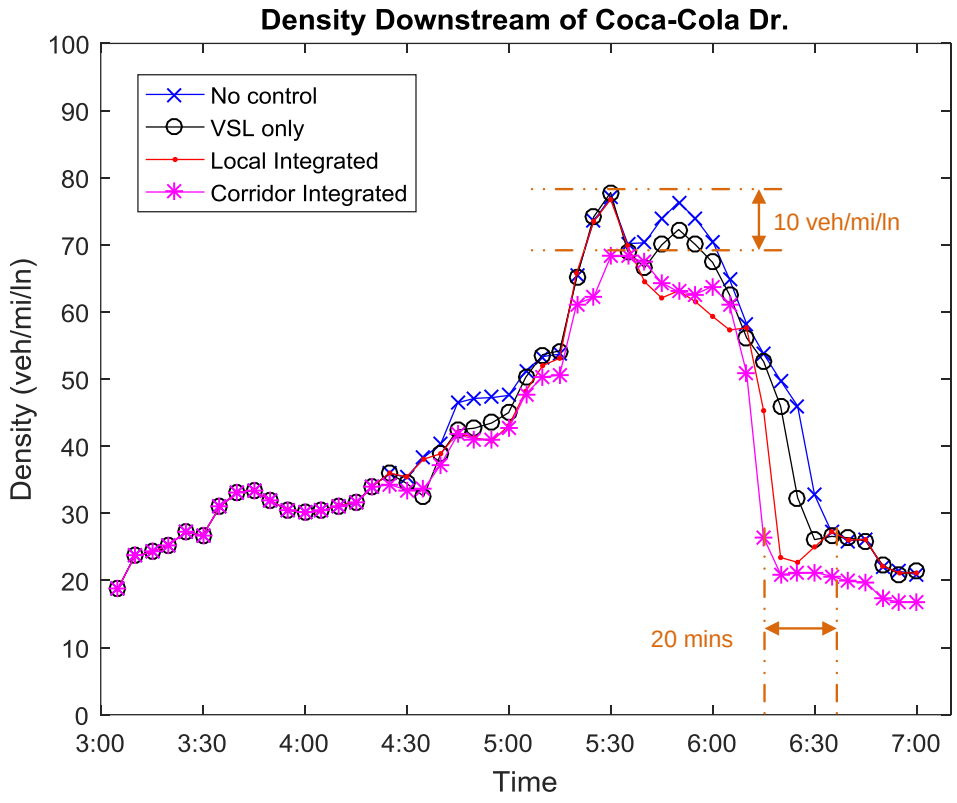

Figure 6.11 Comparison of Bottleneck Density Evolution

Traffic Conditions at the Weaving Segment: Downstream of MD-295 SB

Table 6.6 shows the density profiles at the downstream of MD-295 SB on-ramp. Unlike the condition at the bottleneck location (shown in Table 6.5), all control strategies are effective with respect to the density reduction over the weaving area. Compared with density improvement at the bottleneck segment (i.e., 12.11 percent), the integrated corridor control can clearly achieve better results at this weaving segment (i.e., 20.39 percent).

Table 6.6 Performance Comparison of Average Density Downstream of MD-295 SB On-ramp

Scenario	Ave_Density (veh/mi/ln)	Percentage Improvement over No Control Scenario
No control	46.09	N/A
VSL	43.23	6.22%
Int Local	39.28	14.78%
Int Corridor	36.69	20.39%

The density evolution at the downstream of MD-295 SB is shown in Figure 6.12. Under the no-control scenario, the density will increase from less than 20 veh/mi/ln to about 100 veh/mi/ln. VSL-only only seems to be able to delay the formation of congestion and accelerate the dissipation. Both the integrated local and corridor controls can perform well, as evidenced in reduction of the maximum density from about 100 veh/mi/ln to about 80 veh/mi/ln (i.e., local control) and 75 veh/mi/ln (i.e., corridor control), and also in shortening the congestion period by 20 minutes. Overall, the corridor control outperforms the local one and all other control scenarios with respect to delaying the traffic breakdown, reducing the density in congestion periods, and shortening the duration of congestion.

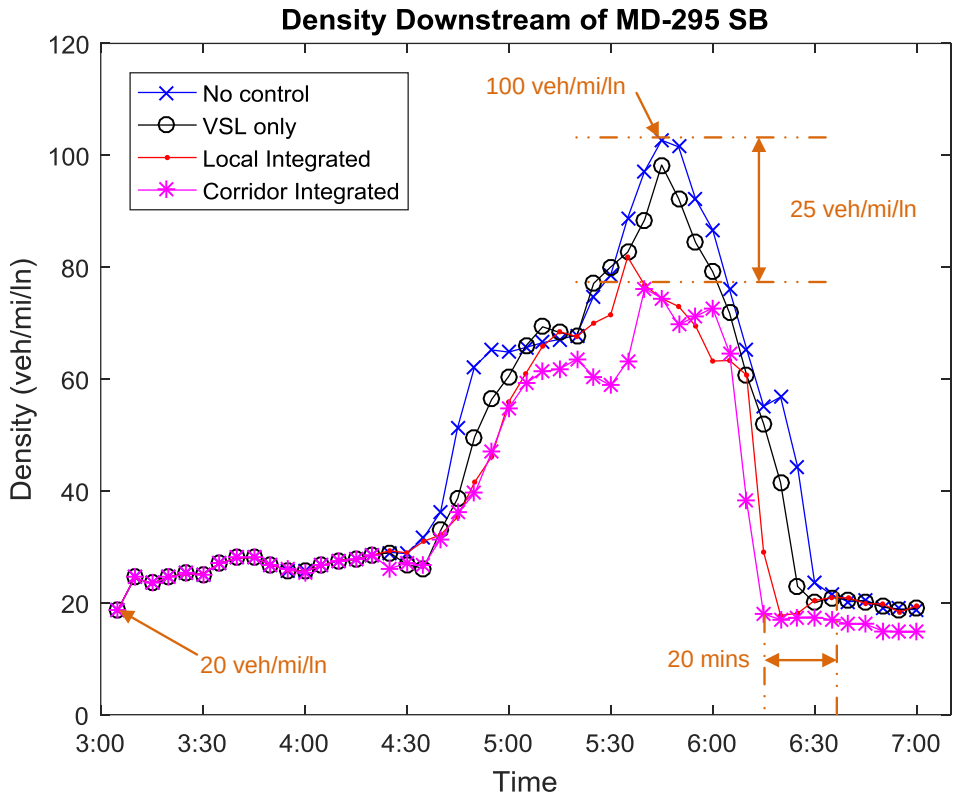

Figure 6.12 Comparison of Density Evolution downstream of MD-295 SB On-ramp

Traffic Conditions at the Weaving Segment: Downstream of MD-295 NB

Due to the close proximity of the MD-295 NB on-ramp and MD-295 SB off-ramp, it is difficult for vehicles to get onto and off the freeway, compared with other segments. As shown in the evolution of traffic breakdown at the downstream bottleneck, this segment's traffic queue will quickly build up at this weaving segment, and the shockwaves will further propagate to its upstream segments. Note that the density at the downstream of MD-295 NB could be even higher than those on the bottleneck segment and the previous weaving segment, where most vehicles are kept in the stop-and-go conditions. As shown in Table 6.7, the average density under no-control is 51.96 veh/mi/ln, and those are 42.9 veh/mi/ln and 46.09 veh/mi/ln at the bottleneck and MD-295 SB on-ramp, respectively. Now, after implementing

the control strategies, the approaching flow rates from both the upstream and metered on-ramps are regulated, and thus result in lower weaving intensity. For instance, under the VSL control alone, one can expect to achieve around 10 percent improvement (i.e., 5.68 veh/mi/ln). Comparing the densities between the local and corridor controls, it is noticeable that 10 percent more density reduction (i.e., 43.60 percent less 31.99 percent) in the congested segment can be achieved with additional ramp meterings.

Table 6.7 Performance Comparison of Average Density Downstream of MD-295 NB On-ramp

Scenario	Ave_Density (veh/mi/ln)	Percentage Improvement over No Control Scenario
No control	51.96	N/A
VSL	46.28	10.94%
Int Local	35.33	31.99%
Int Corridor	29.31	43.60%

As shown in the density evolution profile at the downstream of MD-295 NB in Figure 6.13, the density under the no-control scenario could reach to about 135 veh/mi/ln. VSL control has reduced the density level at the congestion formation period between 4:30 and 5:30 PM, but still cannot prevent the eventual traffic breakdown. The local integrated control cannot prevent the traffic breakdown under the 2015 demand, because the resulting density could be more than 100 veh/mi/ln (around 5:50 PM) in the simulation experiments. The corridor control, however, can perform well, as it significantly reduces the maximum density to about 70 veh/mi/ln, and keep the density at a relatively low level for most of the congestion period between 4:30 and 6:30 PM. For instance, for most time intervals between 4:30 and 5:40 PM (70 minutes) and between 6:10 and 6:25 PM (15 minutes), the corridor control is able to maintain a density below 40 veh/mi/ln.

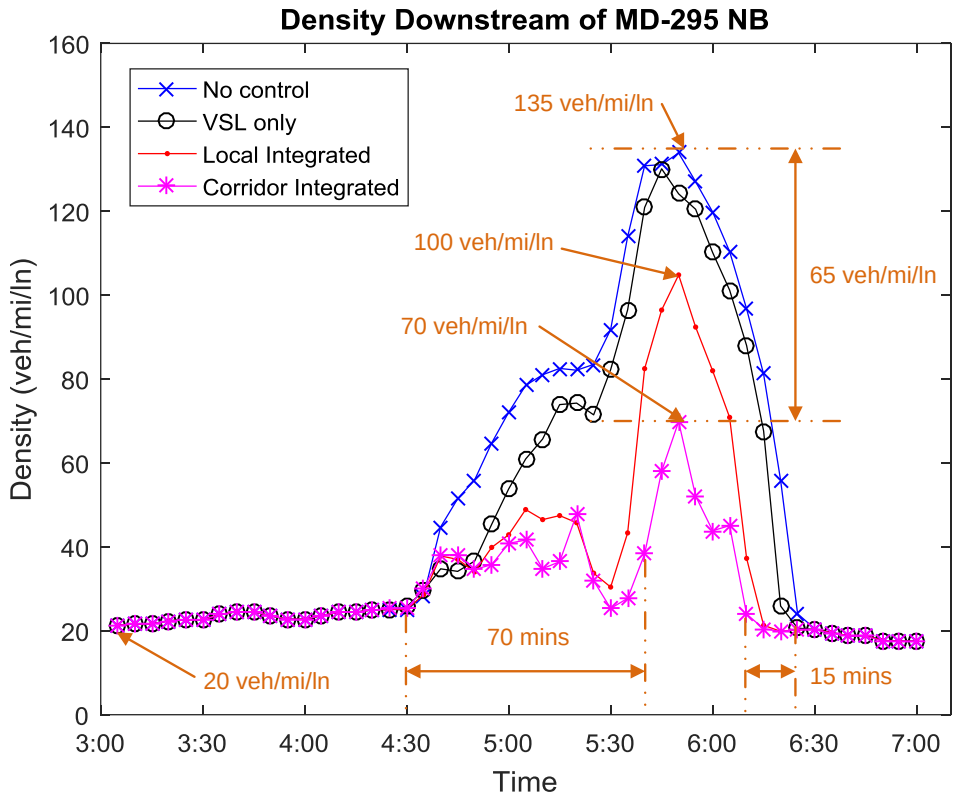

Figure 6.13 Comparison of Density Evolution downstream of MD-295 NB On-ramp

Comparison of Total Time in the Network

By comparing the resulting travel time and density for all experimental scenarios, it is clear that all control strategies can be effective in reducing mainline travel time and densities at critical locations. However, additional ramp metering will inevitably result in longer queues at the on-ramps. Hence, it is essential to further compare the total time of all vehicles within the network during the experimental period, including both the travel time on the mainline and waiting time at on-ramps.

As shown in Table 6.8, the total trip time (including queued duration at on-ramps) can be reduced by 8.33 percent, 16.70 percent, and 23.40 percent with VSL-only, integrated local, and integrated corridor controls, respectively.

Table 6.8 Performance Comparison of Total Time in the Network

Scenario	TTT(h)	Percentage Improvement over No Control Scenario
No control	1082.01	N/A
VSL	991.94	8.33%
Int Local	901.27	16.70%
Int Corridor	828.84	23.40%

Figure 6.14 shows the total time in each roadway segment, where the congestion has reached up to Segment 6, upstream of the MD-713 on-ramp. Taking the bottleneck segment (Segment 13 and 12) for example, not all proposed control strategies yield desirable traffic conditions (e.g., the average speed is around 40 mph over all simulation periods) under the 2015 demand; this indicates the presence of an upper bound on the demand level -- beyond which the congestion cannot be mitigated with the control-side strategies alone -- and thus current deployment of demand-side strategies would be essential.

On the contrary, for the weaving (i.e., Segment 9) and adjacent upstream segments (Segments 7 & 8), the analysis results show that the intensive weavings due to additional demand surge can be reduced effectively by properly distributing those excessive demands over time with those deployed control strategies.

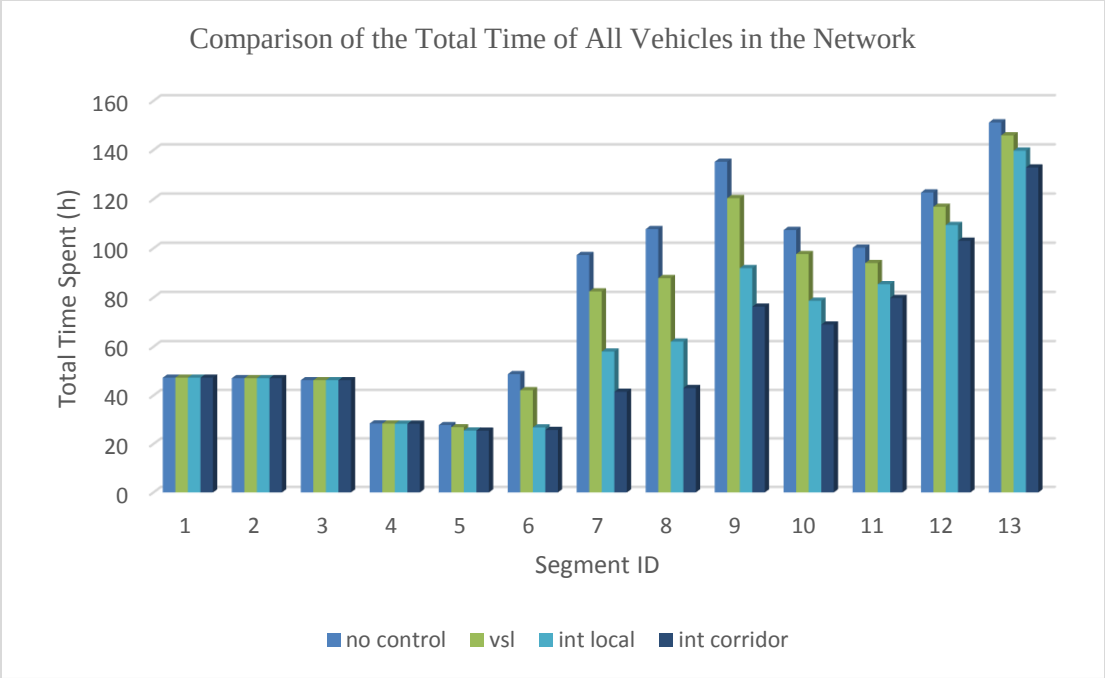

Figure 6.14 Comparison of the Total Time of All Vehicles in Each Segment

Queue Length Comparison

Queue lengths under different controls and the maximum allowable length for all three on-ramps are shown in Figure 6.15 to show whether or not the ramp queue will spill back to the local arterials, and to justify the need to include multiple on-ramps into the metering system.

Within the local integrated control, only the MD-295 SB on-ramp is under metering operations, and its resulting queues have reached their maximum allowable lengths (i.e., 80 vehicles). The density profile in Figure 6.13 clearly shows that the local control has reached its capacity and cannot hold enough vehicles at the on-ramp. The system-wide control has focused on the MD-295 NB on-ramp first, followed by the Coca Cola Dr. on-ramp, and finally switched to the MD-295 SB on-ramp after reaching their respective maximum allowable queue lengths at the previous two on-ramps. The control sequence, generated by the proposed model, seem to make sense, as the weaving density on the segment downstream

of the MD-295 NB on-ramp are much more than those on other segments, justifying the need to implement the ramp metering control.

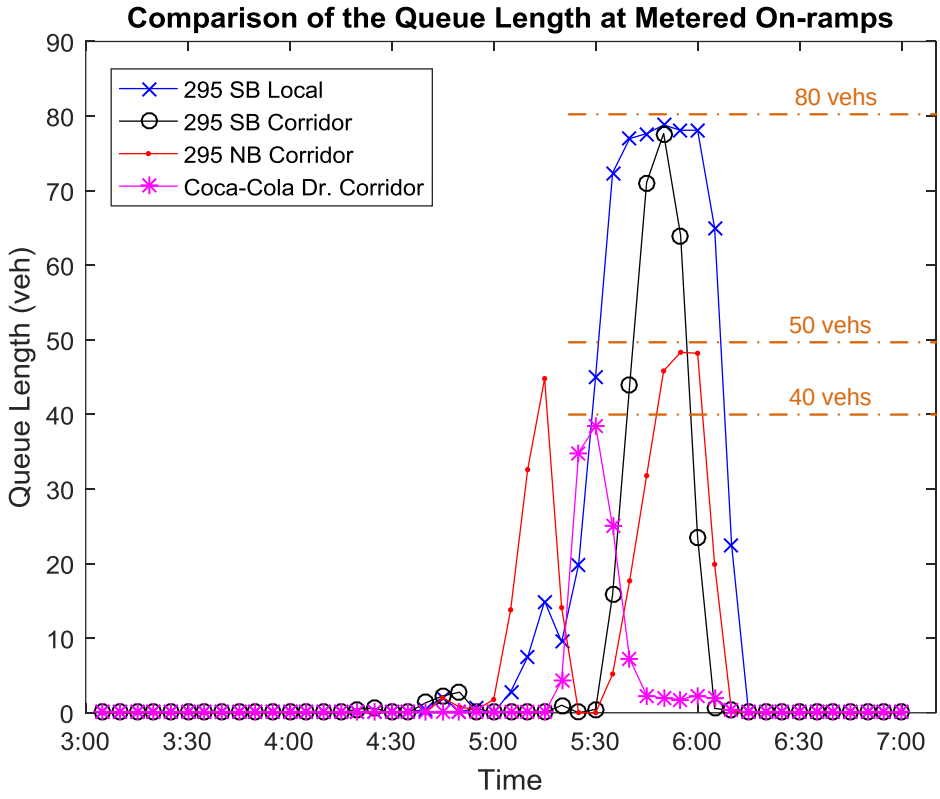

Figure 6.15 Comparison of the Queue Length at Metered On-ramps

As shown in Table 6.9, the average queue length at MD-295 SB ramp under the local control is 13.61 vehicles, and the average total queue length at all three on-ramps under the corridor control is 15.72 vehicles. The increase in queue length at the on-ramps results in increased costs for mobility improvement on the mainline and the reduction in the total trip time of vehicles in the network.

Table 6.9 Comparison of Average Queue Lengths (# of vehs) at Metered On-ramps

Scenario	Coca-Cola Dr.	MD-295 SB	MD-295 NB	Total
Int Local	N/A	13.61	N/A	13.61
Int Corridor	2.51	6.38	6.83	15.72

In addition to improving traffic conditions at metered on-ramps, such control strategies may also benefit drivers at the upstream on-ramp, who are likely to become blocked by mainline queued vehicles. Under the no-control scenario, traffic queues may extend to the upstream of MD-713 on-ramp, thus causing long wait times for the on-ramp. With integrated local and corridor controls, however, the MD-713 on-ramp will not be blocked and most vehicles could merge to the mainline. The total queue length at the MD-713 on-ramp before and after the control operations are shown in Figure 6.16.

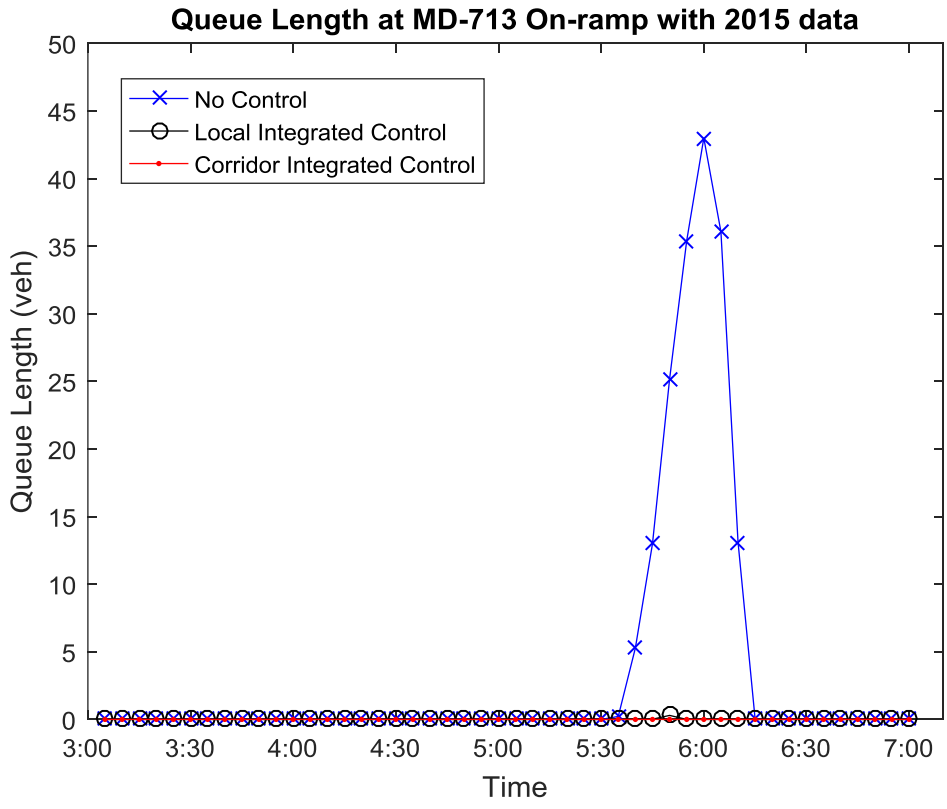

Figure 6.16 Queue Length Comparison at Upstream On-ramp

6.5 Summary

In summary, this chapter presented the evaluation results of all proposed models with the 2015 demand data on MD-100 WB. As expected, all three developed control strategies show their different levels of effectiveness in mitigating the congestion.

Most contributions on travel time savings under these controls come from the density reduction at the weaving segments, which are likely due to: 1) the prevention of increased downstream traffic from breakdown; and 2) fewer weavings under the ramp metering upstream. It has been clear that VSL alone cannot be sufficient to achieve significant improvement, but the local and corridor integrated controls have better capacity to contend with congestion and surging demands.

In terms of the total vehicle time in the target network during the control period, all control strategies show an acceptable level of effectiveness since they are able to: 1) reduce the total time with increased waiting time at the on-ramps; 2) minimize the spatial distribution of the congested area; and 3) reduce the likelihood of causing blockage at upstream on-ramps. Overall, the corridor control can consistently outperform all other strategies in coping with congestion patterns in 2015 on the target segment, because it can result in more equitable distributions of queue lengths among all metered on-ramps.

Chapter 7: Conclusions and Future Research

7.1 Research Summary

To mitigate recurrent congestion caused by freeway bottlenecks and to allow better use of the roadway's available capacity, this study centers on an integrated control system using active traffic management strategies — including both ramp metering and variable speed limit — to keep traffic flows moving near capacity. The developed system with the following key modules has demonstrated effectiveness and efficiency under various experimental scenarios:

- A traffic breakdown prediction model to identify the control boundaries and the activation time, and to determine the control objective to be adopted in the on-line optimal control module: Using the clustering algorithm, the module is capable of identifying the predicted traffic condition to be one of five traffic states. Based on monitored traffic conditions for the entire freeway corridor, the control system can automatically activate this module to predict the time and location of potential traffic breakdown in advance to enable the control center to take actions in time.

- A statistical model to capture the rate of drivers' compliance to VSL messages: This was found to be a function of several important traffic variables, including the speed difference between the prevailing and displayed speeds, and the displayed speed limit.

- A mixed traffic flow model to capture traffic dynamics when only part of the driving population follows the displayed speed reduction: The calibrated model assumes that drivers can be categorized into two groups — following the posted speed limit on the roadside or the dynamically changing speed limit on VSL. Operational guidelines

developed with extensive simulation experiments and field data have been provided to identify critical traffic conditions during which non-VSL-complying vehicles were likely to be affected by those vehicles following the reduced speed limit on VSL.

- An integrated local control module using both local ramp metering and variable speed limits to mitigate the recurrent freeway congestion: Based on the developed traffic flow formulations, the breakdown prediction model allows the control system to determine the optimal activation time. The embedded control algorithm can then function to allocate the targeted reduction in the flow rate between the mainline and the on-ramp, while taking into account both traffic mobility and equity. The output generated from the local control can be further incorporated into an optimized refinement model to achieve system-wide optimal performance.

- An integrated corridor control module, which can activate additional controls on upstream segments to supplement local control operations: Such tasks include determining the control boundaries based on predicted conditions, computing volume reduction distributed to upstream segments, and deactivating the corridor control system in a timely manner.

- Evaluation results from simulation experiments, based on the field-calibrated MD-100 network and the 2015 demand pattern, have demonstrated the effectiveness of the developed integrated control system and its embedded strategies under different traffic scenarios. Major benefits include reductions in total travel time along the freeway mainline and total time spent in the network, as well as density reduction at the bottleneck and the merging areas.

7.2 Future Research

Despite the progress made in this study on control of recurrent congestion, several critical issues remain to be addressed through future research, which include:

Extending the control to local arterials and under non-recurrent congestion scenarios

The system developed in this study has focused only on the freeway network, not the parallel urban arterial. From the network perspective, coordination of both the freeways and the arterials is essential for contending with non-recurrent congestion, such as incidents. Hence, the following issues need to be addressed: 1) how can a network utilize on-ramp metering and signal timing optimization to control traffic flow to ensure it remains under roadway capacity; and 2) how can one divert more vehicles onto the urban network and adjust signal timings at off-ramps under recurrent congestion accordingly.

Enhancing the modeling work on traffic dynamics on weaving/merging areas

In developing a realistic evaluation system, one primary challenge is to estimate traffic conditions at merging areas (i.e., on-ramp and off-ramp). Driving behaviors at such merging areas are very complex, and a more in-depth understanding of such interaction dynamics is essential for the development of any evaluation system. For example, reliable estimation of the capacity at an on-ramp merging area will provide critical information for estimating the breakdown time and for further predicting the traffic evolution. In addition, behavior issues regarding how mainline vehicles would respond to the queued vehicles, that spilled back from off-ramps is also critical to the design and evaluation of control strategies to contend with congestion patterns extending to both freeways and arterials. With advanced modeling of such behaviors, one can more reliably evaluate the trade-off between freeways and arterials and better design an optimal distribution of excessive vehicles.

Enhancing the control under the environment of connected/autonomous vehicles

Connected/Autonomous vehicle (CAV) technologies, which enable communications and information exchange between vehicles and with infrastructure systems, have drawn immense interest from the traffic community. CAV has been tested to show potential in different areas, including safety, mobility, and environment. For example, CAV has been adopted in speed harmonization to improve traffic mobility within a congested area. All control models developed for this study are likely to benefit from the presence of CAV information. Examples of such enhancements include: 1) more reliable estimation of the compliance rate under a variable speed limit (VSL); 2) improved design and evaluation of the signal system's performance along arterials under non-recurrent congestion scenarios, and for current control of freeway and local arterials.

Incorporating active demand management strategies with the integrated corridor control system

Traffic demand management is essential when the capacity of the roadway infrastructure has been fully utilized through the optimal operational management. Multiple state-of-practice strategies on demand management are available to effectively optimize the temporal and spatial distribution of traffic demand, including dynamic pricing, dynamic HOV lanes, on-demand ride-sharing, etc. However, much research needs to be done to ensure better integration of the demand management strategies with active traffic management controls, especially with respect to how travelers will respond to various types of information under different congestion levels. While the information available for travel decisions will be enriched by emerging CAV technologies, much uncertainty at the behavioral side remains to be explored. For example, for one target corridor, a reliable on-line dynamic departure time advisory system could be designed to support the active traffic control, and allow traffic

center operators to tackle both recurrent and non-recurrent congestion patterns. With the support from both demand and operation sides, the congestion could be significantly mitigated.

Bibliography

Abdel-Aty, M., J. Dilmore, and L. Hsia. “Applying variable speed limits and the potential for crash migration.” Transportation Research Record, vol. 1953, pp. 21–30, 2006.

Abdel-Aty, M., R. J. Cunningham, V. V. Gayah, and L. Hsia. “Dynamic variable speed limit strategies for real-time crash risk reduction on freeways.” Transportation Research Record, vol. 2078, pp. 108–116, 2008.

Alessandri, A., A. Di Febbraro, A. Ferrara, and E. Punta. "Optimal control of freeways via speed signalling and ramp metering." Control Engineering Practice, vol. 6, no. 6, pp. 771-780, 1998.

Allaby, P., B. Hellinga, and M. Bullock. "Variable speed limits: Safety and operational impacts of a candidate control strategy for freeway applications." IEEE Transactions on Intelligent Transportation Systems, vol. 8, no. 4, pp. 671-680, 2007.

Bham, G. H., S. Long, H. Baik, T. Ryan, L. Gentry, K. Lall, M. Arezoumandi, D. Liu, T. Li, and B. Schaeffer. “Evaluation of Variable Speed Limits on I-270/I-255 in St. Louis.” No. OR 11-014, 2010.

Bogenberger, K., and A. D. May. "Advanced coordinated traffic responsive ramp metering strategies." California Partners for Advanced Transit and Highways (PATH), 1999.

Bogenberger, K., and H. Keller. "An evolutionary fuzzy system for coordinated and traffic responsive ramp metering." Proceedings of the 34th Annual Hawaii International Conference in System Sciences, 2001.

Bogenberger, K., H. Keller, and S. Vukanovic. "A neuro-fuzzy algorithm for coordinated traffic responsive ramp metering." Proceedings of the IEEE Intelligent Transportation Systems, pp. 94-99, 2001.

Cambridge Systematics, Incorporated. “Twin cities ramp meter evaluation.”, 2001.

Carlson, R. C., I. Papamichail, and M. Papageorgiou. “Local feedback-based mainstream traffic flow control on motorways using variable speed limits.” IEEE Transactions on Intelligent Transportation Systems, vol. 12, pp. 1261–1276, 2011.

Carlson, R. C., I. Papamichail, M. Papageorgiou, and A. Messmer. "Optimal motorway traffic flow control involving variable speed limits and ramp metering." Transportation Science, vol. 44, no. 2, pp. 238-253, 2010.

Chang, G. L., S. Y. Park, and J. Paracha. “Intelligent transportation system field demonstration: integration of variable speed limit control and travel time estimation for a recurrently congested highway.” Transportation Research Record, vol. 2243, pp. 55–66, 2011.

Chang, T. H., and Z. Y. Li. "Optimization of mainline traffic via an adaptive co-ordinated ramp-metering control model with dynamic OD estimation." Transportation Research Part C: Emerging Technologies, vol. 10, no. 2, pp. 99-120, 2002.

Chanut, S, and C. Buisson. “A macroscopic model and its numerical solution for a two-flow mixed traffic with different speeds and lengths” Transportation Research Record, vol. 1852, pp. 209-219, 2003.

Chu, L., H. Liu, M. McNally, and W. Recker. "Development of the Capability-Enhanced PARAMICS Simulation Environment." California Partners for Advanced Transit and Highways (PATH), 2005.

Daganzo, C. F. “A continuum theory of traffic dynamics for freeways with special lanes” Transportation Research Part B, Methodological, vol. 31, no. 2, pp. 485-498, 1997.

Daganzo, C. F. “The cell transmission model, Part II: Network Traffic” Transportation Research Part B, Methodological, vol. 29, no. 2, pp. 79-93, 1995.

Daganzo, C. F. “The cell transmission model: A dynamic representation of highway traffic consistent with the hydrodynamic theory” Transportation Research Part B, Methodological, vol. 28, no. 4, pp. 269-287, 1994.

Daganzo, C. F. “The lagged cell transmission model”, Transportation and Traffic Theory, A. Ceder, Ed., Elsevier, New York, pp. 81-103, 1999.

Drake, J. S., J. L. Schofer, and A. D. May. “A statistical analysis of speed-density hypotheses.” In vehicular traffic science Highway Research Record, vol. 154, pp. 112-117, 1967.

Edie, L. C., R. S., Foote, R. Herman, R. W. Rothery. “Analysis of single lane traffic flow” Traffic Engineering, vol. 21, no. 1, pp. 21-27, 1963.

Finley, M. D., J. Jenkins, and D. S. McAvoy. "Motorists’ speed response to nonvariable and variable work zone speed limits and other work zone conditions." Transportation Research Record: Journal of the Transportation Research Board, vol. 2485, pp. 70-77, 2015.

Franz, M. L. “Development of a decision/deployment support tool for variable speed limits in recurrent congestion.” Ph. D. dissertation, Department of Civil & Environmental Engineering, University of Maryland, 2015.

Fudala, N. J., M. D. Fontaine. “Interaction between system design and operations of variable speed limit systems in work zones.” Transportation Research Record, vol. 2169, pp. 1–10, 2010.

Godunov, S. K. “A difference scheme for numerical solution of discontinuous solution of hydrodynamic equations”, Matematicheskii Sbornik, vol. 89, no. 3, pp. 271-306, 1959.

Gomes, G., and R. Horowitz, “Optimal freeway ramp metering using the asymmetric cell transmission model”, Transportation Research Part C, Emerging Technologies, vol. 14, no. 4, pp. 244-262, 2006.

Greenburg, H., “An analysis of traffic flow”, Operations Research, vol. 7, no. 1, pp. 79-85, 1959.

Greenshields, B. D. “A study in traffic capacity”, Proceedings of Highway Research Record, vol. 14, pp. 448-477, 1935.

Hadiuzzaman, M., T. Z. Qiu. “Cell transmission model-based variable speed limit control for freeways.” Proceedings of Transportation Research Board 91st Annual Meeting, 2012.

Hegyi, A. “Model predictive control for integrating traffic control measures.” Ph. D. dissertation, Netherlands TRAIL Research School, 2004.

Hegyi, A., B. De Schutter, and H. Hellendoorn. "Model predictive control for optimal coordination of ramp metering and variable speed limits." Transportation Research Part C: Emerging Technologies, vol. 13, no. 3, pp. 185-209, 2005.

Hegyi, A., B. De Schutter, J. Hellendoorn. “Optimal coordination of variable speed limits to suppress shock waves.” IEEE Transactions on Intelligent Transportation Systems, vol. 6, pp. 102–112, 2006.

Hegyi, A., S. P. Hoogendoorn. “Dynamic speed limit control to resolve shock waves on freeways – Field test results of the SPECIALIST algorithm.” Proceedings of the 13th IEEE Conference on Intelligent Transportation Systems, 2010.

Hou, Z., J. X. Xu, and J. Yan. "An iterative learning approach for density control of freeway traffic flow via ramp metering."Transportation Research Part C: Emerging Technologies, vol. 16, no. 1, pp. 71-97, 2008.

Jacobson, L. N., K. C. Henry, and O. Mehyar. “Real-time metering algorithm for centralized control.” Transportation Research Record, vol. 1232, 1989.

Jiang, R., and Q. S., Wu. “Extended speed gradient model for mixed traffic”, Transportation Research Record, vol. 1999, pp. 13-22, 2004.

Kang, K. P. “Development of optimal control strategies for freeway work zone operations.” Ph. D. dissertation, Department of Civil & Environmental Engineering, University of Maryland, 2006.

Katz, B., C. O'Donnell, K. Donoughe, J. Atkinson, M. Finley, K. Balke, B. Kuhn, and D. Warren. “Guidelines for the Use of Variable Speed Limit Systems in Wet Weather.” No. FHWA-SA-12-022, 2012.

Kerner, B. S., and P. Konhauser. “Cluster effect in initially homogeneous traffic flow”, Physical Review E, vol. 48, no.4, pp. 2335-2338, 1993.

Kotsialos, A., and M. Papageorgiou. "Efficiency and equity properties of freeway network-wide ramp metering with AMOC." Transportation Research Part C: Emerging Technologies, vol. 12, no. 6, pp. 401-420, 2004.

Kotsialos, A., M. Papageorgiou, and F. Middelham. "Local and optimal coordinated ramp metering for freeway networks." Journal of Intelligent Transportation Systems, vol. 9, no. 4, pp. 187-203, 2005.

Kotsialos, A., M. Papageorgiou, M. Mangeas, and H. Haj-Salem. "Coordinated and integrated control of motorway networks via non-linear optimal control." Transportation Research Part C: Emerging Technologies, vol, 10, no. 1, pp. 65-84, 2002.

Kuhne, R. D. “Macroscopic freeway model for dense traffic-stop-start waves and incident detection”, Proceedings of the Ninth International Symposium on Transportation and Traffic Theory, pp. 20-42, 1984.

Kwon, E., D. Brannan, K. Shouman, C. Isackson, B. Arseneau. “Development and field evaluation of variable advisory speed limit system for work zones.” Transportation Research Record, vol. 2007, pp. 12–18, 2015.

Li, D., P. Ranjitkar, and A. Ceder. "Integrated approach combining ramp metering and variable speed limits to improve motorway performance." Transportation Research Record: Journal of the Transportation Research Board, vol. 2470, pp. 86-94, 2014a.

Li, Y., A. Chow, and D. Cassel. "Optimal control of motorways by ramp metering, variable speed limits, and hard-shoulder running." Transportation Research Record: Journal of the Transportation Research Board, vol. 2470, pp. 122-130, 2014b.

Lighthill, M. J., and G. B. Whitham. “On kinematic waves: I. Flood movement in long rivers”, Proceedings of Royal Society of London, Series A, Mathematical and Physical Sciences, vol. 229, no. 1178, pp. 281-316, 1955a.

Lighthill, M. J., and G. B. Whitham. “On kinematic waves: II. A theory of traffic flow on long crowded roads”, Proceedings of Royal Society of London, Series A, Mathematical and Physical Sciences, vol. 229, no. 1178, pp. 317-345, 1955b.

Lin, P. W., K. P. Kang, and G. L. Chang. “Exploring the effectiveness of variable speed limit controls on highway work-zone operations.” Journal of Intelligent Transportation System, vol. 8, no. 3, pp. 155–168, 2004.

Logghe, S. and L. H., Immers. “Multi-class kinematic wave theory of traffic flow”, Transportation Research Part B, Methodological, vol. 42, no. 6, pp. 523-541, 2008.

Lu, X. Y., and S. Shladover. "Review of Variable Speed Limits and Advisories: Theory, Algorithms, and Practice." Transportation Research Record: Journal of the Transportation Research Board, vol. 2423, pp. 15-23, 2014.

Lu, X. Y., P. Varaiya, R. Horowitz, D. Su, and S. Shladover. "Novel freeway traffic control with variable speed limit and coordinated ramp metering." Transportation Research Record: Journal of the Transportation Research Board, vol. 2229, pp. 55-65, 2011.

Lu, X. Y., T. Z. Qiu, P. Varaiya, R. Horowitz, and S. E. Shladover. "Combining variable speed limits with ramp metering for freeway traffic control." In American Control Conference (ACC), pp. 2266-2271, 2010.

Lyles, R., W. C. Taylor, and J. Grossklaus. "Field test of variable speed limits in work zones (in Michigan)." Michigan Department of Transportation, 2003.

MacDonald, Mott. "ATM Monitoring and Evaluation, 4-Lane Variable Mandatory Speed Limits 12 Month Report (Primary and Secondary Indicators)." Department of Transport, 2008.

Masher, D. P., D. W. Ross, P. J. Wong, P. L. Tuan, H. M. Zeidler, and S. Petracek. "Guidelines for design and operation of ramp control systems." 1975.

Michalopoulos, P. G., P. Yi, A. S. Lyrintzis. "Continuum modeling of traffic dynamics for congested highway", Transportation Research Part B, Methodological, vol. 27, no. 4, pp. 315-332, 1993.

Paesani, G., J. Kerr, P. Perovich, and F. E. Khosravi. "System wide adaptive ramp metering (SWARM)." In Merging the Transportation and Communications Revolutions. Abstracts for ITS America Seventh Annual Meeting and Exposition. 1997.

Papageorgiou, M., "A hierarchical control system for freeway traffic", Transportation Research Part B, Methodological, vol. 17, no. 3, pp. 251-261, 1983.

Papageorgiou, M., and M. Marinaki. "A feasible direction algorithm for the numerical solution of optimal control problems." Dynamic Syst. Simulation Lab., Tech. Univ. Crete, Chania, Greece, 1995.

Papageorgiou, M., E. Kosmatopoulos, and I. Papamichail. “Effects of variable speed limits on motorway traffic flow.” Transportation Research Record, vol. 2047, pp. 37–48, 2008.

Papageorgiou, M., H. Hadj-Salem, and F. Middelham. "ALINEA local ramp metering: Summary of field results." Transportation Research Record: Journal of the Transportation Research Board, vol. 1603, pp. 90-98, 1997.

Papageorgiou, M., H. Hadj-Salem, and J. M. Blosseville. "ALINEA: A local feedback control law for on-ramp metering." Transportation Research Record, vol. 1320, 1991.

Papageorgiou, M., J. M. Blosseville, and H. Hadj-Salem. “Macroscopic modelling of traffic flow on the Boulevard Périphérique in Paris”, Transportation Research Part B: Methodological, vol. 23, no.1, pp. 29-47, 1989.

Papamichail, I., A. Kotsialos, I. Margonis, and M. Papageorgiou. "Coordinated ramp metering for freeway networks–A model-predictive hierarchical control approach." Transportation Research Part C: Emerging Technologies, vol. 18, no. 3, pp. 311-331, 2010.

Papamichail, I., and M. Papageorgiou. "Traffic-responsive linked ramp-metering control." IEEE Transactions on Intelligent Transportation Systems, vol. 9, no. 1, pp. 111-121, 2008.

Papamichail, I., M. Papageorgiou, V. Vong, and J. Gaffney. "Heuristic ramp-metering coordination strategy implemented at Monash freeway, Australia." Transportation Research Record: Journal of the Transportation Research Board, vol. 2178, pp. 10-20, 2010.

Payne, H. J. “Model of freeway traffic and control: Mathematical models of public systems”, Simulation Council Proceedings Series, vol. 1, no. 1, pp. 51-61, 1971.

Pearson, R., J. Black, and J. Wanat, “Ramp metering ITS decision report”, ITS Decision Report, 2001.

Piotrowicz, G., and J. Robinson, “Ramp metering status in North America, 1995 Update”, No. DOT-T-95-17, 1995.

Placer, J. “Fuzzy Variable Speed Limit Device Modification and Testing, Phase II.” No. AZ-466 (2). Arizona Department of Transportation, 2001.

PTV. “VISSIM 5.20 User Manual”. 2009.

Richards, P. I. “Shockwaves on the highway”, Operations Research, vol. 4, no.1, pp. 42-51, 1956.

Schrank, D., B. Eisele, T. Lomax, and J. Bak, “2015 urban mobility scorecard”, Texas A&M Transportation Institute & INRIX, 2015.

Smaragdis, E., and M. Papageorgiou. "Series of new local ramp metering strategies." Transportation Research Record: Journal of the Transportation Research Board, vol. 1856, pp. 74-86, 2003.

Schönhof, M., and D. Helbing. "Empirical features of congested traffic states and their implications for traffic modeling." Transportation Science, vol. 41, no. 2, pp. 135-166, 2007.

Smaragdis, E., M. Papageorgiou, and E. Kosmatopoulos. "A flow-maximizing adaptive local ramp metering strategy." Transportation Research Part B: Methodological, vol. 38, no. 3, pp. 251-270, 2004.

Smulders, S. “Control of freeway traffic flow by variable speed signs.” Transportation Research Part B, vol. 24, pp. 111–132, 1990.

Sparmann, J. "Freeway Operation in Germany: Experiences in Hessen." In Proceedings of the 1st International Symposium on Freeway and Tollway Operations, Athens, Greece. 2006.

Steel, P., R. V. McGregor, A. A. Guebert, and T. M. McGuire. “Application of variable speed limits along the Trans-Canada Highway in Banff National Park.” Proceedings of the Annual Conference of the Transportation Association of Canada, 2005.

Stephanedes, Y. J. "Implementation of on-line Zone Control Strategies for optimal ramp metering in the Minneapolis Ring Road." In Seventh International Conference on Road Traffic Monitoring and Control, pp. 181-184, 1994.

Szeto, W., “Enhanced lagged cell-transmission model for dynamic traffic assignment”, Transportation Research Record, vol. 2085, pp. 76-85, 2008.

Talebpour, A., H. S. Mahmassani, and S. H. Hamdar. “Speed harmonization: effectiveness evaluation under congested conditions.” Proceedings of Transportation Research Board 92nd Annual Meeting, 2013.

Taylor, C., D. Meldrum, and L. Jacobson. "Fuzzy ramp metering: Design overview and simulation results." Transportation Research Record: Journal of the Transportation Research Board, vol. 1634, pp. 10-18, 1998.

Ulfarsson, G. F., V. N. Shankar, and P. Vu. “The effect of variable message and speed limit signs on mean speeds and speed deviations.” International Journal of Vehicle Information and Communication Systems, vol. 1, pp. 69-87, 2005.

Underwood, R.T., “Speed, volume and density relationships: Quality and theory of traffic flow”, Yale University Report, Yale Bureau of Highway Traffic, New Haven, CT, pp. 141-188, 1961.

Wagstaff, K., C. Cardie, S. Rogers, and S. Schrödl. "Constrained k-means clustering with background knowledge." Proceedings of the Eighteenth International Conference on Machine Learning, pp. 577-584, 2001.

Wang, Y., and P. Ioannou. "New model for variable speed limits." Transportation Research Record: Journal of the Transportation Research Board, vol. 2249, pp. 38-43, 2011.

Weikl, S., K. Bogenberger, R. L. Bertini. “Traffic management effects of variable speed limit system on a German Autobahn empirical assessment before and after system implementation.” Transportation Research Record: Journal of the Transportation Research Board, vol. 2380, pp. 48-60, 2013.

Wong, G. C. K., and S. C. Wong, “A multi-class traffic flow model – an extension of LWR model with heterogeneous drivers”, Transportation Research Part A: Policy and Practice, vol. 36, no. 9, pp. 827-841, 2002.

Xin, W., P. Michalopoulos, J. Hourdakis, and D. Lau. "Minnesota's new ramp control strategy: design overview and preliminary assessment." Transportation Research Record: Journal of the Transportation Research Board, vol. 1867, pp. 69-79, 2004.

Xu, J., W. S. Yu, and F. Y. Wang. "Ramp metering based on adaptive critic designs." In IEEE Intelligent Transportation Systems Conference, pp. 1531-1536, 2006.

Yang, X., Y. C. Lu, and G. L. Chang. "Exploratory analysis of an optimal variable speed control system for a recurrently congested freeway bottleneck." Journal of Advanced Transportation, vol. 49, no. 2, pp. 195-209, 2015.

Zhang, H. M., “A theory of nonequilibrium traffic flow”, Transportation Research Part B, Methodological, vol. 32, no. 7, pp. 485-498, 1998.

Zhang, H. M., and S. G. Ritchie. "Freeway ramp metering using artificial neural networks." Transportation Research Part C: Emerging Technologies, vol. 5, no. 5, pp. 273-286, 1997.

Zhang, H. M., and W. W. Recker. "On optimal freeway ramp control policies for congested traffic corridors." Transportation Research Part B: Methodological, vol. 33, no. 6, 417-436, 1999.